Conversion of the ATP synthase subunit *c* into a hydrophilic pore

A Thesis Submitted
to the College of Graduate Studies and Research
in Fulfillment of the Requirements
for the Degree of Master of Science
in the Department of Biochemistry,
University of Saskatchewan,
Saskatoon.

By

Daryna Kulik

Copyright Note

Abstract

Nanopore analysis is a very promising technique for many applications, such as the study of intrinsically disordered proteins, folding and misfolding of proteins and DNA sequencing. Nanopore is a small pore in the lipid bilayer membrane, which can let solutes through. Nanopores of various diameters would be useful for different applications. Currently, the most widely used nanopore is α-hemolysin with an internal diameter of ~1.4 nm. This nanopore is mostly used to study unfolded protein molecules and single-stranded DNA. The limitations of this pore include inability to pass larger folded protein molecules and double-stranded DNA, as well as inability to effectively discriminate biopolymers from smaller molecules.

Our goal was to design a nanopore alternative to α-hemolysin, which would be stable for a long time in the artificial membrane and be suitable for a wider spectrum of applications in nanopore analysis.

We chose *c*-rings of ATP synthase from two bacterial species as scaffolds for a new type of a nanopore: the *c*-ring from *E.coli,* which consists of 10 *c*-subunits, and the *c*-ring from *I. tartaricus,* which consists of 11 *c*-subunits. The size and diameter of the *c*-ring differ from species to species, which makes it a versatile model for a novel nanopore.

We modified each *c*-ring by introducing polar amino acid substitutions into its internal cavity to make the ring interior hydrophilic. We used the wild type *c*-subunit from *E. coli* as a control. Purified monomeric *c*-subunits were reconstituted into proteoliposomes and tested for nanopore formation. Both the wild type and the polar interior versions of the *c*-ring formed stable nanopores with similar electrical properties.

Further studies are needed to investigate the ability of these nanopores to translocate biomolecules and their potential for use in biological assays.

Acknowledgements

I would like to express my gratitude to my scientific advisor Dr. Oleg Dmitriev for the continuous support during my Masters project, for the guidance and immense knowledge. The completion of this project could not have been accomplished without the support of my second scientific advisor Dr. Jeremy Lee. I am deeply grateful for his useful comments, suggestions and help in all the time of research and writing of this thesis. I would like to thank my advisory committee: Dr. Stanley Moore and Dr. Yuliang Wu for their insightful comments and helpful advices. I am grateful to all of those with whom I have had the pleasure to work during this project, including but not limited to Chris O'Grady, Nataliya Dolgova, Sergiy Nokhrin, Corey Yu, Chris Christensen and Elisabet Jakova. I would like to thank Eva Uhlemann for her contribution to this project. I am appreciative to Steve Gagne for sharing his expertise in molecular biology. I would like to thank Dr. George Katselis and his group members for the help with mass spectrometry analysis. This project would have been impossible without the financial support of Proteomics Research in Interactions and Structure of Macromolecules (PRISM) Centre. I would also like to thank my family and especially my husband Dzmitriy for the endless support and encouragement.

Table of Contents

List of Tables

List of Figures

List of Abbreviations

ACMA	9-amino-6-chloro-4-methoxy-acridine
ADP	Adenosine diphosphate
ATP	Adenosine triphosphate
BSA	Bovine serium albumin
Cryo-EM	Cryo-electron microscopy
DDM	n-Dodecyl-β-D-maltopyranoside
DPHPC	1, 2- diphytanoyl-sn-glycero-3-phosphocholine
DTT	Dithiothreitol
DCCD	N,N'-Dicyclohexylcarbodiimide
DNA	Deoxyribonucleic acid
EDTA	Ethylenediaminetetraacetic acid
F	Farad
FCCP	Carbonylcyanide-4-(trifluoromethoxy) – phenylhydrazone
Gu-HCl	Guanidine chloride
IPTG	Isopropyl β-D-1-thiogalactopyranoside
His	Hexa-histidine
HRP	Horseradish peroxidase
LB	Lysogeny broth
LDAO	lauryldimethylamine-N-oxide
NADH	Nicotinamide adenine dinucleotide
Ni-NTA	Nickel-nitrilotriacetic acid
NMR	Nuclear magnetic resonance
OD	Optical density
Ω	Ohm
PBS	Phosphate-buffered saline
PET	Poly(ethylene terephthalate)

PC	Polycarbonate
PCR	Polymerase chain reaction
PI	Polyimide
Pi	Inorganic phosphate
PMSF	Phenylmethanesulfonylfluoride
PVDF	Polyvinylidene fluoride membrane
SDS	Sodium dodecyl sulfate
SDS-PAGE	Sodium dodecyl sulfate polyacrylamide gel electrophoresis
TMH	Transmembrane helix
TCA	Trichloroethanoic acid
Tris	Tris(hydroxymethyl)aminomethane
WT	Wild type

1. Introduction

Nanopore analysis is a modern method for studying single molecules and is becoming widely used for protein research (Madampage *et al.*, 2012). A nanopore is a pore with one to several nanometers in internal diameter, which can pass solutes and small molecules and has great potential for detection and identification of macromolecules in aqueous solution.

Detection of molecules in nanopore analysis is similar to the Coulter counter developed by Wallace H. Coulter in the late 1940s. The Coulter counter consists of a thin glass tube with the small orifice, which is submerged in the electrolyte bath. The diameter of the orifice is usually in the micrometer range. Two electrodes are placed on each side of the glass partition and create an electric field. When the analysed solution is added to the glass tube, vacuum pressure is applied, forcing the particles to move through the orifice. When a single particle traverses the orifice, a resistive pulse occurs, causing a drop in the current. The frequency of the pulses gives an estimate of the concentration of the particles in the solution (Coulter, 1953; Bayley and Martin, 2000). The technique is widely used for counting cells, bacteria and virus particles. Solutes of much smaller size can be detected using nanopore analysis, where molecules are driven through a pore with the diameter in the nanometer range by an electric field rather than by vacuum pressure and the currents are measured in the pA range.

The principle of current detection in nanopore analysis was first used in the patch clamp method. Patch clamp experiments were developed in the early 1980s by Erwin Neher and Bert Sakmann for studying single ion channel molecules. The glass micropipette is used to enclose, or “patch”, the surface of the cell membrane containing a single ion channel, or a group of channels. Currents coming through the channel are then measured using a very sensitive patch clamp amplifier (Sakmann and Neher, 1984).

Essentially, nanopores represent an application of the resistive-pulse technique with the promise of developing sensitivity, specificity and simplicity for many applications (Keyser, 2011). Nanopore analysis can be used for studying intrinsically disordered proteins, protein misfolding and molecule interactions. The method was also successfully employed for real-time DNA sequencing (Eisenstein, 2012).

The widely used α-hemolysin nanopore has a fixed diameter of 1.4 nm. Most proteins are too large to move through the α-hemolysin but it remains the most used biological nanopore due to its commercial availability (Branton *et al.*, 2008). Our goal was to engineer a novel protein nanopore with a controllable diameter for studying a range of molecules of different sizes. Such a nanopore should be stable on a timescale of hours and have internal diameter different from α-hemolysin. We chose the oligomeric *c*-ring of ATP synthase as a scaffold for building the nanopore, as it forms stable structures in the lipid membrane and can consist of a different number of monomers. By changing the number of subunits forming the ring it might be possible to adjust the diameter of a nanopore for various applications.

2. Background information

2.1. Principles of nanopore analysis.

Study of the proteins and other bio-molecules is often hampered by the existence of various conformations and states, which have different properties. The signal obtained from recording many molecules at the same time represents an ensemble averaging, and the properties of individual molecules in dynamics are neglected. Single-molecule experiments enable researches to obtain information about the properties of individual molecules, which cannot be determined from a bulk collection of molecules. A highly sensitive tool is needed to discriminate a single molecule in a solution. Nanopore represents such a tool. Nanopore is a structural element of either protein or synthetic nature with an opening of 1 to several nanometers, located in a membrane and is able to pass analysed solutes through the opening across the membrane, one molecule at a time. The nanopore works as a sensor and provides a reading, which reflects characteristics of the analysed molecule passing though the nanopore.

Currently, two types of nanopores are used in nanopore analysis. Solid-state nanopores are fabricated from different synthetic membranes using a variety of techniques. Biological nanopores are formed by protein molecules embedded in a lipid bilayer and have a hollow core of a few nanometers (Dekker, 2007). Electrical properties of both the biological and the solid-state nanopores can be described using simple laws of physics. The membrane forms a thin insulating layer between two conducting solutions. Therefore, when an electric potential difference is applied across the membrane, it serves as an electric capacitor. A nanopore inserted into the lipid membrane creates an ion channel and becomes an electric conductor. In the presence of electric potential difference, the ion flow through the nanopore creates an electric current, measured in amperes (A), or more conveniently, in picoamperes (pA). According to Ohm's law the current through an ideal conductor (I) is proportional to the applied electric potential difference (V), with proportionality constant defined as electric resistance (R), and measured in ohm (Ω): $V=IR$. Conductance (G) is the inverse of resistance ($G=1/R$), and is commonly used in biophysics to characterize electric properties of the ion channels and nanopores. Conductance is measured in siemens (S), or more conveniently in picosiemens (pS), $1S = 1\ \Omega^{-1}$. From the definition, the higher the nanopore conductance, the higher current will flow through the pore at a

given potential difference. Such pore characteristics as diameter, length and ion selectivity determine its conductance. Another commonly used characteristic is conductivity, which is defined as conductance per unit of conductor length, and is measured in siemens per metre (S/m).

Nanopore analysis is a single-molecule technique used for detection of macromolecules in a solution by analysing changes of electrical current appearing as a result of their interaction with a protein or solid-state nanopore under a constant voltage. An experimental setup of nanopore analysis includes a Teflon partition, which divides two chambers filled with electrolyte solution, and two Ag/AgCl electrodes are placed on each side of the partition creating an electric field. The partition has an aperture of ~150 μm in diameter covered with a lipid, which forms an impermeable membrane. The lipid membrane has very high electric resistance and is stable for many hours. A protein pore of a few nanometers in internal diameter is inserted into the lipid bilayer. The alternative setup would include a solid-state nanopore, which is represented by a single hole in a thin artificial non-lipid membrane. In both cases the nanopore forms the only path between the two chambers (Figure 2.1).

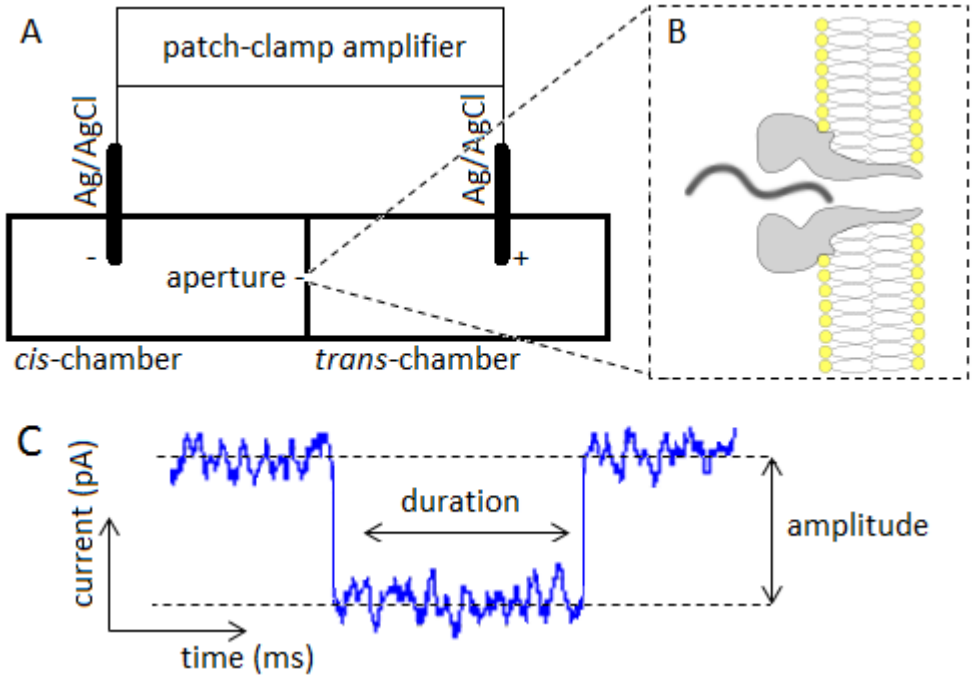

Figure 2.1. The principle of nanopore analysis. (A) A partition with an aperture divides the two chambers filled with an electrolyte solution, each connected to the Ag/AgCl electrode. (B) An artificial membrane in the aperture with the inserted pore translocating a macromolecule. C – Blockade current with the amplitude and duration parameters.

When an electric potential is applied across the membrane, the ionic current through the pore can be measured by using a patch-clamp amplifier. A highly sensitive amplifier is required to record currents in the pA range. Under a constant voltage charged protein molecules tend to translocate according to their electrophoretic mobility. In the experimental setup described above, the *trans*-chamber contains a positively charged electrode, while the *cis*-chamber contains a negatively charged electrode. Negatively charged molecules are added to the *cis*-chamber and driven electrophoretically towards the *trans*-chamber through the pore. Positively charged molecules are added to the *trans*-chamber, and they move towards the *cis*-chamber. If the molecule under study has no charge, it can be added to any chamber as it will diffuse in all directions. The detection and identification of macromolecules in aqueous solution is possible when they translocate through a nanopore, causing displacement of the electrolytes inside the pore. The resistive pulse, corresponding to the drop in the ionic current has an amplitude (I) and time (T), which are measured and analysed. Both these parameters of the resistive pulse depend on the size and shape of the passing molecule, which allows identification of different conformations of the macromolecule.

Each resistive pulse corresponds to either a translocation or bumping event. Translocation event occurs, when a molecule passes through the nanopore, and results in a significant drop in current. A bumping event occurs when a molecule briefly obstructs the pore, causing a short decrease in ionic current, and then diffuses away. The amplitude of bumping events is usually much smaller compared to translocation events. There are also intercalation events, which are characteristic of biological nanopores with large vestibules. In the case of an intercalation event the molecule is trapped inside the vestibule of the pore before diffusing away (Madampage *et al.*, 2012). Translocation events are the most informative, as they directly indicate the size and structural properties of the protein, since the amplitude of the blockade current is proportional to the volume of the pore channel occupied by the translocating molecule (Deamer *et al.*, 2002). The amplitude and time of translocation events are known to be higher for α-helices than β-sheets, for example, β-hairpins (Stefureac *et al.*, 2006; Zhao *et al.*, 2009).

2.2. Solid-state nanopores.

Silicon nitride, silica, polymethylmethacrylate, polyimide, aluminium and graphene are commonly used materials for creation of solid-state nanopores. Glass nanocapillaries were

proved to be efficient in nanopore sequencing (Stein *et al.*, 2004; Keyser, 2011). Several methods for creating the solid-state nanopores have been invented to date. All of them are based on a similar principle: a high energy beam is used to penetrate the membrane creating a small pore.

Ion-track etching is one of the oldest methods, which was developed in the 1960s (Fleischer and Price, 1963). Highly accelerated heavy ions (Xe, Pb, Au or U) are used to penetrate membranes made of poly(ethylene terephthalate) (PET), polycarbonate (PC) or polyimide (PI). Subsequently, strong alkaline solutions are used to increase the diameter of pores up to 10 nm. This process depends on the temperature, base concentration and time, which are used to control the pore diameter (Apel *et al.*, 2001).

The focused ion-beam technique was developed recently (Li *et al*., 2001). A focused high-energy heavy-metal ion beam (Ag^{+}) is used for drilling through a layer of a thin membrane, creating a hole of a few nanometers in diameter. The hole is then narrowed by a diffuse ion beam (Stein *et al*., 2004). Pores up to 1 nm in diameter can be produced by this technique. Although the size of the pore can be controlled, the pore itself is not perfectly symmetrical in shape (Stein *et al*., 2004).

Another method of nanopore design, developed at Delft University (Storm *et al*., 2003), is based on electron-beam lithography to pattern pores in thin membranes made of Si, SiN, or SiO_2 (Dekker, 2007). This method was also successfully employed for single atom layer graphene membranes (Garaj *et al.*, 2010). A direct electron beam is used to drill the pore with direct feedback from a transmission electron microscope (TEM). The result of the electron beam drilling is a pore with a typical diameter of 20 nm. Fine-tuning of the pore is possible to subnanometre precision using a diffuse electron beam. During this process the pore is shrunk to a few nanometers in diameter. The primary advantage of the electron-beam lithography method is the possibility of visually monitoring pore etching and refinement (Dekker, 2007).

Individual nanopores of 1-25 nm in size can be produced in a thin silicon nitride (SiNx) membrane using a recently developed controlled dielectric breakdown technique (Kwok *et al.*, 2014). The experimental setup for nanopore formation is very similar to the nanopore analysis instrumentation described in the previous section. A thin insulating solid-state membrane separates two reservoirs containing electrolyte solution. The two Ag/AgCl electrodes are placed on

both sides of the membrane and trans-membrane potential of up to ±20 V is applied. The nanopore is formed due to structural defects in the membrane, which accumulate under the influence of the electric field. This in turn induces bond breakage inside the membrane, causing a sudden irreversible leakage current. When the current reaches a predetermined threshold, which corresponds to a certain pore diameter, the voltage is turned off.

Solid-state nanopores are very stable and can be used for long experiments. However, they have certain disadvantages. A common problem of the solid-state nanopores is their poor reproducibility. Technological processes used in manufacturing of solid-state nanopores do not allow for perfect reproducibility in terms of size and shape. Also, the length of such a nanopore is limited by the membrane thickness (Keyser, 2011). The other problem lies in the relatively high capacitance of membranes, which results in a high current noise, decreasing the quality of the nanopore signal (Tabard-Cossa *et al.*, 2007).

2.3. Protein nanopores.

Lipid bilayer, which forms the basis of biological membranes, creates an impermeable barrier for solutes. The transport of solutes through the membranes is controlled by the transmembrane proteins such as channels, pumps, and pores. Some of these transporters have no or very low selectivity and remain open for a long period of time. Such transporters can be suitable for use in nanopore analysis if their diameter is in the nanometer range. Biological ion channels, for example, are not suited for use in nanopore analysis, as they have internal diameter of a few angstroms, which is enough for passing through and selecting ions, but is too small for macromolecules, such as peptides and nucleic acids. Some secretins, porins and toxins can be suitable for use in nanopore analysis, as their diameter is much larger than that of channels.

Most of the protein nanopores employed for nanopore analysis were found in bacteria. For example, the opportunistic bacterium *Staphylococcus aureus* secretes a toxin called α-hemolysin. It is isolated as a water-soluble monomeric protein, which is capable of binding to the lipid bilayer. Upon interaction with a membrane, the monomers gain the ability to oligomerize and integrate into the membrane as a heptamer, creating a water-filled transmembrane channel (Gouaux *et al*., 1994; Bayley, 1995). The channel is very stable and allows solutes to pass through the membrane, collapsing ion gradients and causing cell death (Song *et al*., 1996).

The high stability and regular electric properties of α-hemolysin made this pore widely used in nanopore analysis (Figure 2.2 A, B). The α-hemolysin nanopore has a large vestibule in the extra-membranous domain connected to the transmembrane stem domain, forming a mushroom-like structure. The external dimensions of the pore are approximately 100 Å in length and up to 100 Å in diameter. The transmembrane part consists of right-handed β-barrel, formed of 14 antiparallel β-strands (Song *et al*., 1996). The narrowest point in the channel has a diameter of approximately 1.4-1.5 nm, which allows passage of ions, some oligosaccharides, peptides and single-stranded DNA across the membrane (Madampage *et al*., 2012). The pore is characterised by high ionic conductivity with a measured current of 100 pA, when a100 mV voltage is applied across the membrane (Figure 2.3) (Dekker, 2007).

Toxic protein aerolysin from *Aeromonas hydrophila* is another commonly used nanopore with a well-studied structure (Figure 2.2 C, D). Like α-hemolysin, it also forms a heptameric complex in the membrane; however its structure is different from α-hemolysin (Pastoriza-Gallego *et al*., 2011). Aerolysin doesn't have a large vestibule domain. Instead, the cylinder of the pore is surrounded by a disc-like complex about 14 nm in diameter, which lies 2 nm above the membrane surface. The water-filled transmembrane channel of aerolysin is 1.7 nm in diameter, and the length of transmembrane domain is around 5 nm (Parker *et al*., 1994). It was shown that aerolysin has high resistance to strong denaturing agents, such as guanidine chloride (Gu-HCl), which allows the use of this pore to study unfolded proteins (Pastoriza-Gallego *et al*., 2011).

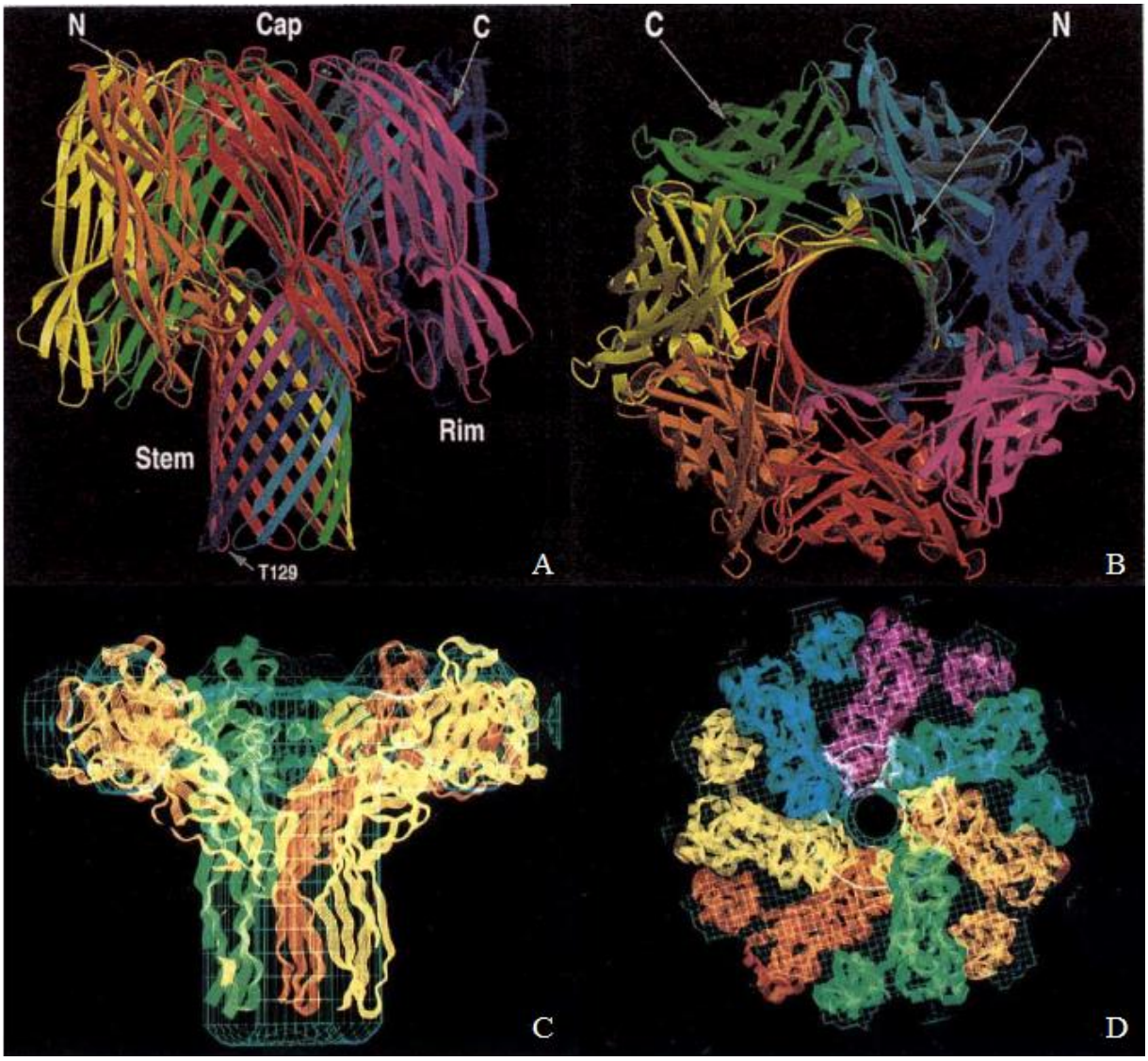

Figure 2.2. Structure representations of α-hemolysin and aerolysin: (A) α-hemolysin, side view; (B) α-hemolysin, top view; (C) aerolysin, side view of the channel; (D) aerolysin, top view. Monomers are represented in different colors (From Song *et al*., 1996. Reprinted with permission from AAAS, and reprinted by permission from Macmillan Publishers Ltd: Nature (Parker *et al.*, 1994), copyright 1994).

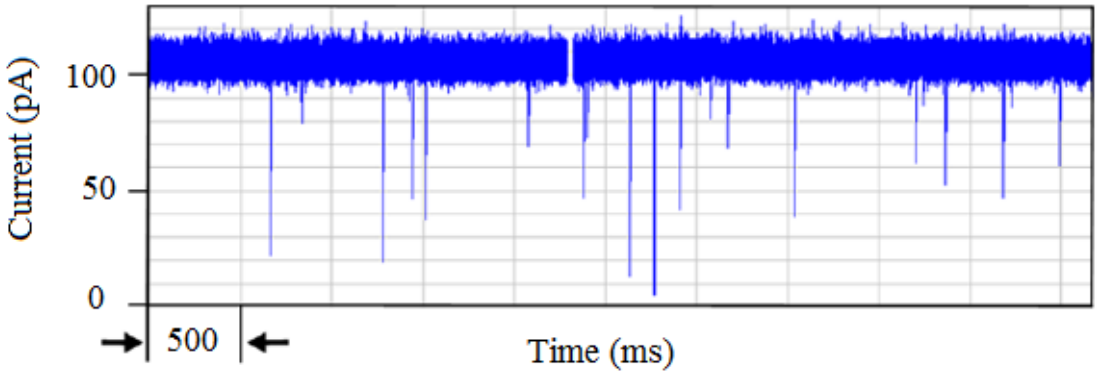

Figure 2.3. Open pore current (100 pA) of α-hemolysin pore. The analyte (RNase A) was added to the electrolyte solution and voltage was applied inducing molecule movement through the pore. Each spike represents an event when a molecule interacts with the pore. Large spikes correspond to translocations and small spikes to bumping events (Krasniqi and Lee, 2014, used under CC BY).

Porin A nanopore, or MspA, was found in *Mycobacterium smegmatis*, where it forms a channel allowing hydrophilic molecules access to the cell interior (Niederweis *et al*., 1999). The unique structure of the protein pore was solved in 2004 (Faller *et al*., 2004). It is represented by a goblet-like octameric polypeptide, which forms a central channel (Figure 2.4 A, B). The diameter of the channel varies from 4.8 nm in the external end of the porin to 1 nm in the 1 nm long constriction area at the periplasmic side. The constriction of the pore may provide a good spatial resolution for translocating molecules, as the blockade current is primarily determined by the molecule translocating through the narrow region. It was shown that the MspA nanopore is very robust and stable for long periods of time. It was successfully used for nucleic acid analysis and has a great potential for DNA sequencing (Butler *et al*., 2008; Manrao *et al*., 2011).

There are other well studied protein pores, which can be used in nanopore analysis, such as secretins and outer membrane proteins. Secretins typically have a cylindrical arrangement of 12–15 subunits, a large vestibule at one end and a gate at the other (Figure 2.4 C, D). GspD secretin from *Vibrio cholerae* has an opening of 7.5 nm in the vestibule and constriction of 5.5 nm in the channel (Korotkov *et al*., 2011).

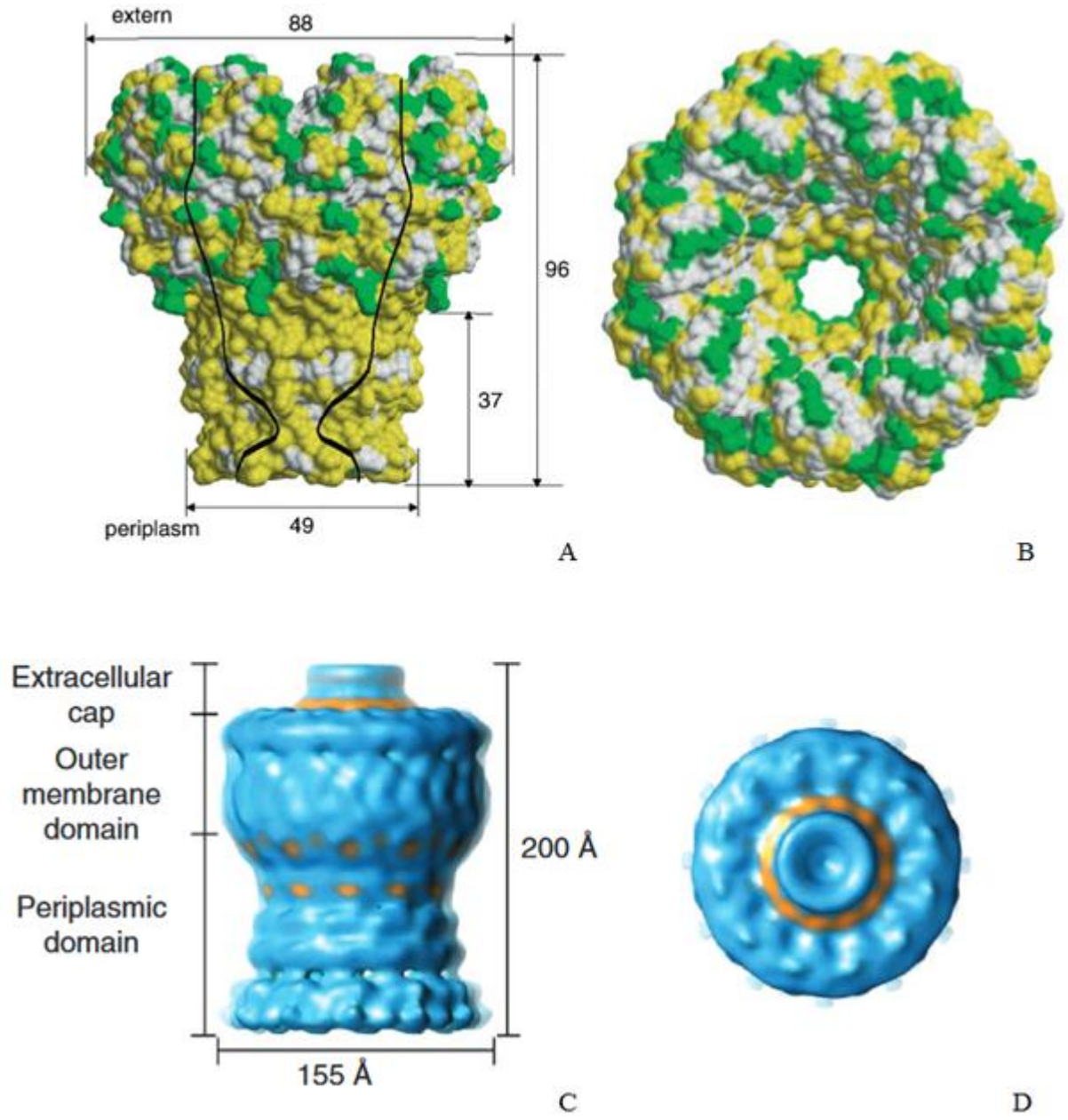

Figure 2.4. Structure representations of MspA porin and GspD from Vibrio volerae: (A) MspA, side view, (B) MspA, top view. The channel lining is shown in black. Polar amino acids are shown in green and nonpolar amino acids in yellow. (C) GspD, side view, (D) GspD, top view (From Faller *et al.*, 2004. Reprinted with permission from AAAS, and reprinted by permission from Macmillan Publishers Ltd: Nature Structural and Molecular Biology (Reichow *et al.*, 2010), copyright 2010).

The robust structure of the bacterial outer membrane porin OmpG provides a promising potential for its use in a nanopore analysis. It has a 1.5 nm diameter of the channel, allowing for the passage of hydrated ions. The major drawback of this nanopore is spontaneous gating, which could be attenuated by protein engineering (Chen *et al*., 2008).

Protein pores offer an effective and convenient tool for nanopore analysis. Unlike solid-state nanopores, they are perfectly reproducible in shape and size; their surface and electric properties remain the same. Another major advantage of protein nanopores is the possibility of introducing local changes in their structures. The amino acid composition can be modified as desired with the help of site-directed mutagenesis for adapting the pore to a specific experiment. Furthermore, other molecules can be fused to the pore. For example, biotin can be added to the chain to probe biotin-binding molecules (Movileanu *et al.*, 2000). Hydrophobic groups, such as cyclodextrins, can be added to bind organic molecules inside the channel thus blocking the pore. This could be used for stochastic sensing, where the individual binding events between analyte molecules and a receptor protein are studied (Gu *et al.*, 1999). Another possibility is attaching oligonucleotides to the protein chain for probing DNA hybridisation. The matching nucleotide sequences bind together and DNA translocation stops until the double helix is unzipped (Howorka *et al.*, 2001).

Most of the protein pores, which are currently used in nanopore analysis have fixed diameter of less than 2 nm, which limits their application range. To date, α-hemolysin is the most widely used nanopore primarily due to its commercial availability. Although it is suitable for sensing single-stranded DNA or RNA and unfolded protein molecules, it is too small for translocating double-stranded DNA or proteins in their native conformation (Keyser, 2011).

Despite the abundance of membrane pores in nature, finding a suitable pore is a challenge, as it should have the proper inner diameter, successfully incorporate into the lipid bilayer and provide a stable current for many hours (Keyser, 2011). A pore with a variable internal diameter could prove useful for many applications, as it would allow translocation of molecules of different sizes. The main purpose of this research is to create such a nanopore. The *c*-ring of F_1F_O ATP synthase forms a circular structure in the membrane and has a different diameter in various species, which makes it a good candidate for this task.

2.4. Molecular structure and function of the F_1F_O-ATP synthase.

F_1F_O ATP synthase (Subscript "O" historically denotes inhibition by oligomycin, a characteristic property of the mitochondrial ATP synthase) is one of the most ubiquitous proteins in all living organisms, which is directly determined by its main function: supplying cells with energy. It catalyzes the synthesis of ATP from ADP and inorganic phosphate (P_i), obtaining energy for this reaction from the gradient of electrochemical potential of H^+ or Na^+ ions across membranes ($\Delta\mu H+$ or $\Delta\mu Na^+$) (Yoshida *et al.,* 2001). Electron-transfer chains in the membranes of microorganisms, mitochondria and chloroplasts work constantly, maintaining the ion gradient sufficient for ATP synthesis (Senior, 1988).

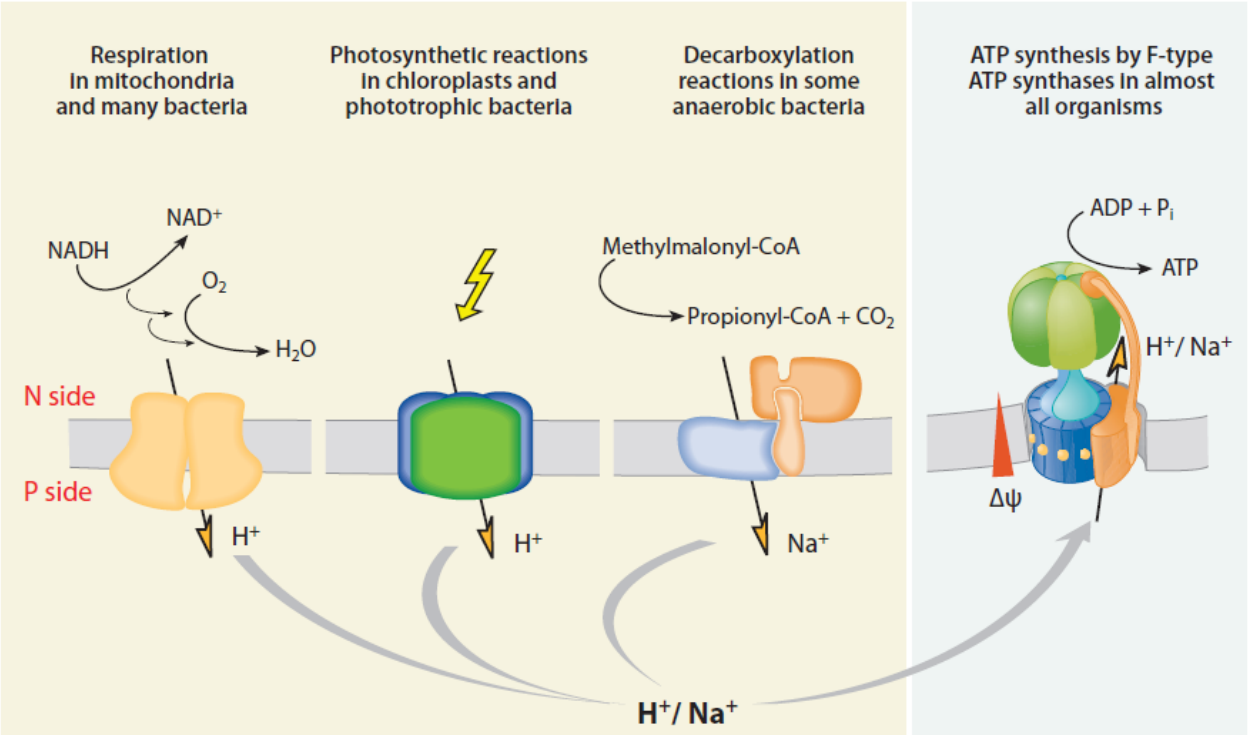

Figure 2.5. Generation of the ion gradients in different organisms. Heterotrophic organisms have respiratory chains, which oxidize reducing equivalents (NADH, succinate) from metabolism of nutrients and convert free energy from oxidation into the electrochemical gradient of protons ($\Delta\mu H^+$) across the membrane. Chloroplasts and phototrophic bacteria use light energy for creation of the $\Delta\mu H^+$ across the membrane. Some anaerobic bacteria, such as *P. modestum* or *I. tartaricus* create the electrochemical gradient of sodium ($\Delta\mu Na^+$) by decarboxylation of methylmalonyl-CoA (von Ballmoos *et al*., 2009).

While most living organisms use the proton gradient produced by the respiratory chain for ATP synthesis, some strict anaerobic bacteria, such as *Propionigenium modestum*, do not have electron transport chains (Figure 2.5). Instead they convert energy from succinate decarboxylation into Na^+ gradients, which is used by the Na^+-dependent ATP synthase to drive ATP synthesis. Despite the use of different coupling ions, both enzymes of *E. coli* and *P. modestum* belong to F-type ATPases and have a remarkably similar subunit composition (Laubinger and Dimroth, 1988). Later discoveries showed that the ion specificity of the ATP synthase is determined primarily by the transmembrane part of the enzyme (Kaim and Dimroth, 1993).

The ATP synthase from *E. coli* is well studied. The enzyme is a large multisubunit complex with an approximate mass of ~500 kDa, consisting of the water-soluble catalytic F_1 complex and the membrane-embedded F_O complex (Figure 2.6). The subunit composition of the *E. coli* F_1F_O ATP synthase is $\alpha_3\beta_3\gamma\delta\varepsilon ab_2c_{10}$ (Hakulinen *et al*., 2012). The F_1 complex contains 5 subunits in stoichiometry $\alpha_3\beta_3\gamma\delta\varepsilon$ with a total molecular weight of ~350 kDa (Yoshida *et al*., 2001; Walker, 2013). The structures of most F_1 subunits are generally well studied and were obtained to a large extent by using X-ray crystallography (Uhlin *et al*., 1997; Wilkens *et al*., 1997; Wilkens and Capaldi, 1998).

Three catalytic centres of the enzyme are created by the subunits α and β, which together form a spherical hexamer of approximately 100 kDa in size. The three nucleotide-binding sites are located at the interface of α- and β-subunits, which are arranged alternately. The $\alpha_3\beta_3$ subunits closely surround the elongated α-helical structure of the γ subunit, which forms the central stalk of the enzyme. It protrudes ~30Å beyond the F_1 catalytic complex and firmly attaches it to the membrane-embedded F_O domain with the help of subunit ε, which interacts with both the subunit γ and cytoplasmic loops of the c_{10} ring (Gibbons *et al*., 2000). The δ-subunit binds to the N-terminal region of one of the three α-subunits and to the subunit *b*. Together with the membrane subunits ab_2 of the F_O complex it forms a side stalk, which connects F_O and F_1 complexes (von Ballmoos *et al*., 2009).

While the F_1 complex is needed for ATP synthesis, the F_O complex translocates protons across the membrane. In ATP synthase from *E. coli* the F_O complex consists of subunits *a, b* and *c* in stoichiometry $a_1b_2c_{10}$ with a total molecular weight of ~150 kDa. Structures of F_O subunits are generally less studied due to the difficulties with crystallization of membrane proteins.

Subunit *a* is a highly hydrophobic protein with a molecular weight of 30.3 kDa. The structure of subunit *a* is currently not known, and the available data of the structural elements have been obtained by separate studies. For example, extramembranous region (Valiyaveetil and Fillingame, 1998; Long *et al*., 1998) and the periplasmic loops of subunit *a* (Wada, 1999) were studied by cysteine substitution mutagenesis. The protein was described to have 5 membrane-spanning segments (Valiyaveetil and Fillingame, 1998; Vik *et al*., 2005), with the N-terminus being located in the periplasmic space, and the C-terminus being located in the cytoplasm.

Subunit *b* of the ATP synthase from *E. coli* has a molecular weight of 17.3 kDa. The subunit *b* is a dimer, which makes tight connections with subunits α and δ of the F_1 complex and subunits *a* and *c* of the F_O complex, thus functioning as stalk, which holds F_1 and F_O together (Dunn and Chandler, 1998; McLachlin and Dunn, 2000; Rodgers and Capaldi, 1998). The only area in subunit *b,* which doesn't have any connections with other subunits can be referred to as the dimerization domain (residues 55-91) and is located between F_O and the lower surface of F_1. Absence of existing interactions with other domains makes the subunit *b* suitable for constructing heterologous chimeric proteins, which have genes from two different species (Claggett *et al.,* 2007; Suzuki *et al.*, 2007).

Subunit *c* is the smallest in the F_O complex with molecular weight of 8.3 kDa (Jiang *et al*., 2001). Each subunit *c* consists of two transmembrane hairpin-shaped α-helices connected with a short loop. The loop of the *c* subunit was described to form a very rigid structure (Dmitriev and Fillingame, 2007). Both termini of the protein are located in the periplasmic space. A conserved R(Q/N)P motif in the subunit *c* is located in the loop and involved in binding of F_1 complex. Substitution of a single residue in this motif results in uncoupling of F_1 from F_O (Mosher *et al*., 1985). Oligomerized *c* subunits form a structure of an hourglass shape called the rotor ring (Girvin *et al*., 1998; Stock *et al*., 1999). It comes in contact with subunits *a* and *b* of the F_O complex and with subunits γ and ε of the F_1 complex.

The proton translocating residue in the *c*-ring from *E. coli* is D61, which is located in TMH2 at the middle of the lipid bilayer. The Na^+-binding residue in *I. tartaricus* is E65. This residue is highly conserved among F_1F_O ATP synthases and is represented only by negatively charged amino acids. It is usually surrounded by residues, with which it forms a hydrogen

bonding network. The protons enter the translocation pathway via an aqueous accessible channel formed by the THM2 of the subunit *c* and TMH5 of the subunit *a*. The channel extends from the periplasm to the centre of the membrane where protons can access the ion-binding residue (Steed and Fillingame, 2013).

It is known that the electrochemical potential of ions across membranes ($\Delta\mu H^+$ or $\Delta\mu Na^+$) is a motive force for ion translocation. When neutralized conserved glutamate or aspartate residue of the subunit *c* enters the *a/c* interface from the hydrocarbon environment and approaches the positively charged conserved arginine of subunit *a*, the change of pKa of the side chain carboxyl facilitates ion release through the exit channel into the cytoplasm. After ion release, the negatively charged carboxyl of the subunit *c* binds the ion entering from the periplasmic half-channel. This binding promotes further rotation of the protonated subunit *c* through the hydrocarbon core and the cycle repeats. Ion translocation in F_O is coupled to the rotation of the rotor ring, which in turn initiates the rotation of the subunits γ and ε tightly connected to the *c*-ring. The side stalk, which consists of subunits δ, *a* and *b*, prevents rotation of F_1 ($\alpha_3\beta_3$) together with the rotor (von Ballmoos *et al*., 2009). Subunit γ forms a long shaft that transmits the rotational energy to the catalytic subunits α and β, taking each β-subunit through 'open', 'loose' and 'tight' conformations sequentially during the catalytic cycle (Abrahams *et al.*, 1994; Capaldi and Aggeler, 2002; Dimroth *et al*., 2003). Inorganic phosphate and ADP enter the active site when subunit β is in the 'open' state. With change of the rotational position of the subunit γ the catalytic site changes conformation, closing the molecules inside and binding them loosely. During the next state the molecules are bound tightly and are forced together resulting in ATP formation. The enzyme then undergoes transition back to the 'open' state, releasing ATP and binding ADP and phosphate for the next cycle (Walker, 2013).

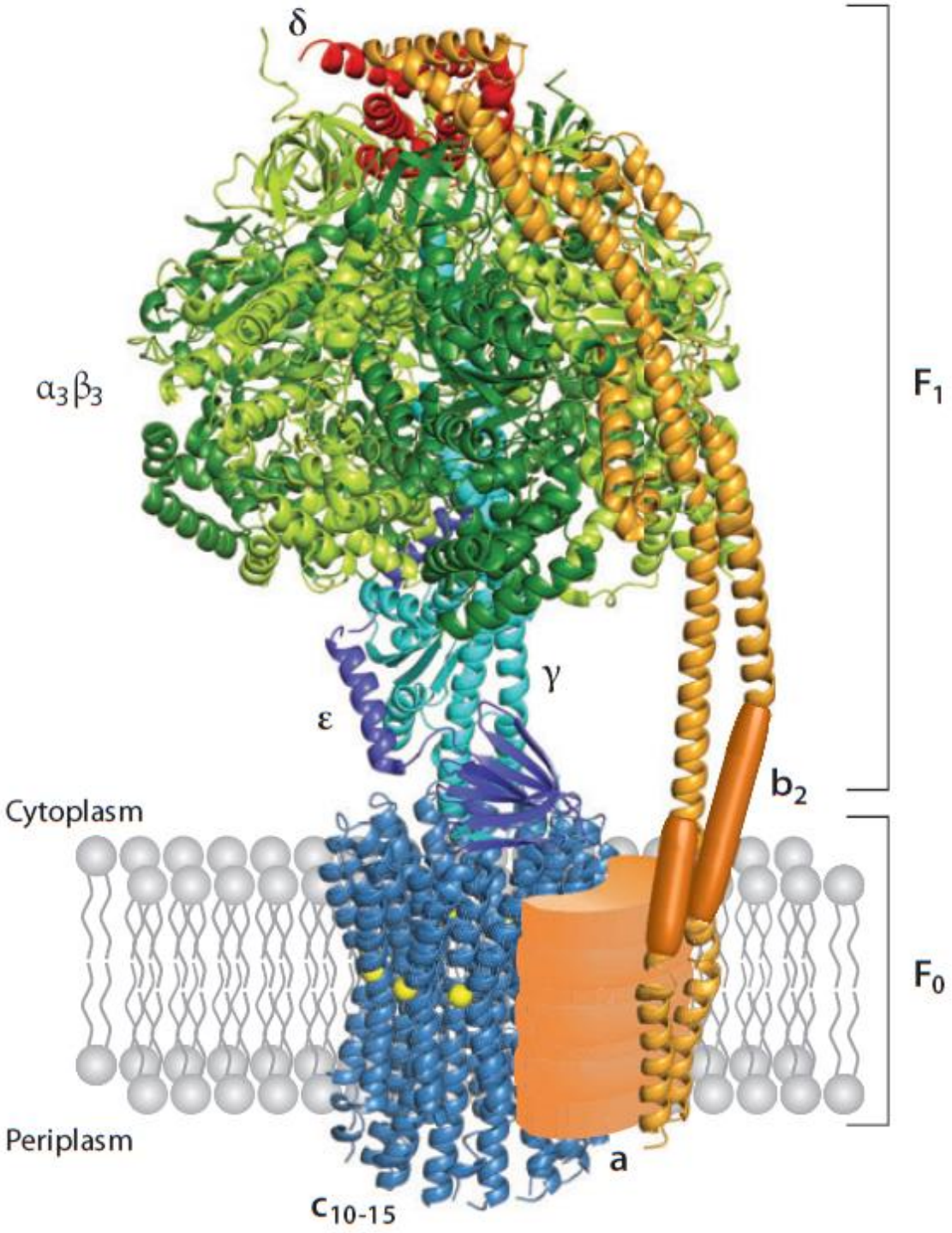

Figure 2.6. Composite representation of ATP synthase and its orientation in the lipid bilayer. Subunits are colored as follows: light green and dark green – subunits α and β, light blue – subunit γ, violet – subunit ε, red – subunit δ, orange – subunit *b*, light orange – subunit *a*, blue – *c*-ring, yellow – proton binding residue (von Ballmoos *et al*., 2009).

2.5. Structure and properties of ATP synthase rotor rings from *E. coli* and *I. tartaricus.*

In order to design a nanopore with desirable properties from the *c*-ring, one has to take into consideration the structure and characteristics of the individual subunits and the protein complex as a whole. The structure of the subunit *c* from *E. coli* was solved by NMR spectroscopy (Girvin *et al*., 1998). Subunit *c* contains 79 amino acid residues. Individual subunits are organized in a cylindrical structure that resembles a membranous pore of a few nanometers in diameter. Each subunit *c* forms a hairpin-like structure with two TMHs connected by a short cytoplasmic loop. In *E. coli* ten transmembrane α-helices surround the central pore of an hourglass shape (Figure 2.7). The N-terminal helix, or TMH1, is located inside the ring, while the C-terminal helix, or TMH2, is located outside (Jones *et al*., 1998). Because the subunit *c* is a substantially hydrophobic protein (Figure 2.8), the internal cavity of the pore is also lined with hydrophobic residues, and apparently filled with lipid. The inner diameter of the *c*-ring from *E. coli* is about 1-1.2 nm (Dmitriev *et al*., 1999). Tight packing and fixed stoichiometry of the subunits makes the overall structure stable and consistent. Such architecture of the ring makes it well suited as a nanopore scaffold.

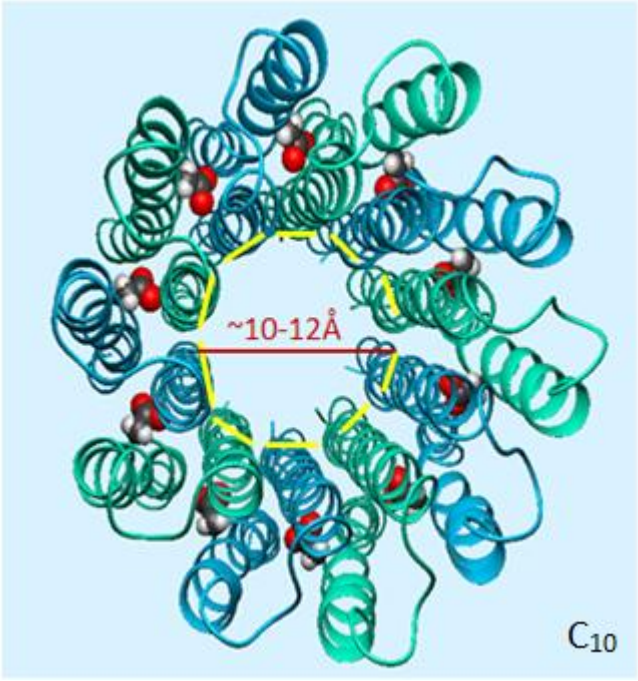

Figure 2.7. Schematic representation of the c_{10} ring from *E. coli*. Estimated internal diameter of the *c*-ring is indicated with red bar. The H^+-binding residue D61 is Van-der-Waals spheres. Subunits are coloured in alternating teal and blue.

I. tartaricus and *P. modestum* are strictly anaerobic gram-negative bacteria, which belong to the *Fusobacterium* branch. It was shown that the c_{11}-rings from *I. tartaricus* and *P. modestum* are very stable, and can resist dissociation by SDS at 100°C for a short period of time (Laubinger and Dimroth, 1988). This property enabled researchers to obtain the structure of the whole C_{11} ring from *I. tartaricus* by using X-ray crystallography at 2.4 Å resolution (Meier *et al.*, 2005). As stability is one of the most desired features of a protein complex for use as a nanopore, the *c*-ring from *I. tartaricus* appears to be a favourable framework for nanopore design.

The amino acid composition of the *c* subunits from *I. tartaricus* and *P. modestum* is very similar (Neumann *at el*., 1998). There are only four different residues: L4, F5, T20 and V63 in *I. tartaricus* correspond to V4, L5, A20 and I63 in *P. modestum*. High resemblance allows using subunits *c* from *I. tartaricus* and *P. modestum* as interchangeable substitutes.

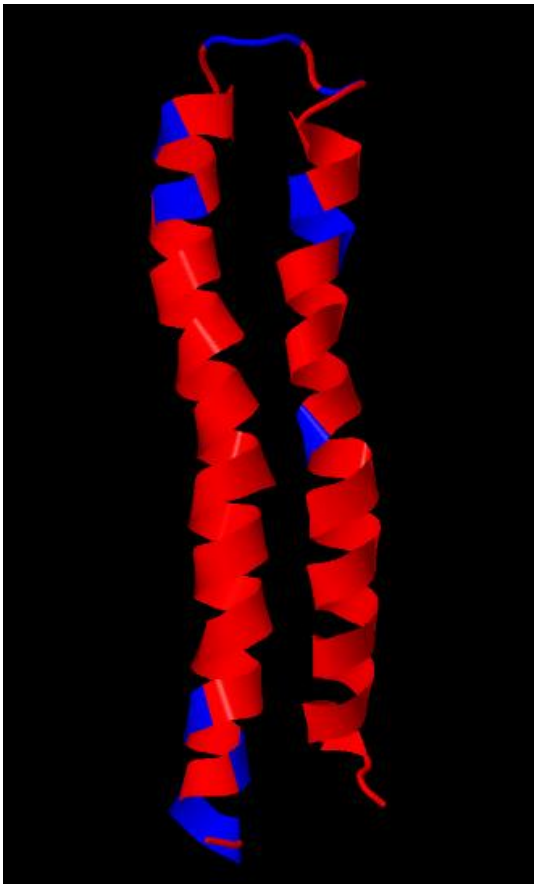

Figure 2.8. Ribbon diagram of the subunit *c* from *E. coli* showing hydrophobic regions in red and hydrophilic regions in blue.

Although this type of the ATP synthase belongs to a Na^+- translocating species, its overall structure resembles one from *E. coli*. The *c*-ring from *I. tartaricus* is an hourglass-shaped membrane protein complex with a height of about 70 Å, and an outer diameter of 40-50 Å (Meier *et al.*, 2005). An electron microscopy study by Vonck *et al.*, 2002 showed that the inner diameter of the undecameric *c*-ring is ~1.7 nm (Figure 2.9).

The structures of the entire *c*-ring from several species were obtained using NMR, X-ray and electron crystallography. All these studies have shown significant variability in the *c*-ring stoichiometry between different species (Watt *et al.*, 2010; Stock *et al.*, 1999; Matthies *et al.*, 2014; Meier *et al.*, 2009; Meier *et al.*, 2006; Preiss *et al.*, 2010; Vollmar *et al.*, 2009; Pogoryelov *et al.*, 2009). The number of *c* subunits per ring varies from 8 to 15 in different species, although it remains constant for a given species (Table 2.1).

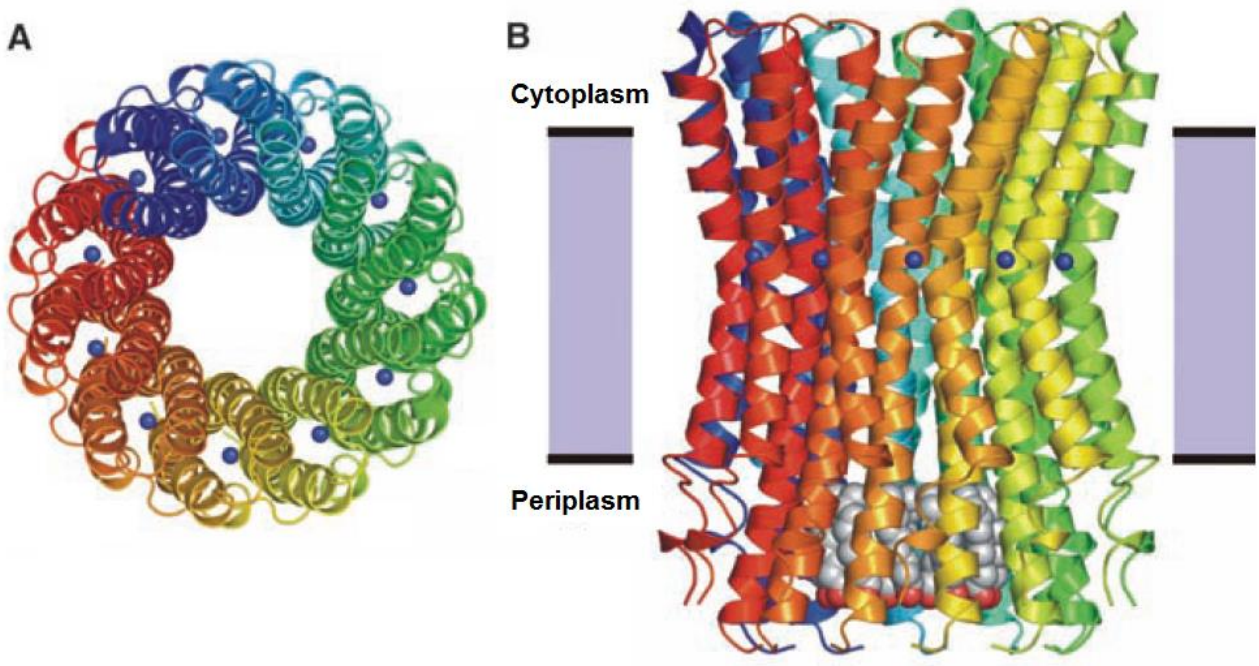

Figure 2.9. Ribbon representation of the c_{11} ring from *I. tartaricus*, individual subunits are shown in different colors. (A) View perpendicular to the membrane from the cytoplasmic side. (B) Side view (From Meier *et al*., 2005. Reprinted with permission from AAAS).

The helix packing motif (GxGxGxG) in TMH1 is responsible for tight transmembrane α-helix packing and ensures constant *c*-ring stoichiometry for a given species. In some species glycine can be partially substituted with bulkier alanine, for example in *E. coli* and *Campylobacter lari* (Steed and Fillingame, 2013). Some species, like the extreme alkaliphile *Bacillus pseudofirmus* OF4 developed a rather unique packing motif AxAxAxA, which is responsible for the C_{13} stoichiometry (Preiss *et al.*, 2013). Structural studies have demonstrated that replacement of the glycine with alanine can increase the number of *c* subunits in the ring (Pogoryelov *et al*., 2012) while alanine-to-glycine changes reduce it (Preiss *et al*., 2013). This implies that the number of *c* subunits in the ring can be altered by introducing mutations in the conserved glycine-rich dimerization motif resulting in *c*-rings of diverse sizes.

One of the most characteristic features of the subunit *c* is the high binding affinity of its H^+/Na^+- binding carboxyl residue to N,N-dicyclohexylcarbodiimide (DCCD). DCCD is a known efficient inhibitor of F_OF_1-ATP synthase, as even a single DCCD molecule is sufficient to block the rotation of the *c*-ring and thus prevent ion translocation across the membrane. In the assembled enzyme, the cyclohexyl groups of DCCD protruding outside from the *c*-ring block its rotation by bumping into subunit *a* (Toei and Noji, 2013). In nanopore design, it may be used as a tool to discriminate between ion translocation through the pore opening and possible ion movement via the ion channel part of a standalone *c*-ring by making the carboxyl residue inaccessible to ions.

Table 2.1. Table of the known *c*-rings, showing number of *c* subunits and the minimal ring diameter, estimated from structural studies (references in the text).

Organism	Number of *c* subunits	Inner diameter
Bos taurus	8	12 Å
Saccharomyces cerevisiae	10	17 Å
Acetobacterium woodii	10	17 Å
Ilyobacter tartaricus	11	17 Å
Clostridium paradoxum	11	17 Å
Bacillus pseudofirmus	13	17 Å
Spinacia oleracea	14	25 Å
Spirulina platensis	15	26 Å

2.6. Membrane insertion and assembly of the membrane subunits of ATP synthase.

Knowledge of protein insertion into the membrane, assembly and adoption of the functional conformation is one of the most important aspects in understanding of the inner membrane proteins biogenesis. However, little is known about assembly of the F_O proteins and their interactions with the F_1 complex to form F_1F_O ATP synthase. For a nanopore design it is important to know whether the *c*-ring can assemble by itself, and which conditions are needed for it to form an assembled pore.

The chaperone-like protein YidC was found to play a crucial role in the biogenesis of chloroplast, mitochondrial and bacterial Sec-independent membrane proteins (de Gier and Luirink, 2003). Several independent studies (Yi *et al*., 2003; van Bloois *et al*., 2004; Van der Laan *et al*., 2004;) confirmed that YidC is strictly required for the membrane insertion of the F_O subunits *in vivo*, even though all of them have a different topology and size (Figure 2.10).

The mechanism of targeting and recognition of the subunit *c* by the YidC chaperone was described recently (Kol *et al*., 2008). Electrostatic interactions of the positively charged residues located at the cytoplasmic loop promote recognition and binding of the subunit *c* and YidC. When bound to subunit *c*, YidC acts as an insertase to assure proper subunit *c* folding into the membrane. A recent study (Kol *et al*., 2006) clarifies the role of YidC in the biogenesis of subunit *c*, which acts only as an insertase and is not responsible for oligomerization, which is a separate process.

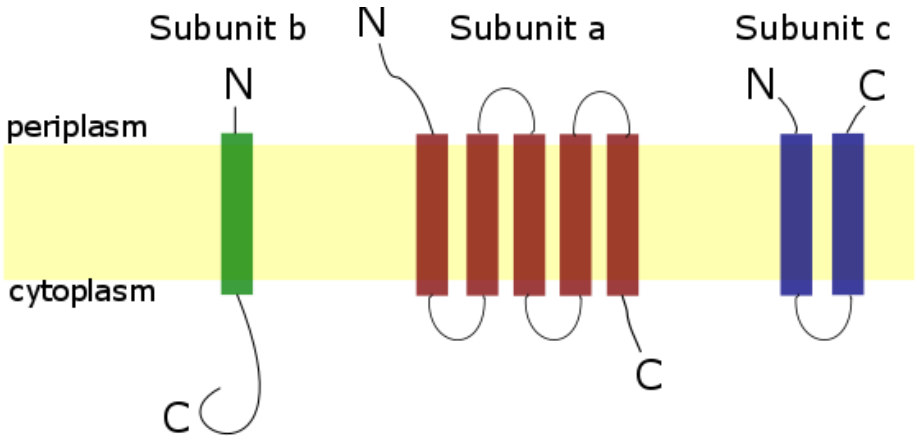

Figure 2.10. Schematic representation of the membrane topology of F_1F_O ATP synthase subunits *a*, *c* and *b*.

The assembly of the *c*-ring of *E. coli in vitro* was demonstrated by Arechaga *et al*., 2002. Overexpressed recombinant subunit *c* was purified in mild detergent solutions and formed annular structures in the absence of other subunits or chaperone molecules. This result suggests that the amino acid sequence determines the ability of the subunit *c* to assemble into the ring. In contrast, in *I. tartaricus* and *P. modestum* a small hydrophobic protein encoded by *atpI* was described to be essential for *c*-ring assembly *in vivo* (Suzuki *et al*., 2007) and *in vitro* (Ozaki *et al*., 2008).

Insertion of subunits *c* and *b* was found to be independent of the presence of the other two subunits of F_O complex. However, incorporation of the subunit *a* into the membrane requires the presence of both subunits *b* and *c* (Hermolin and Fillingame, 1995). It was shown that neither of F_O subunits requires the presence of the proton motive force (PMF) for membrane insertion (Yi *et al*., 2004).

G23D and L31F are naturally occurring mutations, which lead to the formation of a non-functional ATP synthase (Figure 2.11) (Downie *et al*., 1979). They were shown to disrupt assembly of the *c*-ring (Jans *et al*., 1983). The *c* subunit carrying one of these mutations can be used in nanopore experiments as a control for the *c*-ring assembly and incorporation.

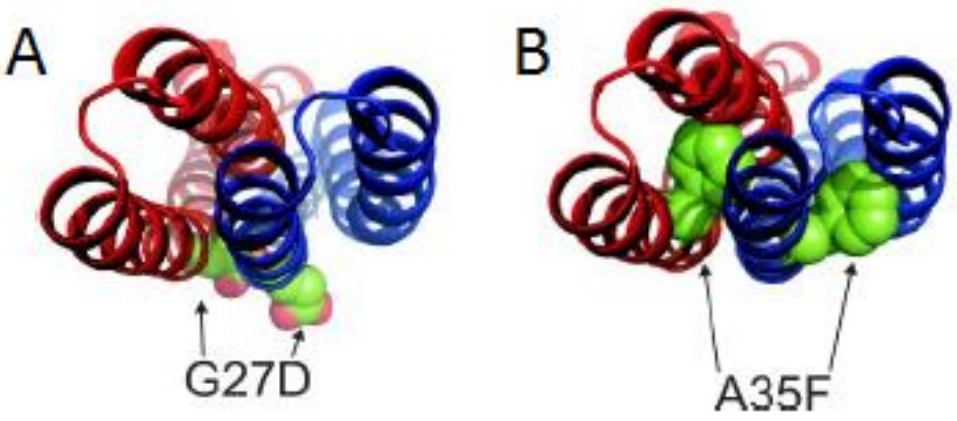

Figure. 2.11. Structural representation of the G27D (A) and A35F (B) mutations in the subunit *c* of the Na^+-ATP synthase from *I. tartaricus*, corresponding to the G23D and L31F in *E. coli*. Individual *c* subunits are coloured in blue and red. Mutated residues are represented as Van der Waals spheres. This research was originally published in Journal of Biological Chemistry (Kol *et al*., 2006).

2.7. Hypothesis and objectives

Our hypothesis is that an engineered pore with a controllable diameter can be created and used for studying a range of molecules of different sizes and it would become an important tool in nanopore analysis, as it could be tuned for every specific application. The main objective of this research is to create a nanopore with a different diameter from α-hemolysin, which would be tunable and stable for several hours in an artificial membrane. The ATP synthase *c*-ring is composed of several *c* subunits. It was chosen as a scaffold for a new nanopore, as it forms stable structures in membranes and can consist of different number of subunits. By changing the number of subunits forming the ring it might be possible to adjust the diameter of a nanopore for various applications.

3. Materials and methods

3.1. Design of a novel protein nanopore

Our goal was to design a stable nanopore with a hydrophilic core using a *c*-ring of ATP synthase as a scaffold. We used the decameric *c*-ring from *E. coli* and undecameric *c*-ring from *I. tartaricus* to achieve this. The amino acid composition of the subunit *c* and its internal cavity, in particular, were shown to be highly hydrophobic. Presumably, the *c*-ring of ATP synthase is filled with lipid (Dmitriev *et al.*, 1999). In order to turn the *c*-ring into a hydrophilic nanopore, its channel should be modified by replacement of residues with aliphatic side chains with residues with polar side chains. We changed both *c*-rings in the same way. The hydrophobic residues facing inside the ring were identified using known protein structures (Figures 2.7 and 2.9). The model of the *E. coli c*-ring was obtained from the monomeric subunit *c* structure and cysteine-cysteine crosslinking studies data by means of molecular dynamics simulation (Dmitriev *et al*., 1999). The structure of the *I. tartaricus c*-ring was solved by X-ray crystallography (Meier *et al*., 2005) and electron crystallography (Vonck *et al*., 2002). We chose serine and asparagine as substituting amino acids because they are hydrophilic and uncharged. Uncharged residues were chosen to avoid ion selectivity. We introduced 6 mutations into the TMH1 of subunit *c* from *E. coli* and 5 mutations into the TMH1 of subunit *c* from *I. tartaricus*. The resulting proteins were named atpES and atpES-IT respectively (atpE is the wild type gene, "S" means "synthetic"). The modifications in the subunit *c* from *E. coli* are shown in Table 3.1 and Figure 3.1. Although the identity of the two protein sequences is only 20.55% and similarity is 31.51%, both structures look alike (Figure 3.2).

Table 3.1. List of mutations introduced in subunits *c* from *E. coli* and *I. tartaricus*

E. coli	***I. tartaricus***
M11N	V9N
V15S	V16N
L19N	I23S
I22N	I26S
I26N	V30N
I30S	

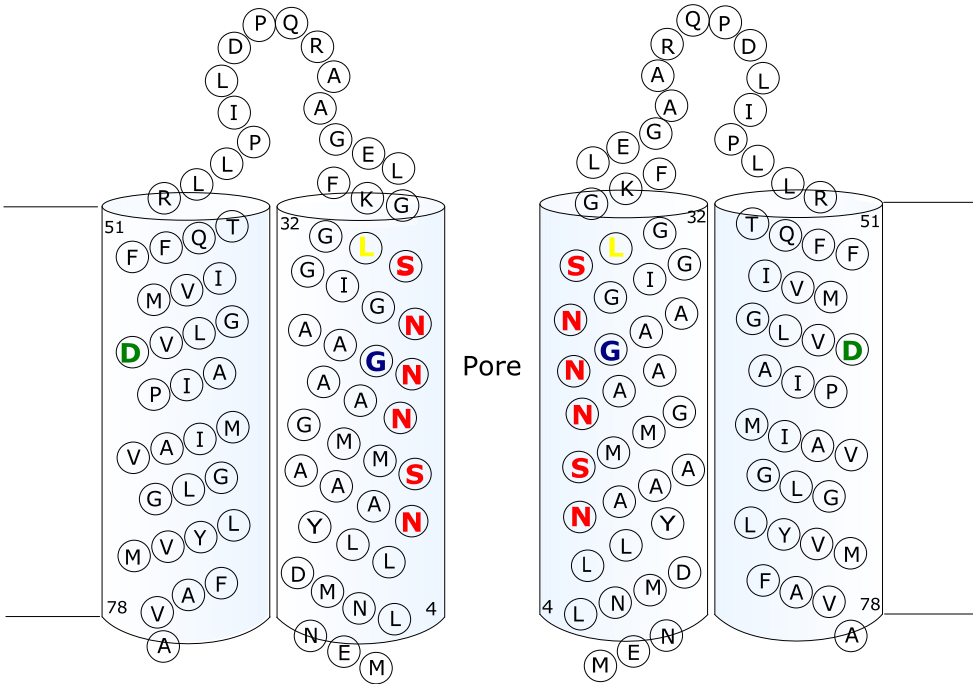

Figure 3.1. Cartoon representation of the nanopore design on the example of atpES from *E. coli*. Two subunits oppose each other in the ring. Substituting amino acids asparagine and serine in the TMH1 are shown in red. Some other amino acid residues discussed in the text are G23 (blue), L31 (yellow), D61 (green).

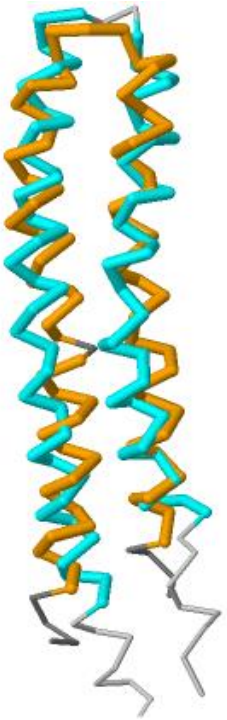

Figure 3.2. Structural alignment of subunit *c* from *E. coli* (orange) and *I. tartaricus* (cyan).

3.2. Molecular biology methods and strain description

Description of strains used in cloning and expression

The *E. coli* BL21(DE3) strain is commercially available (New England Biolabs, Ipswich MA) and is used for overexpression of recombinant proteins. It contains DE3, a λ prophage carrying a gene encoding T7 polymerase. T7 polymerase expression is driven by lac promoter induced by IPTG, while expression of the gene of interest in the expression vector is driven by a strong T7 promoter, and is suppressed until induction by IPTG. The genotype is *fhuA2 [lon] ompT gal (λ DE3) [dcm] Δ*hsdS; *λ DE3 = λ sBamHIo ΔEcoRI-B int::(lacI::PlacUV5::T7gene1) i21 Δnin5*. Plasmids derived from pEXP1-DEST (pDKIE and pDKIES) were cloned into this strain.

The *E. coli* BL21(DE3)star (Invitrogen) is a derivative of BL21 strain with a mutation in *RNAseE*, which makes it less capable of degrading mRNA, resulting in longer half-life for transcripts and enhanced expression levels. It has λ DE3 lysogen, which carries the gene for T7 RNA polymerase under control of the lacUV5 promoter. Expression of the T7 RNA polymerase is induced by IPTG. The genotype is *F- ompT hsdSB (rB-mB-) gal dcm rne131 (DE3)*. Plasmid pNanoΔ4 based on pEXP1-DEST was cloned into this strain for expression analysis.

The *E. coli* OM202 strain has a chromosomal deletion of the entire *atp* operon (Dmitriev, 2004). This strain was a gift from Robert Fillingame and is not commercially available. Plasmids derived from pBWU13 and pBAD102 were cloned into this strain for expression analysis.

The *E. coli* DH5α strain is commercially available (Invitrogen, Burlington ON) and is ideal for cloning and storage of plasmids. DH5a cells have the genotype: F^- Φ80*lac*ZΔM15 Δ(*lac*ZYA-*arg*F) U169 *rec*A1 *end*A1 *hsd*R17 (rK^-, mK^+) *pho*A *sup*E44 λ^- *thi*-1 *gyr*A96 *rel*A1.

Site-directed mutagenesis

Single mutations, deletions and small insertions, like His_6-tag, were introduced into genes using site-directed mutagenesis through the use of specifically designed primers (Figure 3.3). The forward primer has the desired nucleotide change or insertion, with at least 10 complementary nucleotides on the 3′ side of the mutation. The 5′ end of the reverse primer is designed to

anneal back-to-back with 5′ end of the forward primer. The purified PCR product was digested with *Dpn*I to remove the methylated DNA template. Amplified plasmid DNA containing incorporated substitutions or insertions had blunt ends which were ligated.

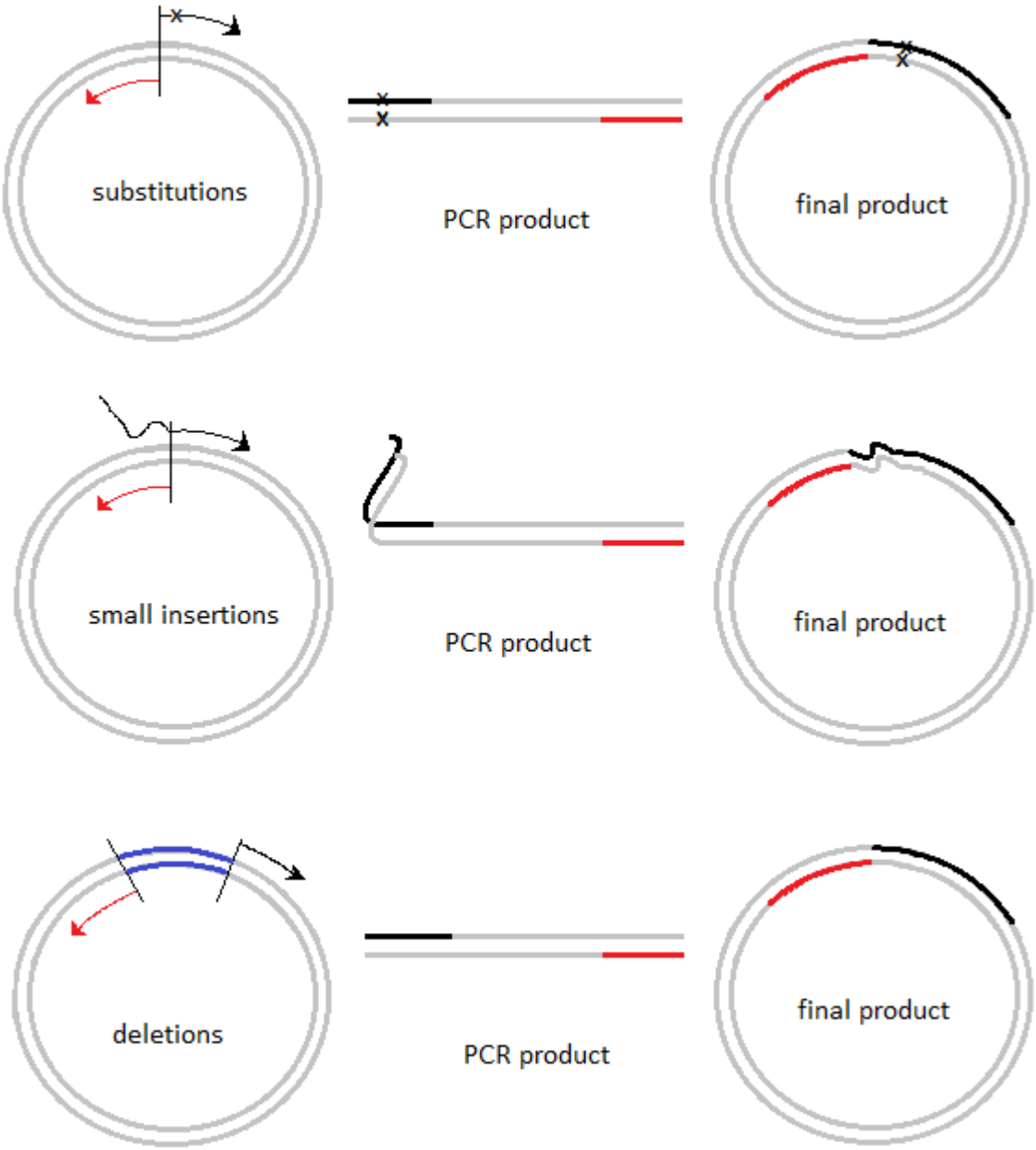

Figure 3.3. Strategies of site-directed mutagenesis to insert, delete and replace genes.

Plasmid preparation

Selection of the mutants was done on LB plates with 100 μg/ml ampicillin. Single colonies were inoculated into 5 mL of liquid LB medium with 100 μg/ml ampicillin, and grown for 16 hours at 37°C with shaking at 220 r.p.m. All plasmids used in the cloning procedure were isolated from liquid *E. coli* cultures using miniprep spin kits (Qiagen, Mississauga, ON). Plasmids were stored at -20°C. Newly constructed plasmids were verified by DNA sequencing (Plant Biotechnology Institute, National Research Council, Saskatoon, Canada, or Eurofins Genomics Company, USA). The DNASTAR Lasergene 8.1 – SeqMan Pro software package was used for data processing.

Restriction, ligation and PCR

All restriction enzymes were purchased from ThermoFisher Scientific (Waltham, MA). Restriction reactions were held at 37°C for 2 hours. T4 DNA ligase (New England Biolabs, Ipswich, MA) was used in ligation reactions, which were held at room temperature for 16 hours. PCR was conducted using Phusion DNA polymerase (Thermo Scientific – Finnzymes, Lafayette, CO).

Transformation of E. coli

Competent cells were prepared using the $CaCl_2$ procedure (Dagert and Ehlrich, 1979). 50 μl of competent cells were added to 2-5 μl of DNA (5-20 ng/μl) and incubated for 45 minutes. Cells were treated with heat shock for 45 seconds at 42 °C, followed by incubation for 10 minutes on ice, and then for 1 hour at 37°C with moderate shaking after addition of 200 μl of LB. The cells were plated on LB agar with ampicillin (100 μg/ml) and incubated at 37°C.

3.3. Generation of plasmids for the expression of subunit *c* variants

Six mutations were introduced into the *atpE* gene encoding the wild type subunit *c* from *E. coli* (Figure 3.1): M11N, A14S, L19N, I22N, I26N, and I30S (prepared previously in Dmitriev lab). The gene had a Histidine tag at the N-terminus and was obtained by chemical synthesis (GenScript, NJ, USA). It was named *His_6-atpES-A14S*. The mutation A14S was introduced by mistake and was corrected by site-directed mutagenesis resulting in *His_6-atpES-*

V15S, which had the intended set of mutations. Both polar versions were tested for expression, but only *His_6-atpES-V15S* was tested for nanopore activity. The *atpES-IT* gene, which differs from the gene encoding the wild type subunit *c* from *I. tartaricus* by five mutations (V9N, V16N, I23S, I26S, and V30N), was also made by chemical synthesis (GenScript, NJ, USA) and had a Histidine tag at the N-terminus, resulting in *His_6-atpES-IT*. Both synthetic genes were cloned in pUC57 plasmid. In bacteria, all the genes encoding the subunits of ATP synthase are grouped in the *atp* operon (Table 3.2).

pBWU13 derived plasmids

The pBWU13 is a plasmid which encodes the whole *atp* operon from *E. coli* and provides resistance to ampicillin (Figure 3.4). This plasmid was used for expressing ATP synthase variants in *E. coli* strain OM202, which lacks the *atp* operon on the chromosome. Mutagenic primers were used to introduce His_6-tag at the N-terminus of the *atpE* gene in pBWU13 following procedure of site-directed mutagenesis resulting in construct pDK7. The *His_6-atpES-A14S* gene was amplified from pUC57 and cloned into pBWU13 using the restriction site for *Nhe*I, replacing wild type *atpE* and producing pDK13. The histidine tag was removed later by site-directed mutagenesis resulting in pDK14.

Table 3.2. The *atp* operon genes and corresponding ATP synthase subunits in *E. coli* and other bacteria.

Genes	**Expression products**
atpI	*i*
atpB	*a*
atpE	*c*
atpF	*b*
atpH	δ
atpA	α
atpG	γ
atpD	β
atpC	ε
Other genes	**Expression products**
atpI-PM	protein *i* from *P. modestum*
atpE-PM	subunit *c* from *P. modestum*
atpES-IT	atpES-IT
atpES-ITopt	atpES-IT
atpES	atpES

During this project, an amino acid sequence error was found in the synthetic *atpES* gene. The gene had A14S mutation instead of the intended V15S. Because of that mistake, previously obtained constructs pDK13 and pDK14 with *atpES* from *E. coli* had to be remade. It was done by site-directed mutagenesis. The constructs pDK13cr and pDK14cr have *atpES* gene with the intended set of mutations. Constructs pDK13S30Icr, pDK13S30Ncr, pDK14S30Icr and pDK14S30Ncr were also made by site-directed mutagenesis using pDK13cr and pDK14cr as templates. They differ from the templates by either isoleucine or asparagine instead of serine in position 30.

To determine the effect of each mutation on the ring assembly (M11N, V15S, L19N, I22N, I26N, I30S), each of them was introduced individually into the *atpE* operon. Mutations were introduced by site-directed mutagenesis. The resulting constructs were named pDKM11N, pDKV15S, pDKL19N, pDKI22N, pDKI26N, pDKI30S and pDKI30T.

We intended to express the atpES-IT *c*-ring in *E. coli*. Previous attempts to express the *atp* operon from *P. modestum* in *E. coli atp* deletion mutant cells were unsuccessful (Gerike *et al.*, 1995). However, the functional chimeric ATPases were created, containing genes of F_O from *P. modestum* and genes of F_1 from *E. coli* (Kaim and Dimroth, 1993), or *Bacillus PS3* (Suzuki *et al.*, 2007). For this reason, we tested expression of the atpES-IT and subunit *c* from *P. modestum* as a part of the chimeric *atp* operon first.

We created chimeric constructs containing the F_1 portion from *E. coli* and the F_O portion from *P. modestum*, with splice points in either the *atpA* (pDK15) or *atpF* (pDKS1) genes. To create pDK15, a fragment containing *atpI*, *atpB, atpE, atpF, atpH*, and the first part of *atpA* gene was amplified by PCR from the pHB plasmid encoding the complete *atp* operon from *P. modestum* and ligated with an amplified fragment of pBWU13, containing the second part of the *atpA, atpG*, *atpD* and *atpC* genes. To create pDKS1, a fragment containing *atpI, atpB, atpE* and a part of the *atpF* gene was amplified by PCR from the pHB plasmid and ligated with an amplified fragment of pBWU13, containing the second part of the *atpF*, *atpH, atpA*, *atpG*, *atpD* and *atpC* genes. Restriction sites for *Nhe*I and *Not*I were introduced into the 3' and 5' ends of PCR products with mutagenic primers. The pDK16 construct differs from pDK15 by substitution of the *atpES-IT* for the *atpE-PM* gene. Gene replacement was done via restriction sites for *Xba*I and *EcoR*V, which were introduced by PCR with mutagenic primers flanking both substi-

tuting and substituted genes. Maps of the plasmids with genes of the chimeric operons are shown in Figure 3.5.

The pDKS2 plasmid (Figure 3.5) was constructed by substituting the *atp* operon of *P. modestum* for the *E. coli atp* operon in pBWU13. The *atp* operon from *P. modestum* and a pBWU13 plasmid without the *atp* operon were amplified with mutagenic primers introducing flanking restriction sites for *Nhe*I and *Not*I, digested with respective enzymes and ligated.

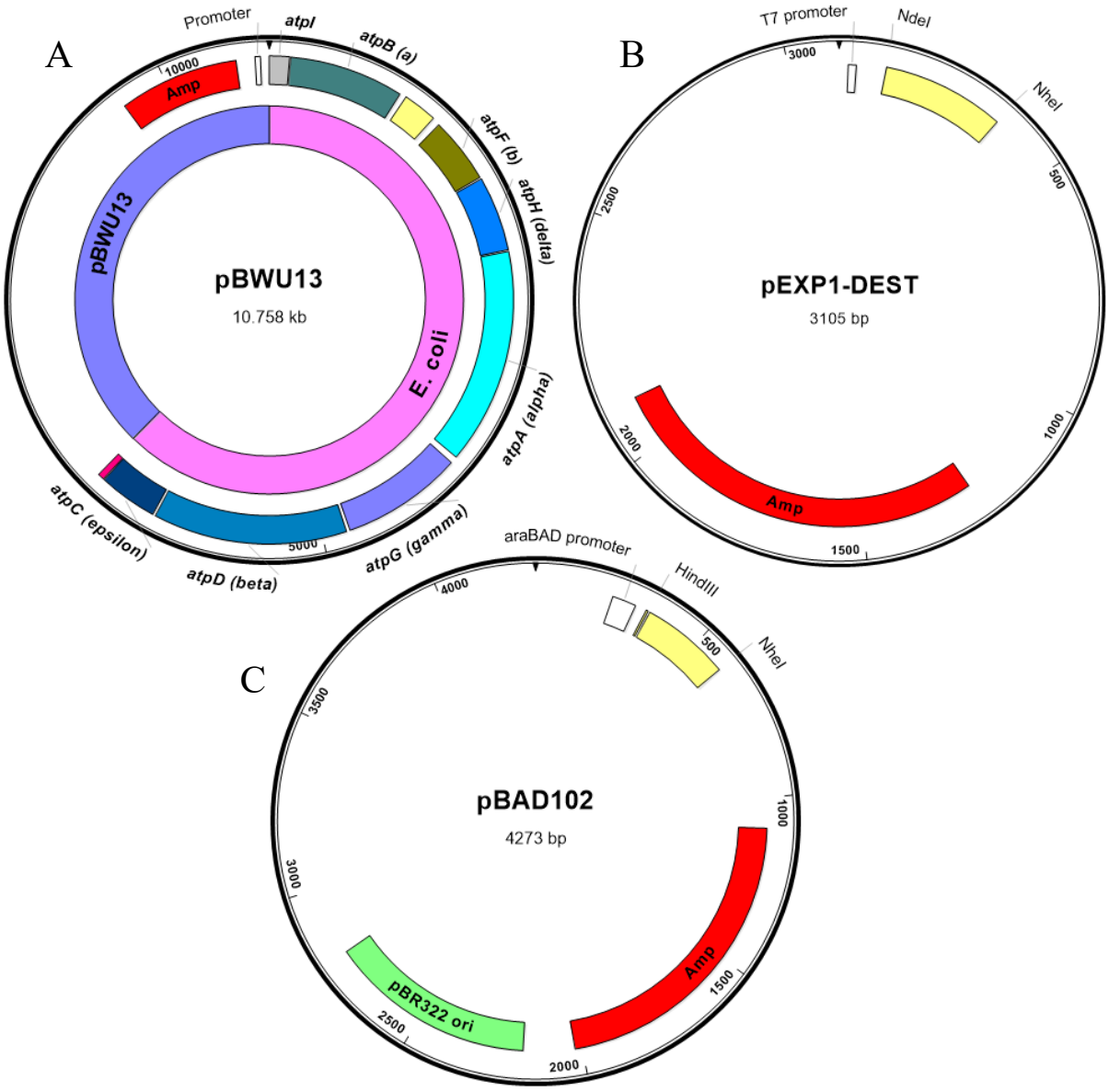

Figure 3.4. Plasmid maps used in cloning. Ampicillin resistance genes are shown in red. Yellow box indicates inserted genes of interest. (A) pBWU13, (B) pEXP1-DEST, (C) pBAD102.

pEXP1-DEST derived plasmids

The plasmid pEXP1-DEST (Invitrogen) is an expression plasmid carrying the T7 promoter (Figure 3.4). The first construct for expression of atpES was created in the Dmitriev lab earlier and contained the pEXP1-DEST vector with the *His_6-atpES-A14S* gene under the control of the T7 promotor – pNanoΔ4. It was transformed into BL21(DE3)star for expression trials.

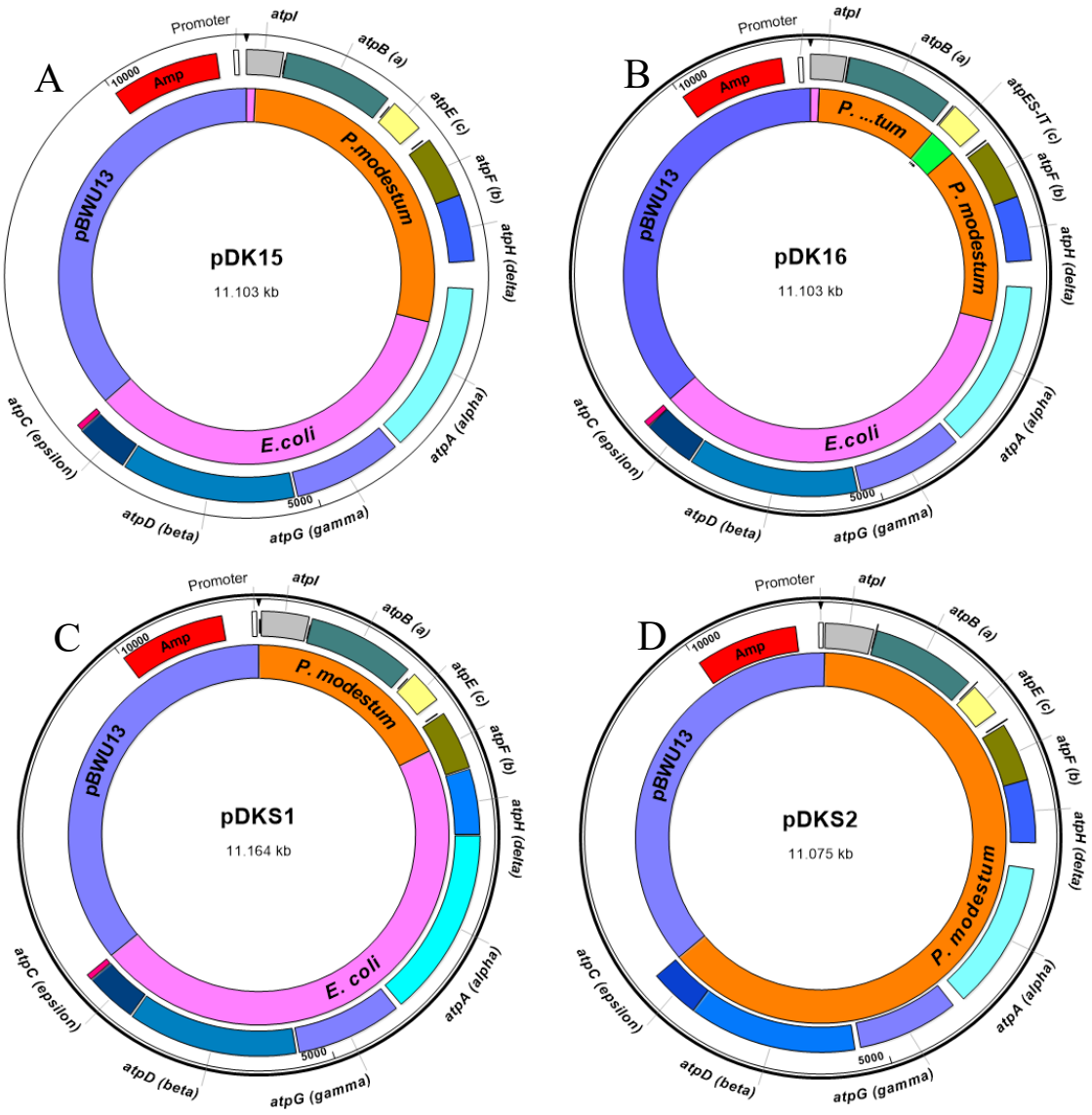

Figure 3.5. Plasmid maps showing the chimeric *atp* operon, containing genes from *E.coli* (magenta) *P. modestum* (orange) and *I. tartaricus* (lime green). (A) pDK15, (B) pDK16, (C) pDKS1, (D) pDKS2.

In order to test expression of the atpES-IT under the control of a strong T7 promoter, genes encoding subunit *c* from *P. modestum* (*atpE-PM*) and a synthetic mutant subunit *c* from *I. tartaricus* (*atpES-IT)* were cloned into pEXP1-DEST with the *atpI* gene upstream. A previously generated construct pNanoΔ4 was used as a template for PCR. Using restriction sites for *Nde*I, *Kpn*I and *Nhe*I, the *His$_6$-atpES-A14S* gene from *E. coli* was replaced with *atpI* and *atpE-PM*, or *atpI* and *atpES-IT*, resulting in constructs *pDKIE* (containing *atpI* and *atpE-PM*) and *pDKIES* (containing *atpI* and *atpES-IT*).

pBAD102 derived plasmids

The plasmid pBAD102 (Invitrogen) is used to express heterologous recombinant proteins in bacteria using L-arabinose as inducer (Figure 3.4). All genes were cloned into pBAD102 plasmid via restriction sites for *Hind*III and *Nhe*I, which were introduced by PCR with mutagenic primers. Constructs based on pBAD102 vector contained His_6-tagged *atpE-PM* or *atpES-IT* following *atpI* from *P. modestum* and were named pDK1H and pDK2H respectively. To test if the *atpI* gene interferes with atpES-IT synthesis, it was deleted from pDK1H and pDK2H, leaving only *atpE-PM* (pDK5) or *atpES-IT* (pDK6) under the control of the *araBAD* promoter. In order to improve translational performance in *E. coli* cells, the sequence of the *atpES-IT* gene was optimised (GenScript USA Inc) for codon usage and GC content. The resulting gene, with a hexahistidine sequence added, *His$_6$-atpES-ITopt* was cloned into the pBAD102, producing pDK9.

The constructs pDK3cr and pDK4cr are also based on the pBAD102 vector and contain the *atpES-V15S* gene with and without the N-terminal hexahistidine tag sequence, respectively. Another pBAD102 derived plasmid, pDK8, contains *His$_6$-atpE.* The mutation G23D was introduced into the *His$_6$-atpE* (pDK8) and *His$_6$-atpES-V15S* (pDK3cr) by site-directed mutagenesis resulting in pDK8-G23D and pDK3cr-G23D. All generated plasmids are listed in Table 3.3.

Table 3.3. List of generated plasmids for expression of subunit *c* variants.

Plasmid Name	Target expression product	Description	Expression organism
pEXP1-DEST derived plasmids			
pNanoΔ4	atpES	Encodes *His_6- atpES-A14S*	BL21(DE3)star
pDKIES	atpES-IT	Encodes *atpI-PM* + *atpES-IT*	BL21(DE3)
pDKIE	Subunit *c* from *P. mod-estum*	Encodes *atpI-PM* + *atpE-PM*	BL21(DE3)
pBWU13 derived plasmids			
pBWU13	Subunit *c* from *E.coli*	Encodes *atp* operon of *E. coli*	OM202
pDK13	atpES	Encodes *atp* operon of *E. coli* with *His_6-atpES-A14S*	OM202
pDK14	atpES	Encodes *atp* operon of *E. coli* with *atpES-A14S*	OM202
pDK13cr	atpES	Encodes *atp* operon of *E. coli* with *His_6-atpES-V15S*	OM202
pDK14cr	atpES	Encodes *atp* operon of *E. coli* with *atpES-V15S*	OM202
pDK13S30Icr	atpES	Encodes *atp* operon of *E. coli* with *His_6-atpES-V15S* with S30I	OM202
pDK13S30Ncr	atpES	Encodes *atp* operon of *E. coli* with *His_6-atpES-V15S* with S30N point mutation	OM202
pDK14S30Icr	atpES	Encodes *atp* operon of *E. coli* with *atpES-V15S* with S30I	OM202
pDK14S30Ncr	atpES	Encodes *atp* operon of *E. coli* with *atpES-V15S* with S30N point mutation	OM202
pDK15	Subunit *c* from *P. mod-estum*	Encodes chimeric *atp* operon *P. modestum/E. coli* with joint in *atpA*	OM202
pDK16	atpES-IT	Encodes chimeric *atp* operon *P. modestum/I. tartaricus/E. coli* with joint in *atpA*	OM202
pDKS1	Subunit *c* from *P. mod-estum*	Encodes chimeric *atp* operon *P. modestum/E. coli* with joint in *atpF*	OM202
pDKS2	Subunit *c* from *P. mod-estum*	Encodes *atp* operon of *P. mod-estum*	OM202
pDK7	Subunit *c* from *E.coli*	Encodes *atp* operon of *E. coli* with *His_6-atpE*	OM202
pDKM11N	Subunit *c* from *E.coli*	Encodes *atp* operon of *E. coli* with point mutation M11N in *atpE*	OM202

pDKV15S	Subunit *c* from *E.coli*	Encodes *atp* operon of *E. coli* with point mutation V15S in *atpE*	OM202
pDKL19N	Subunit *c* from *E.coli*	Encodes *atp* operon of *E. coli* with point mutation L19N in *atpE*	OM202
pDKI22N	Subunit *c* from *E.coli*	Encodes *atp* operon of *E. coli* with point mutation I22N in *atpE*	OM202
pDKI26N	Subunit *c* from *E.coli*	Encodes *atp* operon of *E. coli* with point mutation I26N in *atpE*	OM202
pDKI30S	Subunit *c* from *E.coli*	Encodes *atp* operon of *E. coli* with point mutation I30S in *atpE*	OM202
pDKI30T	Subunit *c* from *E.coli*	Encodes *atp* operon of *E. coli* with point mutation I30T in *atpE*	OM202
pBAD102 derived plasmids			
pDK3cr	atpES	Encodes *His_6-atpES-V15S*	OM202
pDK4cr	atpES	Encodes *atpES-V15S*	OM202
pDK1H	Subunit *c* from *P. mod-estum*	Encodes *atpI* + *His_6-atpE-PM*	OM202
pDK2H	atpES-IT	Encodes *atpI* + *His_6-atpES-IT*	OM202
pDK5	Subunit *c* from *P. mod-estum*	Encodes *His_6-atpE-PM*	OM202
pDK6	atpES-IT	Encodes *His_6-atpES-IT*	OM202
pDK8	Subunit *c* from *E.coli*	Encodes *His_6-atpE*	OM202
pDK9	atpES-IT	Encodes *His_6-atpES-ITopt*	OM202
pDK3cr-G23D	atpES	Encodes *His_6-atpES-V15S* with G23D point mutation	OM202
pDK8-G23D	Subunit *c* from *E.coli*	Encodes *His_6-atpE* with G23D point mutation	OM202

3.4. *E. coli* culture growth and protein expression

Strain BL21(DE3)star expressing atpES from pNanoΔ4 was grown in four different conditions: (i) on M9 minimal medium with 0.4% glucose; (ii) on LB with transfer to M9 before induction; (iii) on LB + 1% glucose with transfer to M9 before induction and (iv) on M9 minimal medium with 0.5% glycerol. Cells were grown at 37°C with shaking at 220 r.p.m. in the presence of 100 μg/ml ampicillin. Induction with 0.5 mM IPTG was done when OD_{600} reached 0.6 after the medium transfer, and growth continued for another 16 hours at 20°C. M9 medium contained 40 mM $Na_2HPO_4 \cdot 7H_2O$, 22 mM KH_2PO_4, 8 mM NaCl, 18 mM NH_4Cl, 2 mM $MgSO_4$, 0.4 % glucose, 0.1 mM $CaCl_2$.

BL21(DE3) cells expressing proteins from pDKIE and pDKIES were grown on LB medium at 37°C with shaking at 220 r.p.m. in the presence of 100 μg/ml ampicillin. Induction with 0.7 mM IPTG was done after 5 min cooling on ice when the OD_{600} reached 0.6. Cell growth continued at 30^{o}C for another 6 hours.

OM202 cells expressing recombinant proteins in the context of the *atp* operon from pBWU13 derived plasmids were grown on LB medium at 37°C with shaking at 220 r.p.m. in the presence of 200 μg/ml ampicillin to late exponential phase.

OM202 cells carrying pBAD102 derived plasmids were grown in LB medium at 37°C with shaking at 220 r.p.m. in the presence of 100 μg/ml ampicillin. Induction with L-arabinose was done when the OD_{600} reached 0.5. Growth continued at 37^{o}C with shaking at 220 r.p.m. for another 4 hours after induction. A range of arabinose concentrations from 0.001% to 1 % was used for screening of the highest subunit *c* expression level. A concentration of 0.1% of L-arabinose was found to produce the largest amounts of the expressed protein.

To analyze expression levels, cells were collected by centrifugation (14,000 g, 5 min) and resuspended in cell lysis buffer (50 mM Tris-HCl (pH 8.0), 1 mM $MgCl_2$, 1 mM PMSF and 1 mM EDTA). The samples with lysed cells for SDS-PAGE were prepared in SDS sample buffer. SDS-PAGE was carried out using 10 % polyacrylamide gels (Schagger and von Jagow, 1987). Protein expression was examined by Western blot analysis of crude cell extracts (antibodies are described in Section 3.15).

3.5. Cell membrane preparation

For membrane preparation, each strain was grown in 2 L of LB medium at 37°C with shaking at 220 r.p.m. to the late exponential phase. Cells were harvested by centrifugation at 6,000 g for 20 minutes and resuspended in TMDG buffer (50 mM Tris-HCl, pH 7.5, 5 mM $MgCl_2$, 1 mM dithiotreitol (DTT), 10% glycerol (v/v), 1 mM phenylmethylsulfonyl fluoride (PMSF), 5 mM *p*-aminobenzamidine-HCl). The homogenized cell suspension was passed through a cell disruptor (Constant Systems, Kennesaw, GA) at 35,000 p.s.i. twice. Cell debris was removed by centrifugation at 6,000 g for 15 minutes. The supernatant was centrifuged at 120,000 g for 75 minutes. The pelleted membranes were resuspended in cold TMDG buffer and ultracentrifugation was repeated. The membrane pellet was resuspended in TMDG buffer, homogenised, freshly frozen in liquid nitrogen and kept at -80°C.

3.6. Isolation of F_1 complex from the cell membranes

Cell membranes were incubated in F_1 stripping buffer (1 mM Tris-HCl, pH 7.5, 0.5 mM EDTA, 10 % v/v glycerol) at a protein concentration of 5 mg/ml for 2 hours at room temperature under moderate shaking, and pelleted at 150,000 g for 1.5 hour. Separated soluble detached F_1 fraction was found in the supernatant.

3.7. Isolation of F_O complex from the cell membranes

F_o complex was isolated essentially as described previously (Schneider and Altendorf, 1984). Birefly, the cell membranes stripped of F_1 were washed in stripping buffer three more times as described (Section 3.7). To solubilize F_O, the membranes were suspended in 50 mM Tris-HCl, pH 8.0, buffer, containing 10% glycerol, 0.1 mM EDTA, 0.1 mM PMSF and 0.1 mM DTT. Ammonium sulfate, sodium cholate and octyl-β-D-glucopyranoside were added slowly and drop wise under constant stirring on ice to the final concentrations of 10% (w/v), 0.5% (w/v) and 1.5% (w/v) respectively. After stirring on ice for 20 minutes and ultracentrifugation for 1 hour at 120,000 g supernatant containing F_O was collected. Protein was fractionated by precipitation with 65% (w/v) ammonium sulfate and incubated on ice for 20 minutes. The solution was then pelleted at 27,000 g for 25 min and the pellet containing F_O was solubilized in buffer (10 mM Tris-HCl, pH 8.0, 150 mM NaCl, 10% Glycerol, 0.2 mM PMSF, 1% Na-

cholate). The isolated F_O fractions were aliquoted, frozen in liquid nitrogen and stored at -80 °C.

3.8. Purification of the *c*-ring by ammonium sulphate precipitation

Purification of subunit *c* from BL21(DE3) and OM202 was done essentially as described (Pogorelov *et al*., 2012, Meier *et al*., 2005). The membrane pellet was solubilized in buffer A (10 mM Tris-HCl, pH 8.0, 5 mM EDTA), containing 1% DDM at room temperature. After centrifugation (200,000 g) for 45 min at 20°C the supernatant was precipitated with 65% (w/v) $(NH_4)_2SO_4$ and incubated for 20 minutes at room temperature. The precipitate was collected by centrifugation at 39,000 g for 20 min and solubilized in buffer A, containing 2% (w/v) N-lauroylsarcosine by incubation at 65 °C for 12 min. After subsequent incubation at 20 °C for 20 min and another round of precipitation with 65% (w/v) $(NH_4)_2SO_4$ and centrifugation, supernatant containing the *c*-subunit was filtered and dialysed against 5 L of 10 mM Tris-HCl, pH 8.0, using a dialysis membrane with the molecular weight cut-off of 3 kDa.

3.9. Purification of subunit *c* variants by LDAO extraction and affinity chromatography

Subunit *c* was purified following the extraction with LDAO, based on a previously described protocol (Arechaga *et al.*, 2002). Harvested cells were suspended in cold 50 mM potassium phosphate buffer, pH 8.0, containing 1 mM DTT and 1 mM PMSF at a ratio 8 ml of buffer per 1 g wet weight cells. The homogenized cell suspension was passed through a cell disruptor (Constant Systems, Kennesaw, GA) at 35,000 p.s.i. twice. Cell debris was removed by centrifugation at 12,000 g for 20 minutes at 4°C. The supernatant was centrifuged at 120,000 g for 70 minutes at 4°C. The membranes were resuspended in cold 20 mM Tris-HCl, pH 8.0, containing 4 mM EDTA (at a protein concentration of 25-30 mg/ml), and ultracentrifugation was repeated. The membranes were resuspended in 20 mM Tris-HCl, pH 8.0, with 300 mM NaCl and 2% LDAO and gently agitated for 1 h at RT. The suspension was pelleted down at 120,000 g for 70 min and supernatant was collected. Ni-NTA agarose (Qiagen, Missisauga, ON) was prewashed with 5 column volumes (CV) of ddH_2O and with 10 CV of the buffer containing 20 mM Tris-HCl, pH 8.0, with 0.3M NaCl and 0.05% LDAO. The supernatant was mixed with Ni-NTA and the mixture was gently agitated for 1 h at RT before it was loaded into a column. The column was eluted by gravity flow. The contaminating proteins were washed with 10 column volumes

(CV) of wash buffer (20 mM Tris-HCl, pH 8.0, 300 mM NaCl, 0.05% LDAO and 35 mM imidazole). The protein was eluted with 5 CV of elution buffer (20 mM Tris-HCl, pH 8.0, 300 mM NaCl, 0.05% LDAO and 150 mM imidazole). All fractions were analysed using SDS-PAGE with subsequent Coomassie staining. Fractions containing the pure protein were pooled, concentrated by centrifugation in an Amicon Ultra-15 concentrator (Merck Millipore Ltd., Ireland) with molecular weight cut-off of 3 kDa and stored in liquid nitrogen.

3.10. Size exclusion chromatography

Size exclusion chromatography was performed using ÄKTA prime system (GE Healthcare, Mississauga, ON). Superdex 75 16/60 column (GE Healthcare, Mississauga, ON) was equilibrated with 1 column volume of 20 mM Tris-HCl, pH 8.0, containing 300 mM NaCl and 0.05% LDAO. The protein sample was eluted at a flow rate of 1 ml/min with 1 column volume of the same buffer, 3 ml per fraction. Collected fractions were analysed with SDS-PAGE and silver staining. Fractions containing the purified protein were pooled, concentrated by centrifugation in VivaSpin concentrator (Sartorius, Göttingen, Germany) with molecular weight cut-off of 3 kDa and stored in liquid nitrogen.

3.11. Proteoliposome preparation

Liposomes were pre-formed using a chloroform solution of 1,2-diphytanoyl-*sn*-glycero-3-phosphocholine (DPhPC) (Avanti polar lipids, Alabaster, AL). Chloroform was evaporated under a gentle stream of argon and the lipid was dissolved in 20 mM phosphate buffer, pH 8.0, containing 2 mM β-mercaptoethanol and 1.5% octylglucoside (w/v), to a final lipid concentration of 25 mg/ml. Dissolved liposomes were dialyzed against 20 mM potassium phosphate, pH 8.0, containing 2 mM β-mercaptoethanol using a 12 - 14 kDa molecular weight cut-off SpectraPor dialysis tubing to remove the detergent. The liposomes were stored in liquid nitrogen until use.

Reconstitution of the nanopore variants into the proteoliposomes was carried out using Bio-Beads SM-2 (BioRad Laboratories Ltd., Mississauga, Ontario). Bio-beads were mixed with 100% MeOH at a 1:7 ratio (w/v) for 15 minutes and then washed with 200 ml of 100% MeOH and 700 ml of ddH_2O. Bio-beads were degassed overnight prior to use. The liposomes made

either from total *E. coli* lipid (Haji, 2012) or 1,2-diphytanoyl-*sn*-glycero-3-phosphocholine (DPhPC) were passed through a mini-extruder (Avanti Polar Lipids) 20 times, using a Whatman polycarbonate membrane (GE Healthcare) with a 100 nm pore size. Purified protein was added to the liposomes at a protein to lipid ratio of 1:25 (w/w) and Triton-X 100 was added to a final concentration of 0.5%. Proteoliposomes were then incubated at 30°C for 15 minutes with moderate shaking. Then pre-treated Bio-Beads in the amount of 10, 10, 20, 20 and 60 mg were added to the liposomes and then removed sequentially every 30 min at 30°C to remove the detergent. Proteoliposomes were dialysed against 10 mM phosphate buffer, pH 8.0, with 1M KCl, using 3 kDa molecular weight cut off SpectraPor dialysis tubing for buffer exchange.

3.12. Test for oxidative phosphorylation by cell growth on succinate

A single colony of an examined strain was streaked onto a plate with M9 minimal medium, containing either 0.6% succinate or 0.6% glucose as a sole source of carbon. Control cells were: F_1F_O-deficient OM202 strain, unable to sustain growth on succinate, and OM202 strain with the pBWU13 plasmid, containing the *atp* operon from *E. coli*, and able to grown on succinate. Growth levels of bacterial cells on succinate and glucose as a control were recorded after 2-3 days of incubation at 37°C.

3.13. ATP dependent proton transport assay

ACMA (9-amino-6-chloro-2-methoxyacridine) fluorescence was used to measure ATP dependent proton transport in membrane vesicles. In the presence of ATP, active ATPase pumps protons inside the vesicles. When uncharged, ACMA can freely move across the membrane, but when it is protonated its positive charge no longer allows it to cross the membrane, resulting in accumulation of ACMA in the vesicles, which is observed by concentration dependent fluorescent quenching.

Isolated membrane vesicles, containing 100 µg total protein, were added to 1 ml of ACMA quench buffer (20 mM Tricine-NaOH, pH 8.0, 10 mM $MgCl_2$, 300 mM KCl). ACMA was added to the reaction mixture to a final concentration of 2 µM. Fluorescence was recorded at 490 nm with excitation at 410 nm. When a stable baseline was reached, proton transport was initiated by addition of ATP to a final concentration of 0.2 mM. To dissipate the proton gradient

across the membrane at the end of the assay as a control, proton uncoupler FCCP (carbonylcyanide-4-(trifluoromethoxy)-phenylhydrazone) was added to the reaction mixture to a final concentration of 2 μM.

3.14. Nanopore experiments

The nanopore experiments were conducted using the patch-clamp instrument, which consists of amplifier (Axopatch 200B), digitizer (Digidata 1322A), Faraday cage (Warner instruments), perfusion unit with electrodes and a personal computer.

The perfusion unit consists of a Teflon perfusion bilayer chamber and a Delrin perfusion bilayer cup. Together they form two 1 ml compartments (*cis* and *trans*). The *trans* compartment includes the measuring electrode with a low-noise integrating headstage, while the *cis* compartment includes the reference electrode. Perfusion units and electrodes are placed inside a Faraday cage to block external electromagnetic noise. The signal from the electrodes is transmitted through the integrating headstage (model CV203BU) to the patch-clamp amplifier, which converts the voltage to current. The signal from the amplifier is then transmitted to the analog-to-digital converter. The patch-clamp instrument is connected to the personal computer with the Clampex 9.2.1.4 software.

The experiment was started by applying a DPhPC/decane solution to the 150 μm aperture of the perfusion cup. After the lipid excess was dried under a stream of nitrogen, both compartments were filled with electrolyte solution (1M KCl in 10 mM potassium phosphate, pH 8.0). Two Ag/AgCl electrodes were placed into each compartment and the electric potential of 100 mV was applied across the perfusion units. A lipid solution in decane was applied with a fine paintbrush over the aperture in the perfusion bilayer cup to form a lipid multilayer. The multilayer was subsequently thinned to a bilayer by removing excess lipid with the paintbrush. The proper membrane thickness for the effective pore incorporation was evaluated by monitoring capacitance values (which should be >12 pF) using Clampex software. Cessation of the electric current through the aperture was another indicator of the formation of a stable lipid bilayer. The proteoliposomes, prepared as previously described, were added to the buffer in the *cis*-chamber in aliquots of 80 μl. After addition of the proteoliposomes, the electric potential

difference was switched to 200 mV. Pore incorporation was observed as a spontaneous change in the recorded current during one hour after addition of the proteoliposomes.

3.15. Analytical methods

Protein concentration was determined by Lowry assay (Lowry *et al*., 1951), with 3 – 60 μg of BSA standard curves.

SDS-PAGE was performed according to Schagger and von Jagow (Schagger and von Jagow, 1987), with 3% stacking and 10% separating gels.

Western blot analysis was performed as described (Towbin *et al*., 1979). A polyvinylidene fluoride membrane (PVDF) was used for protein transfer. The monoclonal anti-pentahistidine HRP conjugate antibody (Qiagen) was used for hexahistidine tag detection at a dilution of 1:5,000. For the detection of subunit *c,* primary polyclonal rabbit anti-*c* antibody (1:60,000, diluted in PBS with 0.1 % Tween-20 and 2 % BSA) and secondary goat anti-rabbit HRP-conjugated antibody (ThermoFisher Scientific, 1:10,000 dilution in PBS with 0.1 % Tween-20) were used.

4. Results

4.1. Effects of mutations in the *c*-ring interior on *E. coli* ATP synthase assembly and function.

The goal of this project was to create a nanopore using a *c*-ring of F_1F_O ATP synthase as a scaffold. We modified the channel of the *c*-ring of *E. coli* and *I. tartaricus* by substituting hydrophobic amino acids with hydrophilic uncharged serine and asparagine. Six mutations were introduced into the *atpE* gene encoding subunit *c* from *E. coli* to engineer atpES protein (performed previously in Dmitriev lab). Two polar versions of subunit *c* were created: atpES-A14S (created by mistake) and atpES-V15S. Both of them have six polar substitutions in the TMH1, with either the A14S or V15S mutation.

Although isolated *c*-rings appear to be stable (Arechaga *et al.*, 2002, Meier *et al.*, 2005), the other Fo subunits may facilitate ring assembly. It is known that the YidC chaperone is required for the membrane insertion of subunit *c* in *E. coli* (Yi *et al.*, 2003, Kol *et al.*, 2006). Also, the 14 kDa hydrophobic protein encoded by the *atpI* gene of the *atp* operon is crucial for *P. modestum c*-ring assembly (Ozaki *et al.*, 2008). Considering this, it would be beneficial to express mutant variants of subunit *c* in the context of the *atp* operon and use a well-established procedure to purify the assembled *c*-ring (Meier *et al.*, 2005).

We employed an ATP synthase deficient strain, OM202, for expressing the polar version of subunit *c* from *E. coli*, atpES, using plasmids based on pBWU13, which encode the entire *atp* operon of *E. coli*. First, we tested expression of the mutant variant atpES-A14S. The plasmids pDK13 and pDK14 had the *atpES-A14S* gene with and without a His_6-tag at the N-terminus respectively. Examination of the atpES-A14S expression was done in comparison with the OM202 strain without a plasmid and OM202/pBWU13 which encodes the *atp* operon with the wild type subunit *c*. No atpES-A14S protein was detected in isolated vesicles using anti-subunit *c* or anti-pentahistidine antibody (Figure 4.1, A and B). The assembly of the ATP synthase was analysed for the presence of the α and β subunits. These are the largest subunits of the F_1 complex with molecular weights of 55.3 kDa and 50.3 kDa respectively (Yoshida *et al.*, 1979). They are water-soluble and can be visualised by using SDS-PAGE followed by Coomassie staining. Normally, presence of the α and β subunits indicates that the ATP synthase is

assembled in cells. In our results the absence of the subunits α and β (Figure 4.1, C) means that atpES interferes with the proper ATP synthase assembly.

As the tested polar version of subunit *c* was not expressed in the context of the *atp* operon, it is likely that one or several introduced mutations had a disruptive effect on the *c*-ring. For this reason we tested each mutation separately for the potential to disrupt *c*-ring assembly in the cell. They were introduced into the *atpE* gene by means of site-directed mutagenesis, and the expression of the mutant subunit *c* variants was done in the context of the *atp* operon in the *E. coli* F_1F_O-deficient strain OM202. The assembly and function of the mutant enzymes was studied by various methods. Assembly of the ATP synthase mutants was evaluated by the presence of subunits α and β of the F_1 complex, analysed by SDS-PAGE followed by Coomassie staining. Both of these subunits were present in cells with ATP synthase carrying mutations M11N, V15S, L19N, I22N and I26N in the subunit *c*. However, mutation I30S caused disruption of the enzyme assembly, as no subunits α and β were detected (Figure 4.2 A).

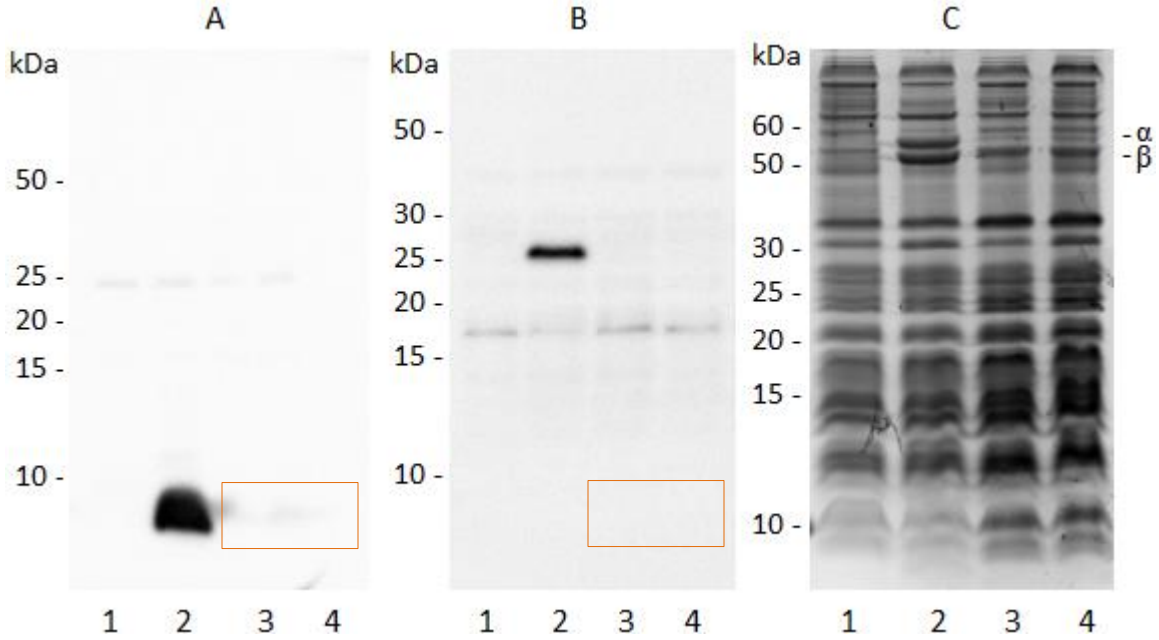

Figure 4.1. Expression test of atpES-A14S in the context of the *atp* operon in the OM202 strain. The samples were analysed by Western blot with polyclonal anti-subunit *c* antibody, 1:60,000 (A), HRP-conjugated anti-pentahistidine antibody, 1:10,000 (B), SDS-PAGE followed by Coomassie staining (C). 1 – negative control OM202, 2 – positive control OM202/pBWU13 with His-tagged subunit *a*, 3 – OM202/pDK13 (N-His_6-atpES-A14S), 4 – OM202/pDK14 (atpES-A14S). The positions of the subunits α and β are shown. Orange rectangles indicate expected positions of the atpES-A14S band.

To examine if the mutants remained active, we tested the ability of cells with the mutant ATP synthase to sustain growth on succinate as a sole source of carbon. The bacterial cells with non-functional ATP synthase fail to grow on succinate as they lose the ability to carry out oxidative phosphorylation. Unlike other mutants, the cells with the I30S mutation in subunit *c* didn't grow on succinate (Table 4.1). These results prompted us to test ATP-dependent active H^+-transport of the mutants by using the ACMA fluorescence quenching assay. Wild type ATP synthase was used as a control and showed a strong response of ACMA fluorescence quenching after the addition of ATP. Mutants L19N, I22N and I26N had activity comparable to the wild type ATPase (Figure 4.3). Mutants M11N and V15S showed approximately half of the activity of the wild type (Figure 4.3). Mutant I30S showed negligible activity, which was consistent with the lack of oxidative phosphorylation activity in this strain (Table 4.1). Our results demonstrated that five of the mutations had no or little effect on the enzyme assembly and function, and one, I30S, had a strongly disruptive effect.

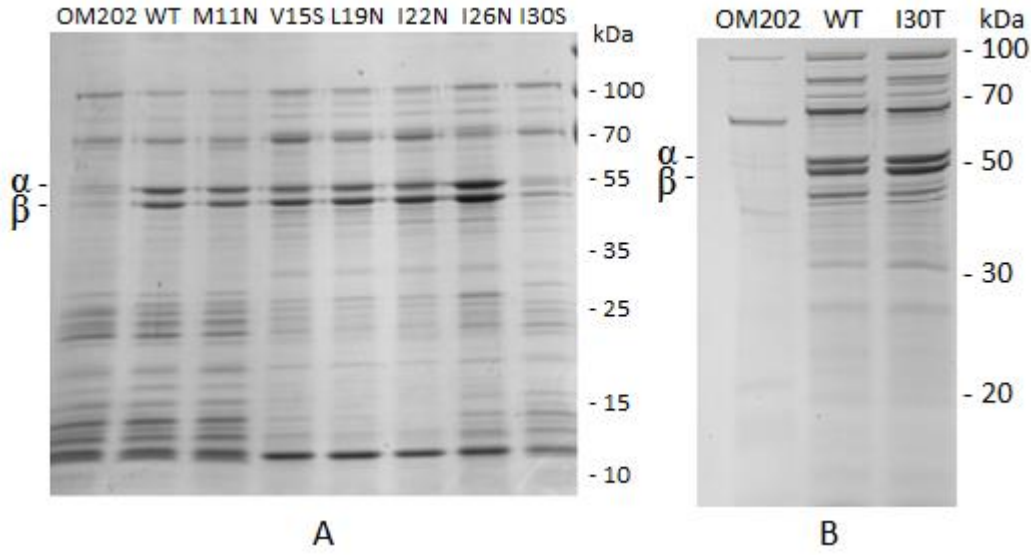

Figure 4.2. Evaluation of the assembly of ATP synthase mutants in the OM202 strain. The F_1 portion was extracted for better visualisation of the α and β subunits. The samples were analysed by SDS-PAGE followed by Coomassie staining. OM202 (no ATP synthase) and OM202/pBWU13 with wild type (WT) ATP synthase were negative and positive controls respectively. The positions of subunits α and β are shown on the left. Each lane is labelled with the mutation introduced in subunit *c*.

Table 4.1. Test for oxidative phosphorylation by cell growth on succinate. The bacterial growth was examined after 72 hours at 37°C on minimal media agar plates containing 0.6% succinate or 0.6% glucose as a positive control.

Construct name	Growth on glucose	Growth on succinate
no plasmid	+	-
wild type *E. coli* ATP synthase	+	+
M11N	+	+
V15S	+	+
L19N	+	+
I22N	+	+
I26N	+	+
I30S	+	-
I30T	+	+

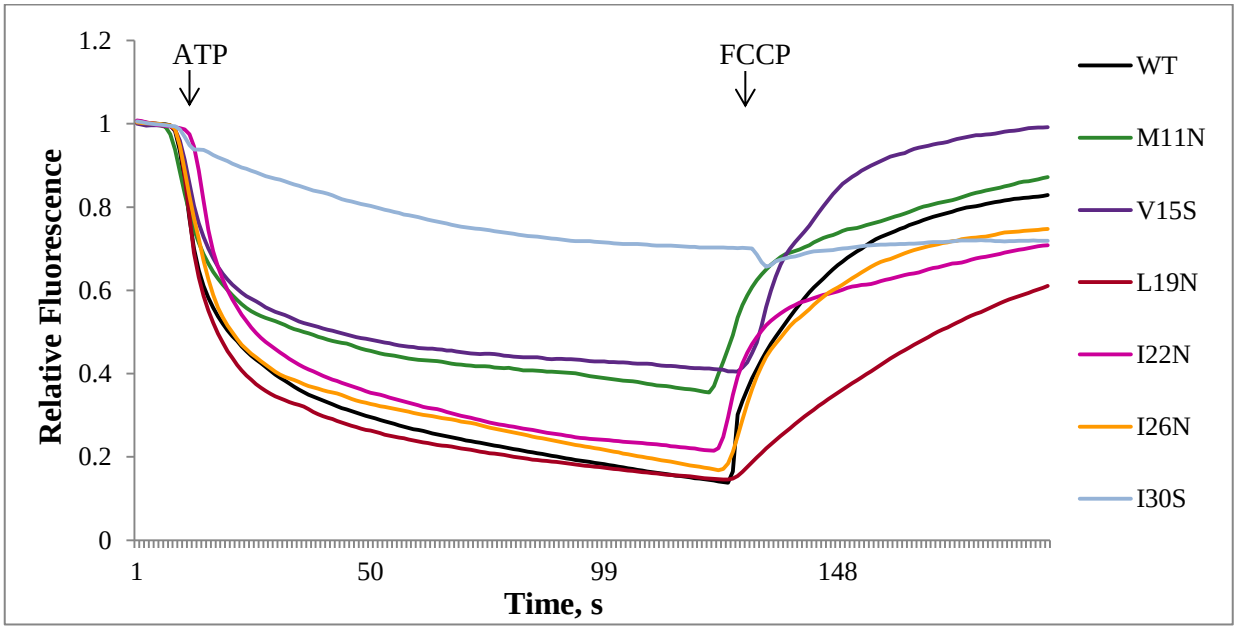

Figure 4.3. ATP-dependent active H^+ - transport measured by ACMA fluorescence quenching. Six constructs with single mutations were tested for the ATPase activity. Wild type ATP synthase was used as a control.

Because the mutation I30S in subunit *c* wasn't tolerated as well as the other mutations and led to disruption of enzyme assembly *in vivo*, we tested threonine as an alternative substitute for isoleucine at position 30; threonine is similar to isoleucine and has a β-branched side-chain. To examine the effect of the I30T mutation on ATP synthase assembly, the F_1 fraction was extracted from the membranes and analysed by SDS-PAGE. Normal levels of α and β subunits of ATP synthase were detected in the strain expressing the I30T variant of subunit *c* (Figure 4.2 B), indicating proper enzyme assembly. The I30T mutant showed normal growth on succinate, indicating that the cells had a functioning ATP synthase (Table 4.1). ATP-dependent H^+-transport in the membranes from the OM202 strain, OM202 with wild type ATP synthase and the I30T mutant cells was measured by ACMA fluorescence to estimate activity of the mutant enzyme (Figure 4.4). The I30T mutant had H^+-transport activity comparable to the wild type ATP synthase. This result is consistent with the ability of the mutant cells to grow on succinate by oxidative phosphorylation. We conclude from these results that the I30T mutation does not cause any major conformational changes in the protein and can be used in further pore optimization instead of I30S.

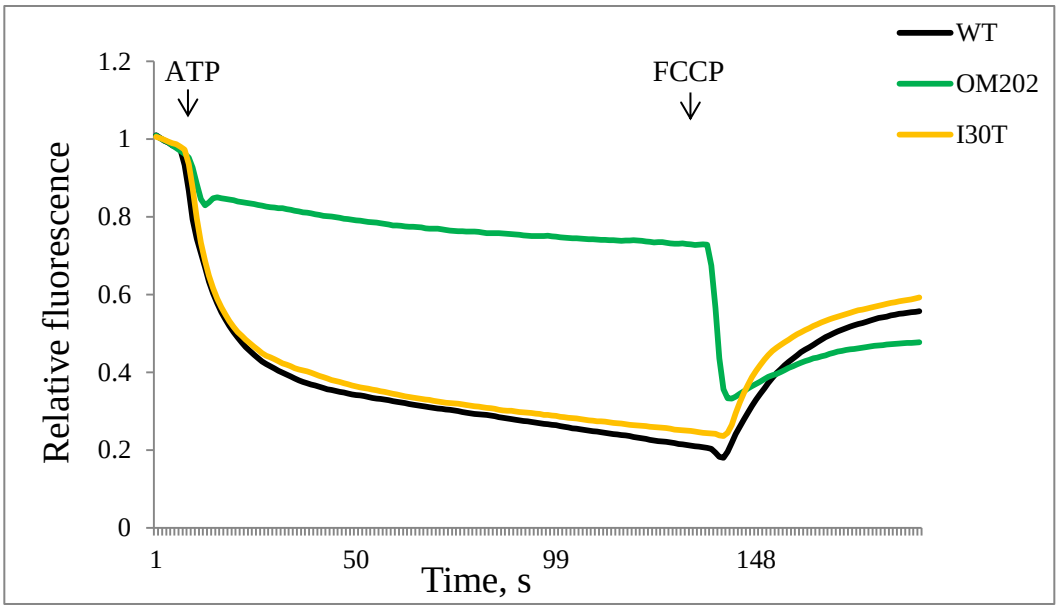

Figure 4.4. ATP-dependent active H^+ - transport of I30T ATP synthase in comparison with WT ATP synthase as a positive control and OM202 without a plasmid as a negative control, measured by ACMA fluorescence quenching.

4.2. Expression of subunit *c* variants in the context of the complete *atp* operon.

Previously we found that the mutation I30S disrupts enzyme assembly (Section 4.1). In order to prevent the disruptive effect of I30S on the *c*-ring assembly and incorporation, we reintroduced isoleucine at position 30 in atpES-V15S mutant variant, so only 5 mutations were left in the *atpES* gene. This protein was tested with and without a histidine-tag at the N-terminus (His_6-I30-atpES-V15S and I30-atpES-V15S). In another variant, we changed I30 to asparagine to test a different polar substitution at this position, resulting in His_6-I30N-atpES-V15S and I30N-atpES-V15S. As above, we tested expression of the mutants in comparison with the background strain OM202 and OM202/pBWU13. We found that although subunits α and β were present, no subunit *c* was detected with polyclonal anti-subunit *c* antibody (Figure 4.5). The test for oxidative phosphorylation showed that all the ATP synthases with atpES variants were non-functional and didn't grow on succinate (Table 4.2).

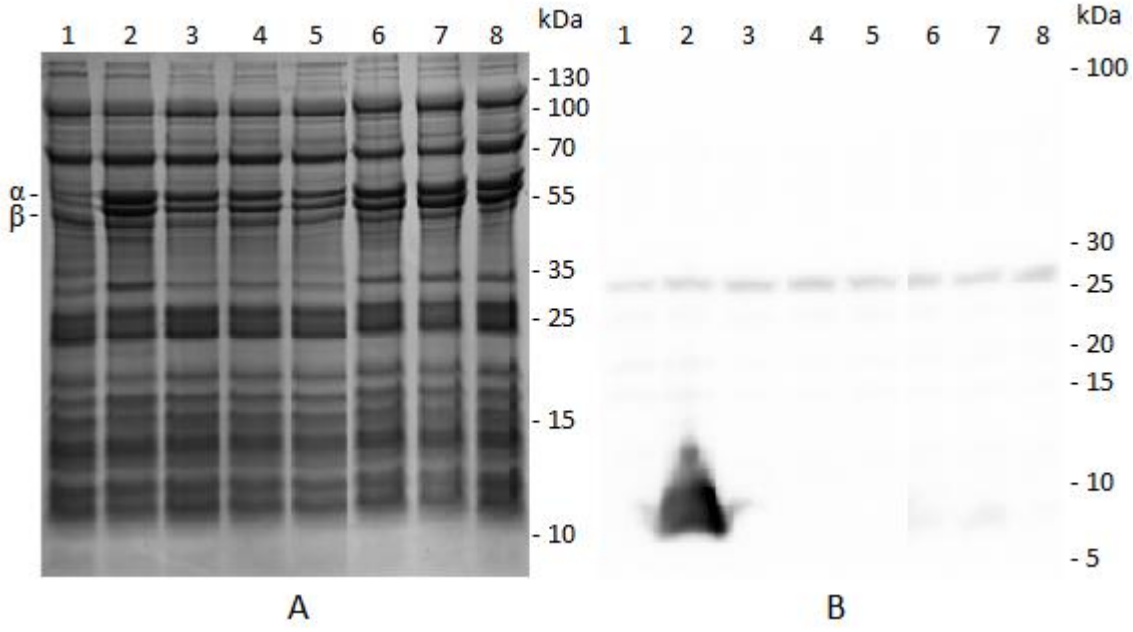

Figure 4.5. Test of the expression of ATP synthases with atpES-V15S variants in OM202 strain. F_1 was extracted for better visualisation of α and β subunits. The samples were analysed by SDS-PAGE followed by Coomassie staining (A) and Western blot with polyclonal anti-subunit *c* antibody, 1:60,000 (B). 1 – OM202, no plasmid; 2 – OM202/pBWU13 (wild type *E. coli* ATP synthase); 3 – OM202/pDK13cr (His_6-atpES-V15S); 4 – OM202/pDK13S30Icr (His_6-I30-atpES-V15S); 5 – OM202/pDK13S30Ncr (His_6-I30N-atpES-V15S); 6 - OM202/pDK14cr (atpES-V15S); 7 –OM202/pDK14S30Icr (I30-atpES-V15S); 8 - OM202/pDK14S30Ncr (I30N-atpES-V15S). The positions of the subunit α and β are shown.

The activity measurements using the ACMA fluorescence quenching assay confirmed that the mutant enzymes were non-functional (Figures 4.6 and 4.7).

Summarizing the data described above, the tested ATP synthases with mutant atpES-V15S have subunits of the F_1 complex but lack subunits of the F_O complex, and they were inactive, as expected. A seeming contradiction in our results – the presence of subunits α and β, and absence of subunit *c* – prompted us to isolate and analyse the F_O fraction of the mutant enzymes more thoroughly. Only variants without the His_6-tag were examined. The results presented in Figure 4.8 show that all mutant ATP synthases have subunit *b* but lack subunits *a* and *c*. This means that mutant ATP synthases are present in cells in an incompletely assembled form. Apparently, multiple mutations in subunit *c* disrupt assembly of the *c*-ring and prevent formation of the F_O complex, resulting in incomplete enzyme assembly. These results can be explained by the cumulative effect of introduced mutations, which interfere with the association of subunits *a* and *c*. The result also indicates that it is impossible to synthesize polar variants of subunit *c* as a part of the *atp* operon in OM202 cells.

Table 4.2. Test for oxidative phosphorylation by cell growth on succinate. The bacterial growth was examined after 72 hours at 37°C on minimal media agar plates containing 0.6% succinate or 0.6% glucose as a positive control.

Construct name	Growth on glucose	Growth on succinate
OM202, no plasmid	+	-
OM202/pBWU13 (wild type *E. coli* ATP synthase)	+	+
OM202/pDK13cr (His_6-atpES-V15S)	+	-
OM202/pDK13S30Icr (His_6-I30-atpES-V15S)	+	-
OM202/pDK13S30Ncr (His_6-I30N-atpES-V15S)	+	-
OM202/pDK14cr (atpES-V15S)	+	-
OM202/pDK14S30Icr (I30-atpES-V15S)	+	-
OM202/pDK14S30Ncr (I30N-atpES-V15S)	+	-

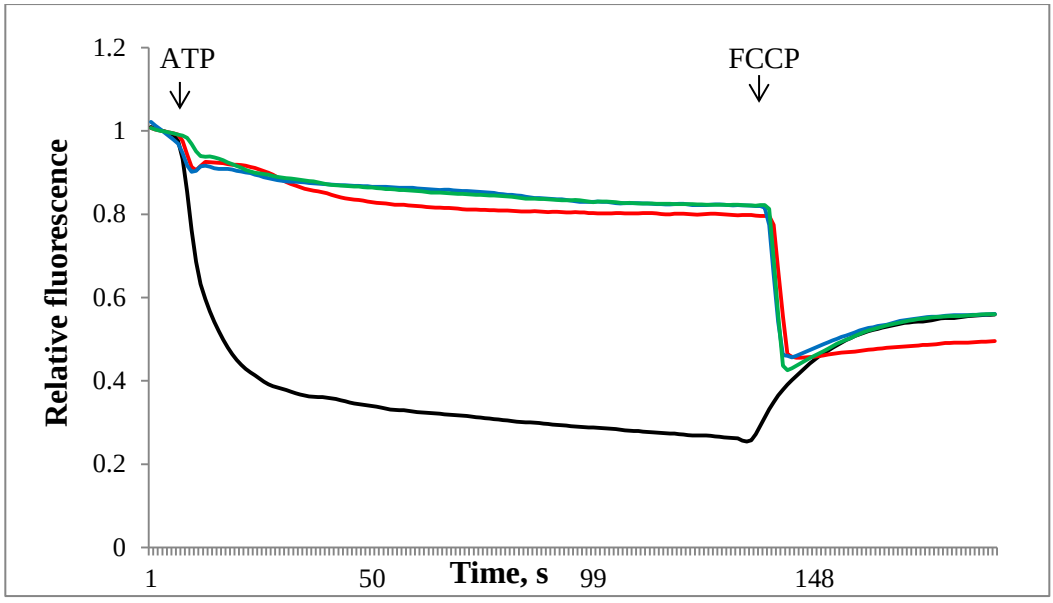

Figure 4.6. ATP-dependent active proton transport of 3 His-tagged subunit *c* mutants of ATP synthases and wild type ATP synthase, measured by ACMA fluorescence quenching. Black line indicates OM202/pBWU13 (wild type ATP synthase), red line – OM202/pDK13cr (His_6-atpES-V15S), blue line – OM202/pDK13S30Icr (His_6-I30-atpES-V15S), green line – OM202/pDK13S30Ncr (His_6-I30N-atpES-V15S).

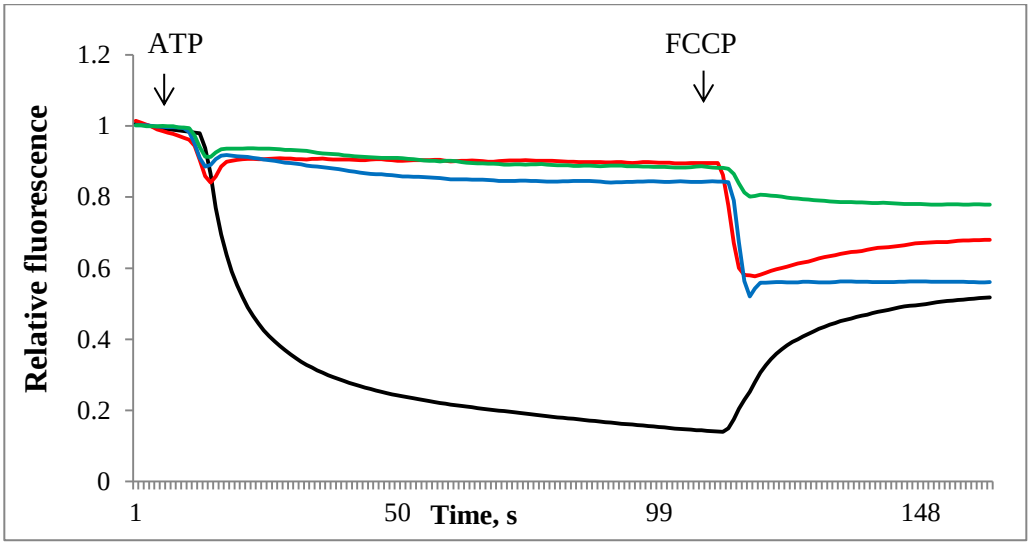

Figure 4.7. ATP-dependent active proton transport of 3 subunit *c* mutants of ATP synthases and wild type ATP synthase, measured by ACMA fluorescence quenching. Black line indicates OM202/pBWU13 (wild type ATP synthase), red line – OM202/pDK14cr (atpES-V15S), blue line – OM202/pDK14S30Icr (I30-atpES-V15S), green line – OM202/pDK14S30Ncr (I30N-atpES-V15S).

Expression of the polar version of subunit *c* from *I. tartaricus*, atpES-IT, was also tested in the context of the *atp* operon. We chose *I. tartaricus c*-ring as a scaffold for a nanopore because it forms a remarkably stable complex which can resist boiling in SDS for several minutes (Laubinger and Dimroth, 1987, Meier *et al.*, 2003) and can be purified as an entire *c*-ring (Meier *et al.*, 2005). The high resolution structure of the *I. tartaricus c*-ring is available (Meier *et al.*, 2005). Like the *c*-ring of *P. modestum*, it consists of 11 subunits made up of tightly packed pairs of membrane-spanning α-helices of a hairpin shape, connected by a short cytoplasmic loop.

Previously it was shown that *E. coli* doesn't express the *atp* operon from *P. modestum* or *I. tartaricus* (Gerike *et al.*, 1995), but fully assembled and active chimeras were obtained and characterized (Kaim and Dimroth, 1993; Suzuki *et al.*, 2007). We attempted to reconstruct the described chimeras using the pBWU13 plasmid with genes of the *atp* operon from *E. coli* and the OM202 strain. Two of the chimeric ATP synthases combined the F_1 complex from *E. coli* with the F_O complex from *P. modestum* with the gene splicing either in *atpA* (subunit *α*) or *atpF*

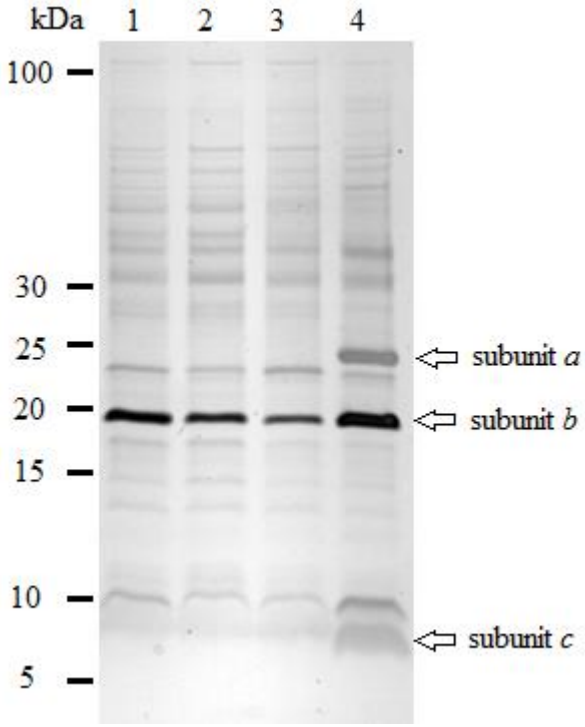

Figure 4.8. Purified F_O fraction from mutant ATP synthase mutants and wild type ATP synthase expressed in the OM202 strain. The samples were analysed by SDS-PAGE followed by silver staining. 1 – OM202/pDK14cr, 2 - OM202/pDK14S30Icr, 3 - OM202/pDK14S30Ncr, 4 – OM202/pBWU13 (wild type ATP synthase). The positions of the subunits *a*, *b* and *c* are shown.

(subunit *b*) (Figure 3.4) resulting in pDK15 and pDKS1 respectively. Subunit *c* from *I. tartaricus* can be substituted for the wild type *P. modestum* subunit *c*, as they share 95% sequence similarity and differ by only 4 amino acids: L4V, F5L, T20A and V63I. The third chimeric ATP synthase contained the F_1 complex from *E. coli,* spliced with the F_O complex from *P. modestum* in *atpA*, and *atpES-IT* substituted for the *atpE-PM* (pDK16). The construct with the complete *atp* operon of *P. modestum* in pBWU13 plasmid was created as well (pDKS2).

We tested expression of the chimeras by analysing the ATP synthase assembly. The F_1 fraction was extracted from the membranes for better visualisation of subunits α and β. Subunits α and β were absent in all chimeric constructs and the untransformed OM202 strain (negative control), but present in pBWU13/OM202 expressing ATP synthase from *E. coli* (positive control) (Figure 4.9).

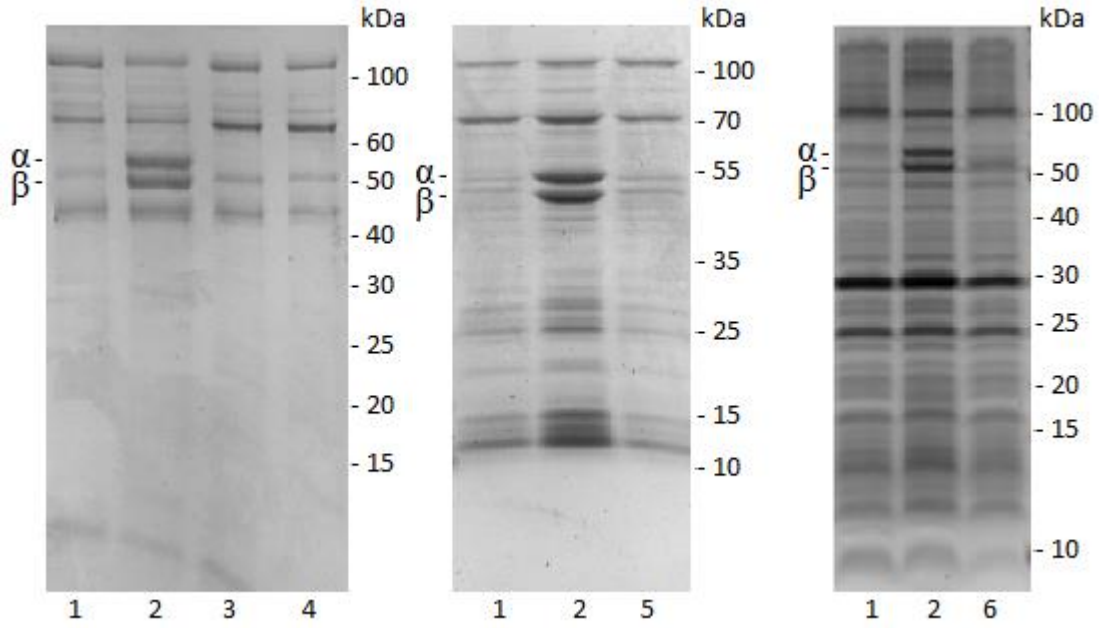

Figure 4.9. Evaluation of assembly of chimeric ATP synthase mutants in the OM202 strain. The F_1 portion was extracted from the membrane for better visualisation of the α and β subunits. The samples were analysed by SDS-PAGE followed by Coomassie staining. 1 – OM202 strain, no plasmid, 2 – OM202/pBWU13 (wild type ATP synthase), 3 – OM202/pDK15, 4 – OM202/pDK16, 5 – OM202/pDKS1, 6 – OM202/pDKS2. The positions of subunits α and β are shown.

Table 4.3. Test for oxidative phosphorylation by cell growth on succinate. The bacterial growth was examined after 72 hours at 37°C on minimal media agar plates containing 0.6% succinate or 0.6% glucose as a positive control.

Construct name	Growth on glucose	Growth on succinate
OM202, no plasmid	+	-
OM202/pBWU13 (wild type *E. coli* ATP synthase)	+	+
OM202/pDK15	+	-
OM202/pDK16	+	-
OM202/pDKS1	+	-
OM202/pDKS2	+	-

The test for oxidative phosphorylation showed that chimeric constructs and the OM202 strain without a plasmid were unable to support growth on succinate as a sole source of carbon, indicating that ATP synthase is either non-functional or absent in these cells. The control OM202/pBWU13 cells sustained a good growth on succinate (Table 4.3).

We conclude from our results that chimeric ATP synthases and the *atp* operon from *P. modestum* were not expressed in pBWU13 based plasmids in the F_1F_O-deficient OM202 strain. Because atpES-A14V was not expressed in the context of the *atp* operon either, a different expression system was developed and tested, which included expression of a single or a pair of genes under the control of an inducible promoter in a different plasmid.

4.3. Expression of subunit *c* variants under the control of T7 promoter.

Previously our attempts to express the polar version of subunit *c* from *E. coli* in the context of the *atp* operon were unsuccessful due to the cumulative effect of several mutations (Section 4.2). Expression experiments of the polar version of subunit *c* from *E. coli* with 6 mutations including A14S, His_6-atpES-A14S, were carried out using pEXP1-DEST based expression plasmid pNanoΔ4, previously constructed in Dmitriev lab, under the control of the T7 promoter in BL21(DE3)star. Four different conditions were screened for the best expression levels of the

atpES-A14S protein: M9 minimal medium containing 0.4% glucose, LB with transfer to M9 before induction, LB containing 1% glucose with transfer to M9 before induction and M9 minimal medium containing 0.5% glycerol.

The His_6-atpES-A14S protein in the crude cell extract was visualised by using anti-pentahistidine antibody. The expression was analysed before and after induction with IPTG. Good levels of the protein expression were observed initially (Figure 4.10). The amounts of the His_6-atpES-A14S were similar before and after induction in all tested conditions. M9 minimal medium containing 0.4% glucose was chosen for further optimisation of the His_6-atpES-A14S expression.

Despite our attempts to optimize expression of the target protein, the overall decrease of His_6-atpES-A14S expression was observed in our subsequent experiments. We examined and compared protein amounts in crude cell extract before induction and every hour after induction. His-tagged subunit *a* from pBWU13 in the *atp*-deficient OM202 strain was used as a control because this plasmid constitutively expresses ATP synthase (Figure 4.11).

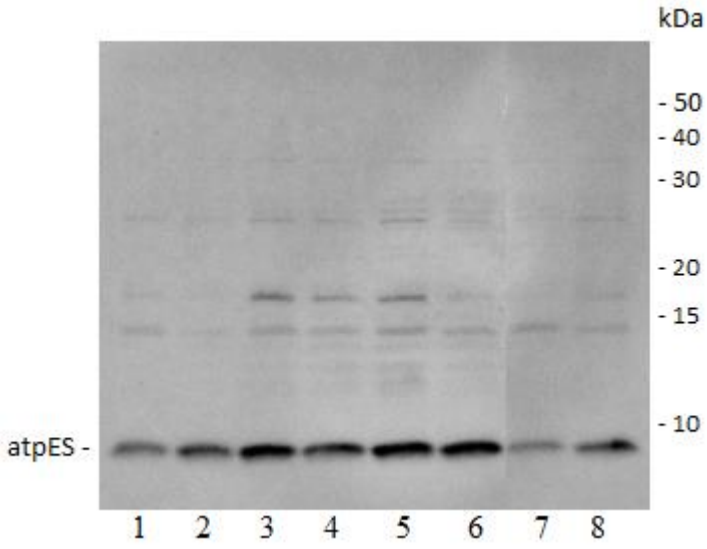

Figure 4.10. Expression of His_6-atpES-A14S in BL21(DE3)star under different conditions. The samples were analysed by Western blot with HRP-conjugated anti-pentahistidine antibodies, 1:5,000. 1 - M9 + 0.4% glucose, before induction, 2 – M9 + 0.4% glucose, after induction, 3 – LB/M9, before induction, 4 – LB/M9, after induction, 5 – LB + 1% glucose/M9, before induction, 6 – LB + 1% glucose/M9, after induction, 7 – M9 + 0.5% glycerol, before induction, 8 – M9 + 0.5% glycerol, after induction. The position of the atpES is shown.

Our results showed that protein yields of the His_6-atpES-A14S didn't change after induction and they were significantly lower compared to the subunit *a* expressed in a pBWU13 plasmid. One explanation is that there are high levels of basal expression which lead to selection of cells with low expression of the potentially toxic atpES protein. The basal level of expression might be abnormally high due to the properties of the expression vector and the bacterial strain, in which there is extremely high activity of T7 RNA polymerase and increased stability of mRNAs.

Because His_6-atpES-A14S protein wasn't produced in sufficient quantities in this expression system, and it wasn't expressed in the context of the *atp* operon either (Sections 4.1 and 4.2), we tested expression of the atpES-V15S under the control of *araBAD* promoter in the OM202 strain.

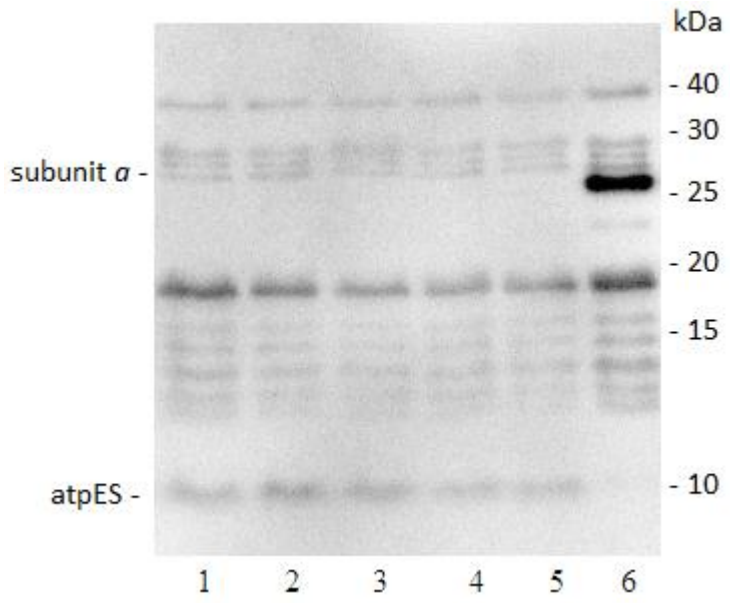

Figure 4.11. Expression of His_6-atpES-A14S in BL21(DE3)star, grown in M9 + 0.4% glucose. The samples were analysed by Western blot with HRP-conjugated anti-pentahistidine antibodies, 1:5,000. 1 – before induction, 2 – 1h after induction, 3 – 2h after induction, 4 – 3h after induction, 5 – 4h after induction, 6 – OM202/pBWU13 with His-tagged subunit *a*. Positions of the subunit *a* and atpES are shown.

4.4. Expression of subunit *c* variants under the control of *araBAD* promoter.

Our previous attempts to overexpress His_6-atpES-A14S in the context of the *atp* operon and under the control of T7 promoter were unsuccessful. We devised an alternative way to overexpress His_6-atpES-V15S using the pBAD102 vector and the OM202 strain. The OM202 strain was chosen because it has no wild type subunit *c*, which might be co-purified with the polar version. The expression was induced in the range of L-arabinose from 0.001% to 1%. No protein was detected before induction, and the highest protein yield was observed with 0.1% of L-arabinose (Figure 4.12). The absence of basal His_6-atpES-V15S expression before induction is important for preserving high protein yield with time as it prevents the selection of cells with lower expression levels of this potentially toxic protein. This result demonstrates that the protein can now be obtained from *E. coli* cells in sufficient quantities for nanopore experiments.

Figure 4.12. Expression of the His_6-atpES-V15S from pDK3cr in OM202 under the control of *araBAD* promoter as a function of arabinose concentration. Western blot with anti-pentahistidine HRP-conjugated antibody (1:5,000), using crude cell extract. 1 – before induction, 2 – 0.001% of L-arabinose; 3 – 0.01% of L-arabinose; 4 – 0.1% of L-arabinose; 5 – 1% of L-arabinose. The position of atpES is shown.

Expression of the His_6-atpES-IT protein was also tested in the same expression system. pBAD102 based constructs contained the *atpI* and *atpES-IT* genes under the control of the *ara-BAD* promoter. The atpI protein was preserved because it was described as essential for the assembly of the *c*-ring from *P. modestum* (Suzuki *et al.*, 2007). Analysis of expression was done under the same conditions as for the His_6-atpES-V15S in the range of L-arabinose from 0.001% to 1%. No protein was detected in crude cell extract under any tested conditions using anti-pentahistidine antibody (Figure 4.13). Because the presence of the *atpI* gene could interfere with His_6-atpES-IT expression, it was deleted, but still no His_6-atpES-IT was detected in the cell extract with any arabinose concentration tested (Figure 4.14). The gene encoding His-tagged wild type subunit *c* from *P. modestum* was cloned into the same cloning site as *His_6-atpES-IT*, and expression was tested in the same conditions. Still, no protein was detected with anti-pentahistidine antibody (Figure 4.14).

Figure 4.13. Test of expression of the atpI- His_6-atpES-IT in OM202 under the control of the *araBAD* promoter as a function of arabinose concentration. The samples were analysed by Western blot with anti-pentahistidine HRP-conjugated antibody (1:5,000) using crude cell extract. The plasmid contains *atpI* and *atpES-IT* genes. 1 – before induction, 2 – 0.001% of L-arabinose; 3 – 0.01% of L-arabinose; 4 – 0.1% of L-arabinose; 5 – 1% of L-arabinose 6 – atpES from OM202/pDK3cr. The position of the atpES is shown. The blue rectangle indicates the expected positions of the His_6-atpES-IT bands.

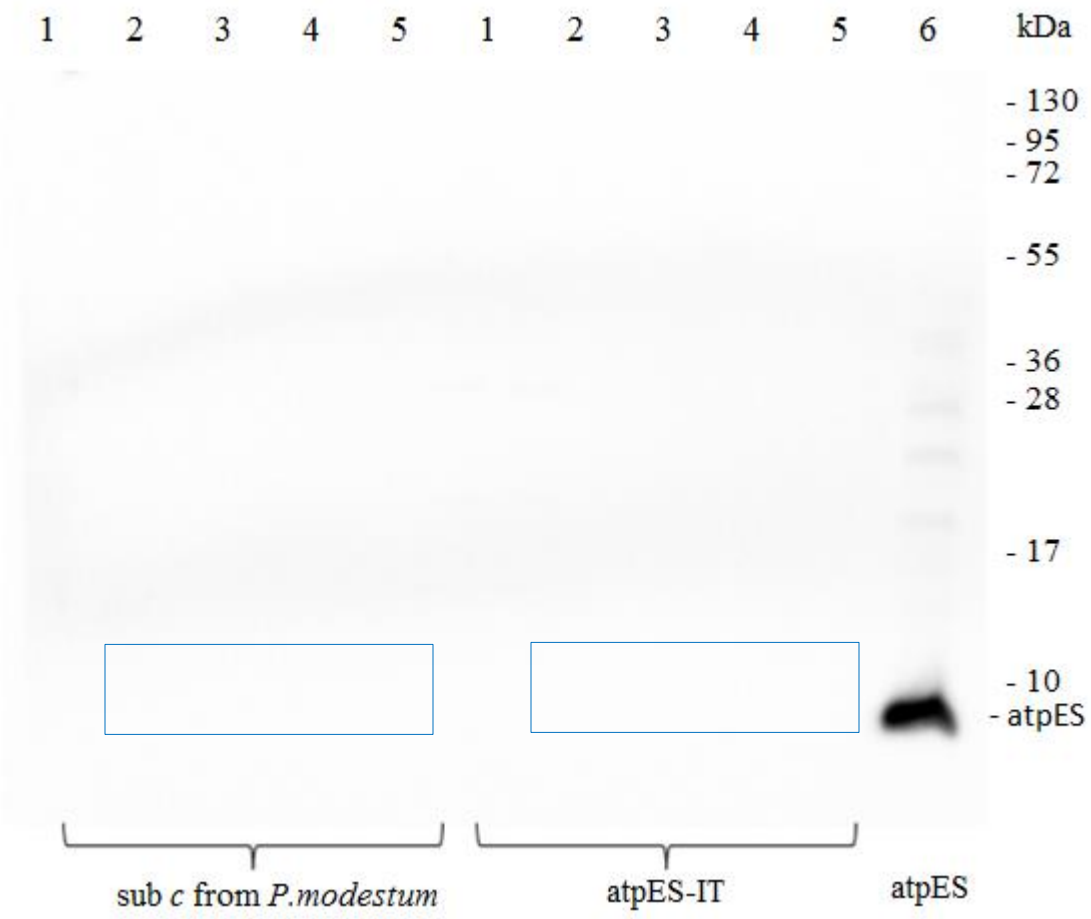

Figure 4.14. Test of expression of His-tagged wild type subunit *c* from *P. modestum* (pDK5) and His_6-atpES-IT (pDK6) in OM202, under the control of the *araBAD* promoter as a function of arabinose concentration. Neither plasmid contains *atpI*. The samples were analysed by Western blot with anti-pentahistidine HRP-conjugated antibody (1:5,000), using crude cell extract. 1 – before induction; 2 – 0.001% of L-arabinose; 3 – 0.01% of L-arabinose; 4 – 0.1% of L-arabinose; 5 – 1% of L-arabinose; 6 – atpES from pDK3cr, crude cell extract. The position of the atpES is shown. Blue rectangles indicate the expected positions of the subunit *c* from *P. modestum* and atpES-IT bands.

It is possible that the proteins were not expressed because the codon frequency in the *atpES-IT* and *atpE-PM* genes is rather different from the *E. coli* host cells. A new construct with codon optimized *His_6-atpES-IT* gene sequence was tested under the same conditions. Expression of the His-tagged wild type subunit *c* from *E. coli* in the pBAD102 plasmid (pDK8), His_6-atpES-V15S in the pBAD102 plasmid (pDK3cr) and His-tagged wild type subunit *c* from *E. coli* in the context of the *atp* operon (pDK7) were tested as well. Neither His_6-atpES-IT or the wild type subunit *c* from *E. coli* was detected with anti-pentahistidine antibody (Figure 4.15).

Figure 4.15. Test of expression of the His-tagged wt subunit *c* from *E. coli* and His_6-atpES-IT in OM202 under the control of the *araBAD* promoter as a function of arabinose concentration, using crude cell extracts. The *His_6-atpES-IT* gene sequence was optimized. The samples were analysed by Western blot with anti-pentahistidine HRP-conjugated antibody (1:5,000). The position of the atpES is shown.
1 – His_6-atpES-V15S from pDK3cr;
2 – 6 - His-tagged wt subunit *c* from pDK8: 2 – before induction; 3 – 0.001% of L-arabinose; 4 – 0.01% of L-arabinose; 5 – 0.1% of L-arabinose; 6 – 1% of L-arabinose;
7 – 11 - His_6-atpES-IT from pDK9: 7 – before induction; 8 – 0.001% of L-arabinose; 9 – 0.01% of L-arabinose; 10 – 0.1% of L-arabinose; 11 – 1% of L-arabinose;
12 - His-tagged wt subunit *c* from pDK7 expressed in the context of *atp* operon.
Green rectangles indicate the expected positions of the His-tagged wt subunit *c* from *E. coli*.
Blue rectangle indicates the expected positions of the His_6-atpES-IT bands.

Summarising the results, expression of the His_6-atpES-V15S in the pBAD102 vector in the OM202 strain was successful. It means that this expression system can be used for protein purification. Unlike His_6-atpES-V15S, His-tagged wild type subunit *c* from *E. coli* and His_6-atpES-IT were not detected in the same expression system and in the context of the *atp* operon (pDK7). The absence of signal could be due to the absence of expression or low binding affinity of antibody to these proteins. Because His_6-atpES-V15S was expressed very well in the same conditions, and the wild type subunit *c* from *E. coli* was previously expressed in the context of the *atp* operon (Figure 4.1), it is likely that the antibody does not bind efficiently to the His-tagged wild type subunit *c* and to the His_6-atpES-IT. To test this hypothesis all proteins were purified and analysed by SDS-PAGE and Western blot.

4.5. Purification of subunit *c* variants.

The purification procedure for the *P. modestum* and *I. tartaricus* *c*-ring was described previously (Meier *et al.*, 2005). The procedure was designed for fast and efficient purification of the entire *c*-ring expressed heterologously in *E. coli*. We aimed to replicate the purification procedure for the atpES-IT and unmodified *c*-ring from *P. modestum*.

According to the study of Ozaki *et al.*, 2008, the 14-kDa hydrophobic protein encoded by the *atpI* gene is required for the assembly of the *c*-ring from *P. modestum*. In order to get an assembled ring, the gene encoding the atpI protein was cloned in front of the *atpES-IT* or *atpE-PM* gene. The plasmids pDKIES and pDKIE encoding the atpES-IT and WT subunit *c* from *P. modestum* respectively were transformed into BL21(DE3) strain. Briefly, the purification procedure includes isolation of the membranes from disrupted cells, protein solubilisation in a detergent and treatment of the solubilized protein with 65% of ammonium sulphate. As a result the stable *c*-ring remains in the solution, while contaminating proteins precipitate. The detection of the purified *c*-ring is possible using SDS-PAGE followed by silver staining, as the ring doesn't dissociate in SDS as a result of its extreme stability, and stronger denaturing agents are needed to disassemble it.

Bands corresponding to the *c*-ring and the monomeric subunit *c* of ~90 kDa and ~8 kDa respectively were the expected outcome of the purification. Both these bands were present in the purified samples (Figure 4.16 A). In order to disassemble the *c*-ring and oligomers, the pro-

teins in the suspension were treated with trichloroacetic acid (TCA) to a final concentration of 5% (Ozaki *et al.*, 2008). Most of the high molecular bands disappeared after treatment with TCA (Figure 4.16 B) indicating that they belonged to oligomers of the *c*-ring.

Because bands of ~8 kDa might belong to contaminating proteins from the host *E. coli* cells, mock purification was done as a control using BL21(DE3) cells without a plasmid. The band distribution appeared to be similar to the purified proteins (Figure 4.16 C). Qualitative examination of the putative monomeric and c_{10} bands was done by Mass-spec analysis, which confirmed absence of the target protein in the samples. Only proteins of the host *E. coli* cells were detected by mass spectrometry in the analysed sample. From this we conclude, that either the purification procedure didn't work, or the protein wasn't expressed. Because the wild type

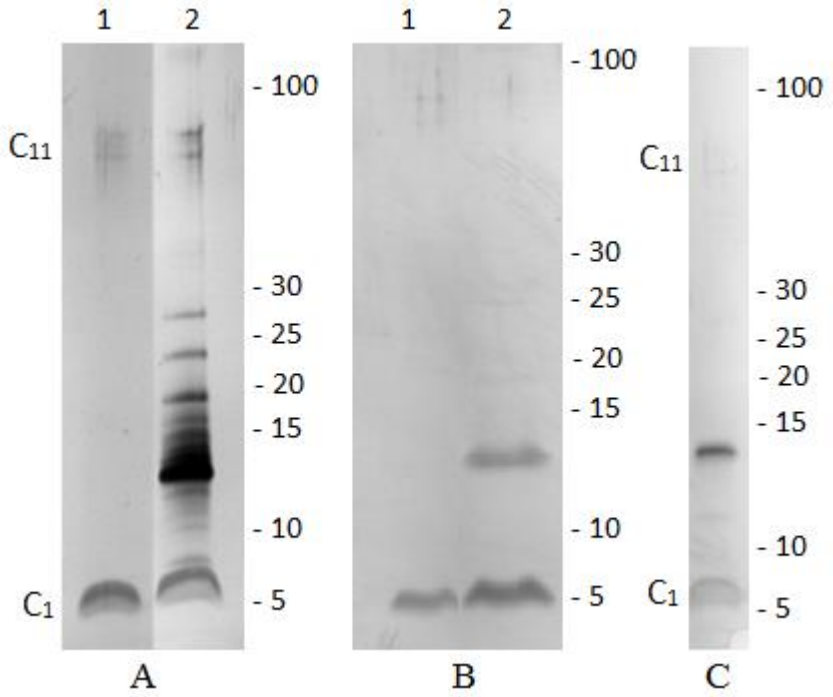

Figure 4.16. Preparations of subunit *c* from *P. modestum* and atpES-IT from BL21(DE3) in monomeric and oligomeric forms. The samples were analysed by SDS-PAGE followed by silver staining. 1 – *P. modestum* subunit *c* from pDKIE, 2 – atpES-IT from pDKIES. (A) before treatment with TCA. (B) after treatment with TCA. (C) mock purification from BL21(DE3) strain without a plasmid. The positions of the monomeric subunit *c* and the *c*-ring are shown.

subunit *c* from *P. modestum* and the atpES-IT proteins didn't have a histidine tag, the expression analysis of these proteins wasn't possible. To clarify whether the protein was lost during the ammonium sulphate precipitation, we performed the same purification procedure for the His_6-atpES-V15S, as it can be detected with anti-pentahistidine antibody and was successfully expressed under the control of the *araBAD* promoter in OM202 cells (Section 4.4). Although a ~8 kDa band was detected with silver staining (Figure 4.17, A), this band did not show any reaction with anti-subunit *c* antibody (Figure 4.17, B), and therefore it does not belong to atpES.

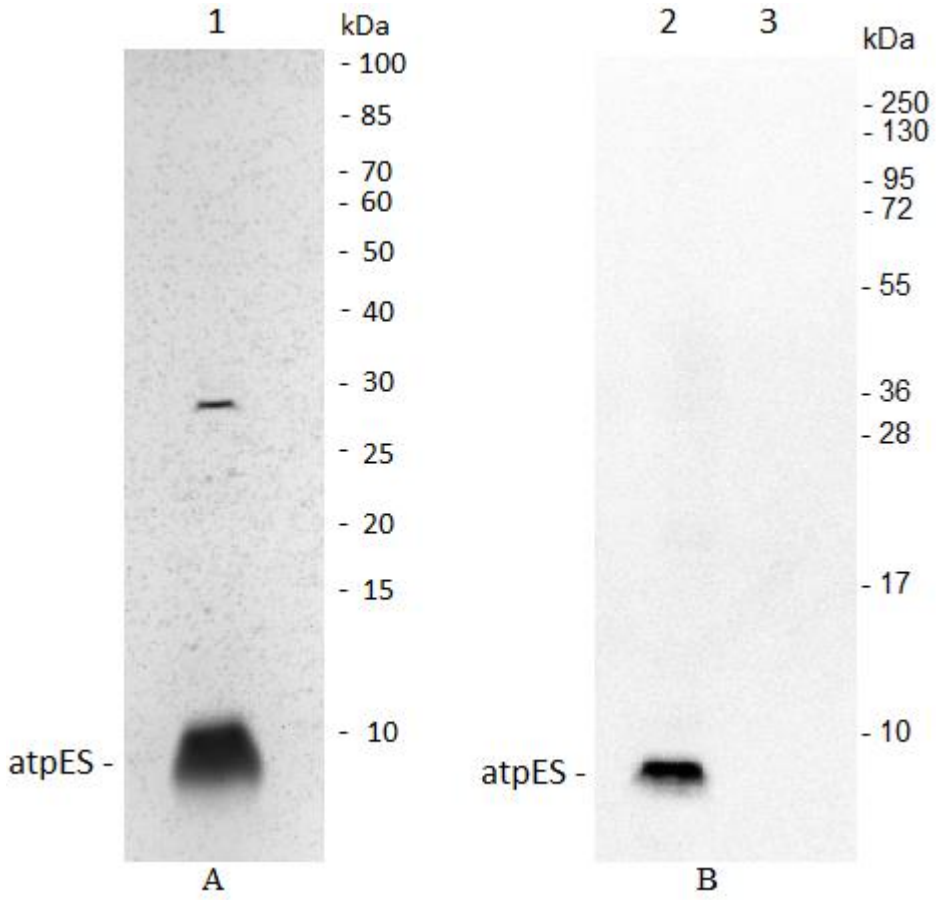

Figure 4.17. Preparation of His_6-atpES-V15S from pDK3cr expressed under the control of the *ara*BAD promoter in OM202 with 0.1% of L-arabinose and purified by ammonium sulphate precipitation. The samples were analysed by SDS-PAGE followed by silver staining (A) and Western blot with polyclonal anti-subunit *c* antibody, 1:60,000 (B). 1 – purified atpES; 2 – atpES from crude cell extract; 3 – sample expected to contain purified atpES. Positions of the atpES band are shown.

It is possible that the protein precipitated during the treatment with ammonium sulphate. According to Meier's procedure (Meier *et al.*, 2005), the *c*-ring and monomeric subunit *c* should stay in the supernatant fraction, while all contaminating proteins are precipitated with 65% (w/v) of ammonium sulphate. A titration with 30-60% (w/v) ammonium sulphate was done in order to find out if the protein was being lost during the precipitation step. Samples were collected from both pellet and supernatant and analysed by Western blot with polyclonal anti-subunit *c* antibody (Figure 4.18). The protein was found in the pellet in much greater quantities than in the supernatant indicating that atpES was precipitating. The atpES was almost completely absent in the supernatant sample, which was treated with 60% (w/v) ammonium sulphate. This means that the purification procedure did not work as expected and the ~8 kDa band did not contain atpES, which was confirmed by mass-spec analysis.

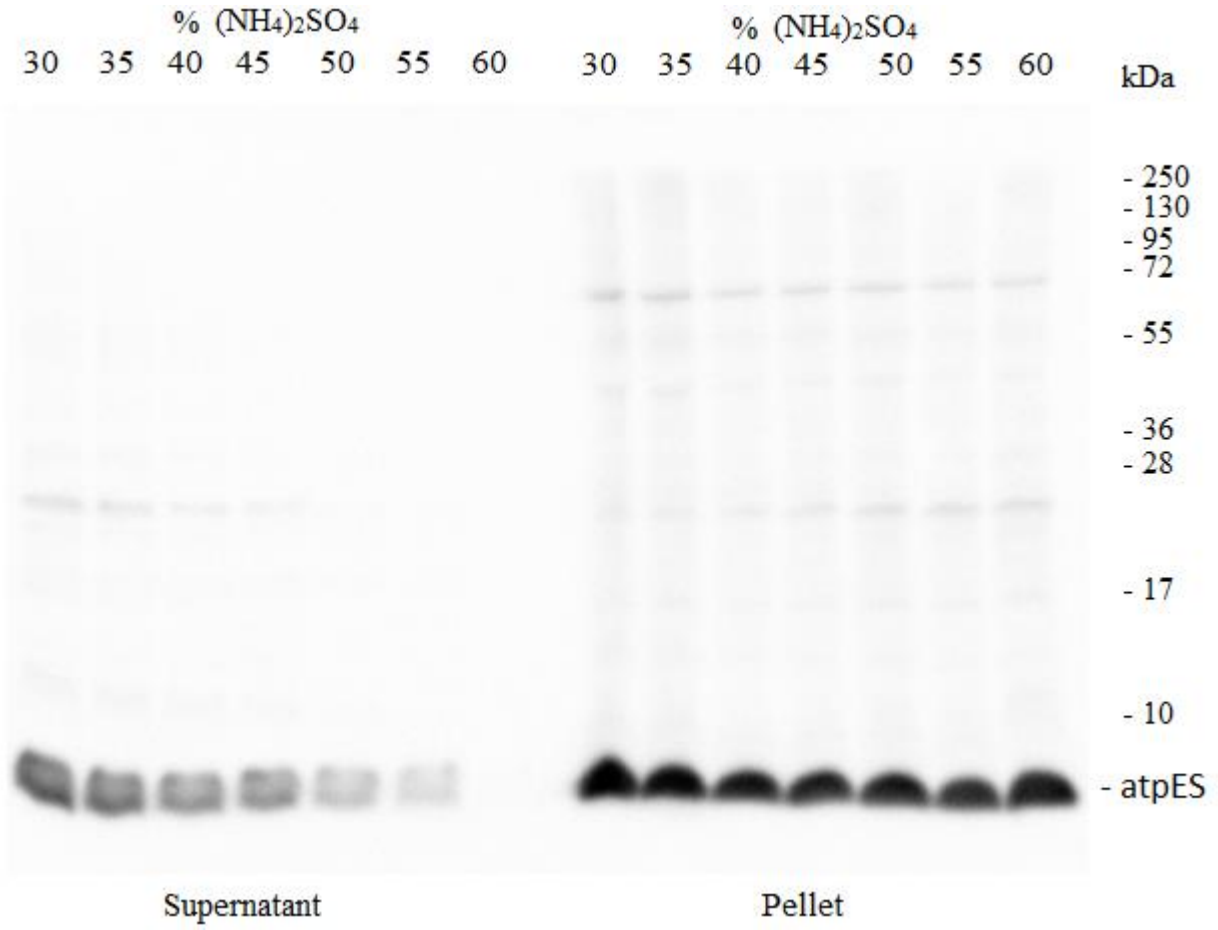

Figure 4.18. Fractionation of solubilized membranes of OM202/pDK3cr expressing atpES by ammonium sulfate precipitation. The samples were analysed by Western blot with polyclonal anti-subunit *c* antibody, 1:60,000. Position of the atpES is shown.

Although a similar pattern of bands was observed with the purified samples compared to the literature (Meier *et al.*, 2005), subunit *c* wasn't present there in any form, indicating that the purification procedure didn't work as described. For this reason another purification procedure was devised, suitable for purification of all subunit *c* variants in monomeric form.

A new purification procedure for subunit *c* variants included membrane isolation from disrupted cells, protein solubilisation in 2% LDAO, affinity chromatography on Ni-NTA, gel filtration and concentration. LDAO was chosen because it was found to yield the highest protein purity (Arechaga *et al.*, 2002). All the subunit *c* variants were successfully purified, and their identity was confirmed by Western blot analysis (Figure 4.19).

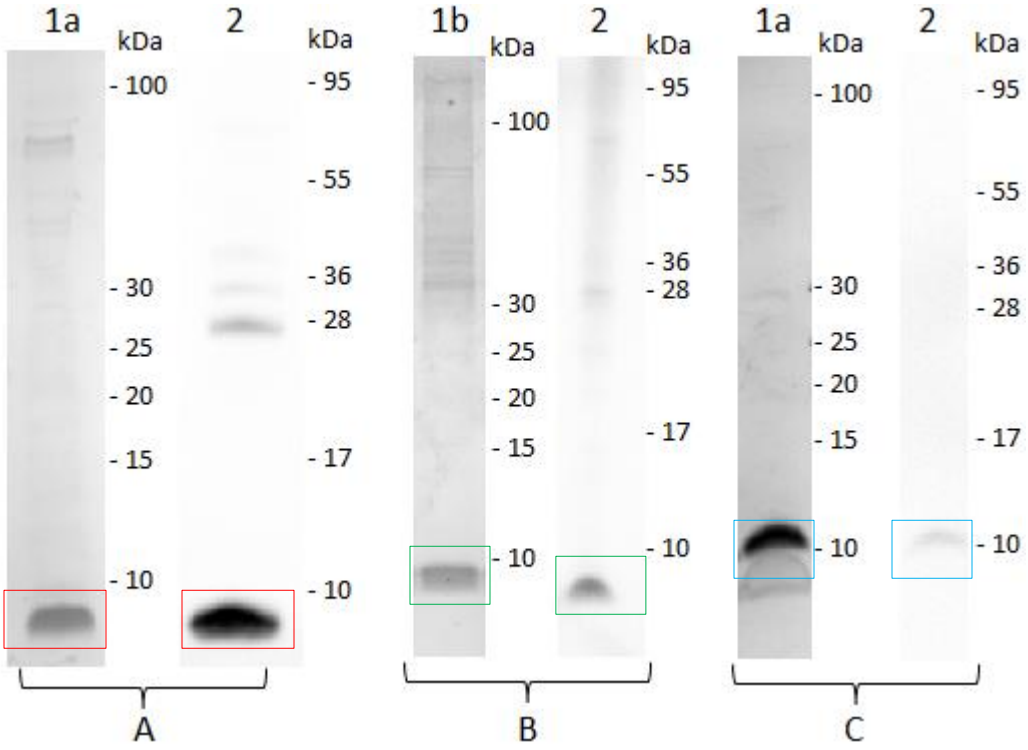

Figure 4.19. His_6-atpES-V15S (A), His-tagged wild type *E. coli* subunit *c* (B) and His_6-atpES-IT (C) purified from OM202/pDK3cr, OM202/pDK8 and OM202/pDK9 respectively by affinity chromatography on Ni-NTA agarose followed by gel filtration and concentration. The samples were analysed by SDS-PAGE followed by silver staining (1a) or Coomassie staining (1b) and Western blot with anti-pentahistidine antibody, 1:5,000 (2). Red rectangles indicate positions of the His_6-atpES-V15S. Green rectangles indicate positions of the His-tagged wt subunit *c* from *E. coli*. Blue rectangle indicates positions of the His_6-atpES-IT.

This result confirmed the hypothesis that the proteins His_6-atpES-IT and the His-tagged wild type subunit *c* from *E. coli* were expressed in OM202/pDK9 and OM202/pDK8 but not visualised with anti-pentahistidine antibody, possibly due to the low amount of expressed protein in the crude cell extract. Consistent with this explanation, the purified concentrated proteins showed good antibody reactivity.

The same purification procedure was used for atpES and the wild type subunit *c* with the G23D mutation (called atpES-G23D and atpE-G23D, respectively). This mutation was reported to disrupt *c*-ring assembly (Kol *et al.*, 2006). We intended to use the G23D variants to confirm that the open pore currents are produced by the *c*-ring nanopores. Subunit *c* with the G23D mutation is not supposed to oligomerize into the *c*-ring and yet it produced currents of the same value and electrical properties as other nanopore variants (see below).

Mutation G23D introduced into the His_6-atpES-V15S led to the formation of oligomers, which were clearly visible on SDS-PAGE and Western blot with anti-pentahistidine antibody (Figure 4.20 B). Unlike His_6-atpES-V15S, wild type subunit *c* with the G23D mutation didn't form oligomers (Figure 4.20 A).

Because the purified nanopore variants still contained contaminants, mock purification was done with OM202 cells without a plasmid for use as a control in nanopore analysis. After gel filtration we collected the same fractions that contained subunit *c* variants in our previous purifications: 17-19, corresponding to the fractions collected for the wild type subunit *c,* and 21-23, corresponding to all other subunit *c* variants (Figure 4.21). The collected samples lacking subunit *c* were concentrated and reconstituted into proteoliposomes using the standard procedure.

During this project, the expression of subunit *c* variants was tested in the context of the *atp* operon in the OM202 strain, in the BL21(DE3) strain under the control of T7 promoter, and in the OM202 strain under the control of the *araBAD* promoter. Only the last system was successful and resulted in a good yield of the protein of interest. Unfortunately, the purification procedure of the intact *c*-ring didn't work as it was described in literature, so a different method for purification of subunit *c* variants was developed, using LDAO for protein solubilisation, followed by Ni-NTA and gel filtration. Using this purification procedure, however, several issues

arise. First, the purity of the protein is not sufficient for use in nanopore analysis. For this reason, mock purification of OM202 cells was done in order to examine the ability of the contaminant proteins, which are co-purified with nanopore variants to form conductive nanopores. Second, the protein can be purified in the monomeric state only using this purification procedure. Although the monomers should self-assemble into the *c*-ring during reconstitution into lipid, it is still not possible to verify the presence of the assembled *c*-rings in proteoliposomes. Taken together, this means that the verification of the identity of a protein producing an open pore current is crucial. For this reason, we tested and compared all subunit *c* variants, including G23D mutants and proteins from mock purification for the potential to form conductive nanopores.

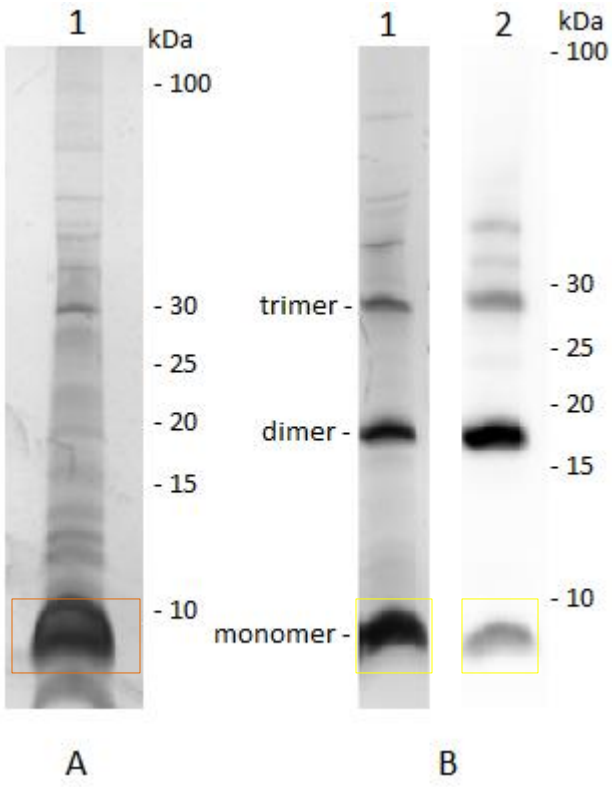

Figure 4.20. His_6-atpE-G23D (A) and His_6-atpES-G23D (B) purified from OM202 by affinity chromatography on Ni-NTA agarose followed by gel filtration and concentration. The samples were analysed by SDS-PAGE followed by silver staining (1) and Western blot with anti-pentahistidine antibody, 1:5,000 (2). The orange rectangle indicates the position of His_6-atpE-G23D. Yellow rectangles indicate the positions of His_6-atpES-G23D in monomeric form.

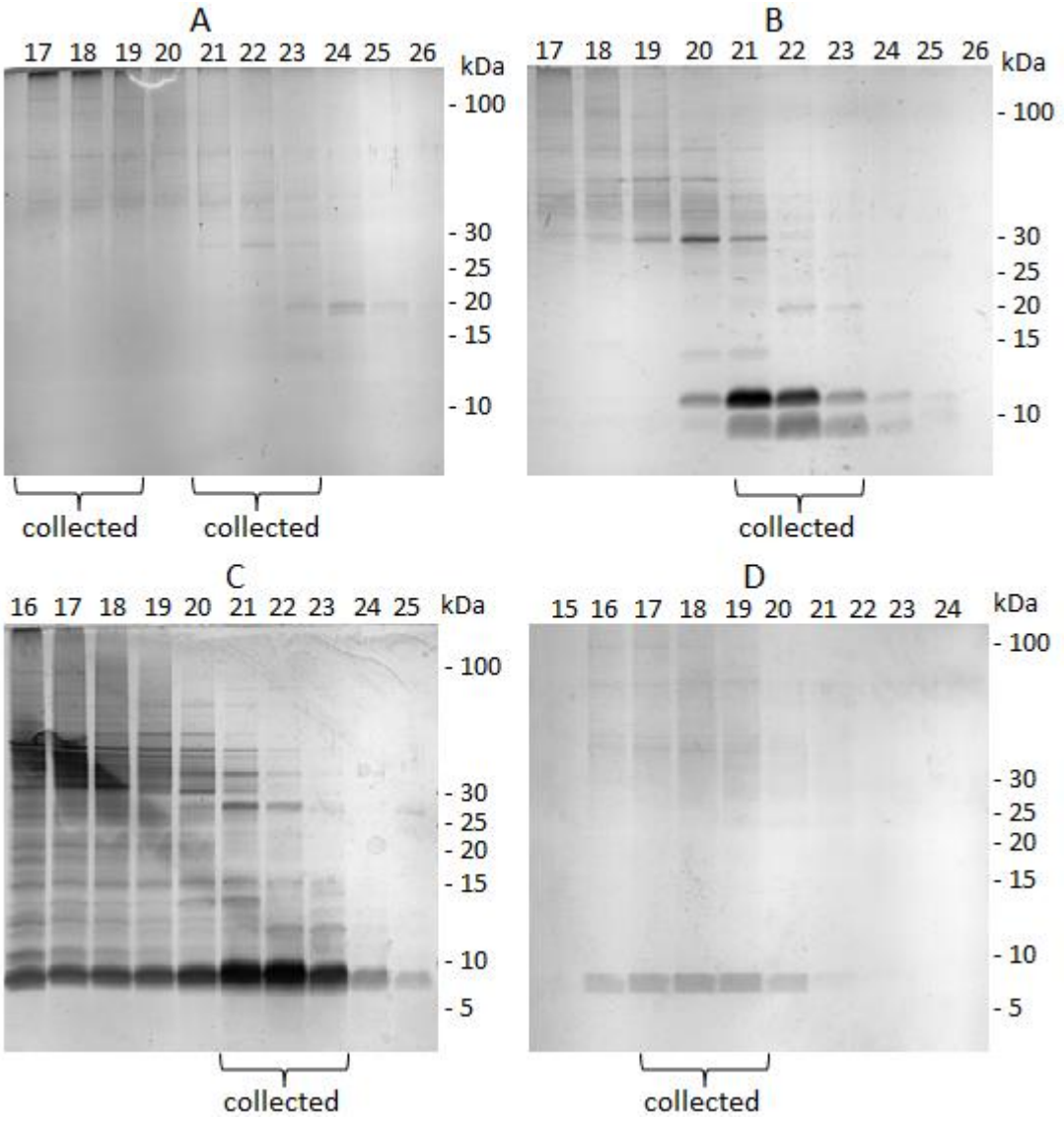

Figure 4.21. Gel filtration profile of mock purification of OM202 strain without a plasmid (A), His_6-atpES-IT (B), His_6-atpES-V15S (C) and His-tagged wild type subunit *c* from *E. coli* (D). The samples were analysed by SDS-PAGE followed by Coomassie (A, D) and silver (B, C) staining. Fractions 17-19 and 21-23 were pooled separately and concentrated.

4.6. Testing subunit *c* variants for nanopore activity.

We tested polar variants of subunit *c* from *E. coli* and *I. tartaricus* – His_6-atpES-V15S and His_6-atpES-IT for nanopore activity. We also used His-tagged wild type subunit *c* from *E. coli*, G23D mutants and proteins from mock purification as controls, which were not supposed to produce open pore currents during tests for nanopore activity. All purified proteins were reconstituted into proteoliposomes made of DPhPC lipid. After formation of a stable membrane the proteoliposomes containing one of the purified proteins were added to the electrolyte solution. Pore formation was registered as a stepwise increase in current from 0 to ~700 pA. The open pore current lasted for a few seconds up to several hours, until the pore collapsed by itself. In the course of an experiment additional pore incorporations could have occurred with the same or a different open pore current.

The control experiments with DPhPC liposomes without a protein were performed to eliminate the possibility of pore formation by lipid. As expected, pore formation didn't occur with DPhPC liposomes. Pores were formed and the currents of different values were recorded with all tested proteoliposomes, including wild type subunit *c* from *E. coli*, G23D mutants and proteins from mock purification (Figures 4.22, 4.23, 4.28). We conclude that the wild type subunit *c* and the contaminant proteins, which were co-purified together with the *c*-ring nanopore variants, were also able to form pores in tested conditions. The open pore currents of 103 pA, 206 pA and 309 pA were regularly observed with the proteoliposomes containing His_6-atpES-V15S, His_6-atpES-IT and wild type subunit *c* from *E. coli* (Figure 4.22), and no such currents were recorded with proteins from the mock purification or wild type subunit *c* with G23D mutation. As the open pore current is proportional to the number of simultaneously incorporated nanopores, the currents 103 pA, 206 pA and 309 pA belong to the same protein, which formed 1, 2 and 3 pores in the membrane concomitantly. The consistency of these currents for three different nanopore variants indicates that all of them have similar internal diameter and stoichiometry. For an open pore the ratio of its diameter to the electric current is constant and can be calculated using formula:

$$\mathrm{I} = k \cdot \frac{d^2}{l},$$

where I is the open pore current, k is a constant at a given voltage, d is the pore diameter, and l is the length of the pore. The length of the undecameric pore from *I. tartaricus* calculated from AFM and cryo-EM measurements is ~7 nm (Stahlberg *et al.*, 2001; Vonck *et al.*, 2002). An open pore current of ~103 pA belongs to a single nanopore. Using these data the approximate diameter of the undecameric *c*-ring is ~1.8 nm. This is consistent with the diameter of the undecameric *c*-ring measured by electron cryo-microscopy, which is ~1.7 nm (Vonck *et al.*, 2002).

Unexpectedly, the wild type subunit *c* from *E. coli* also produced pores similar to the nanopore variants. Although the central cavity of the *c*-ring has a strong affinity for hydrophobic molecules, the central plug of phospholipid could be removed from the channel during pore incorporation under a constant voltage of 200 mV. The ring could remain stable after removal of the central plug due to the tight protein-protein interactions stabilizing the entire complex (Meier *et al.*, 2001).

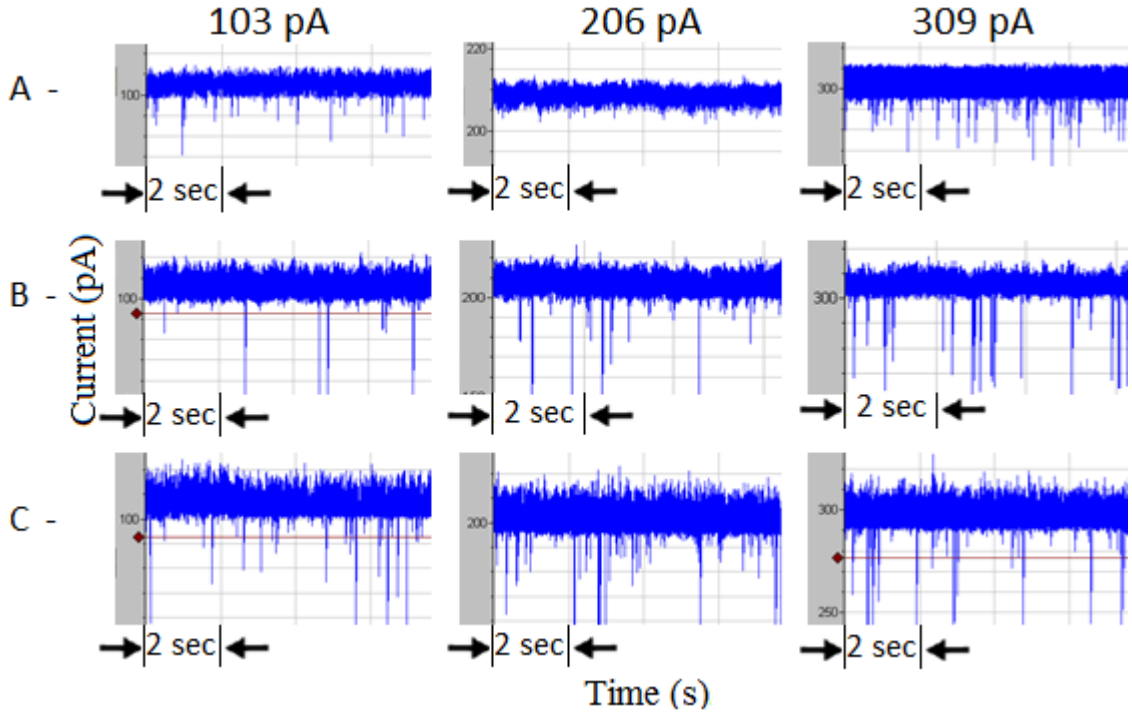

Figure 4.22. Open pore currents recorded with different nanopore variants during independent experiments. (A) wild type subunit *c* from *E. coli*; (B) His_6-atpES-V15S, (C) His_6-atpES-IT. Number of inserted pores at the same time is proportional to the observed current as follows: 103 pA – single pore, 206 pA – two pores, 309 – three pores. Open pore current values are shown above current traces.

Control DPhPC proteoliposomes were prepared using fractions after gel filtration of the OM202 mock purification, which correspond to the fractions containing nanopore variants purified by the same method (Figure 4.21). The control proteoliposomes produced various currents (Figure 4.23), ranging from 38 pA to 286 pA, with prevailing current of 133 pA. The previously described currents of 103 – 309 pA, which most likely correspond to the nanopore variants of the *c*-ring, were not observed in the control experiments with proteins from mock purification. Rates of current appearances for each nanopore variant and proteins from mock purification are shown in Figure 4.24.

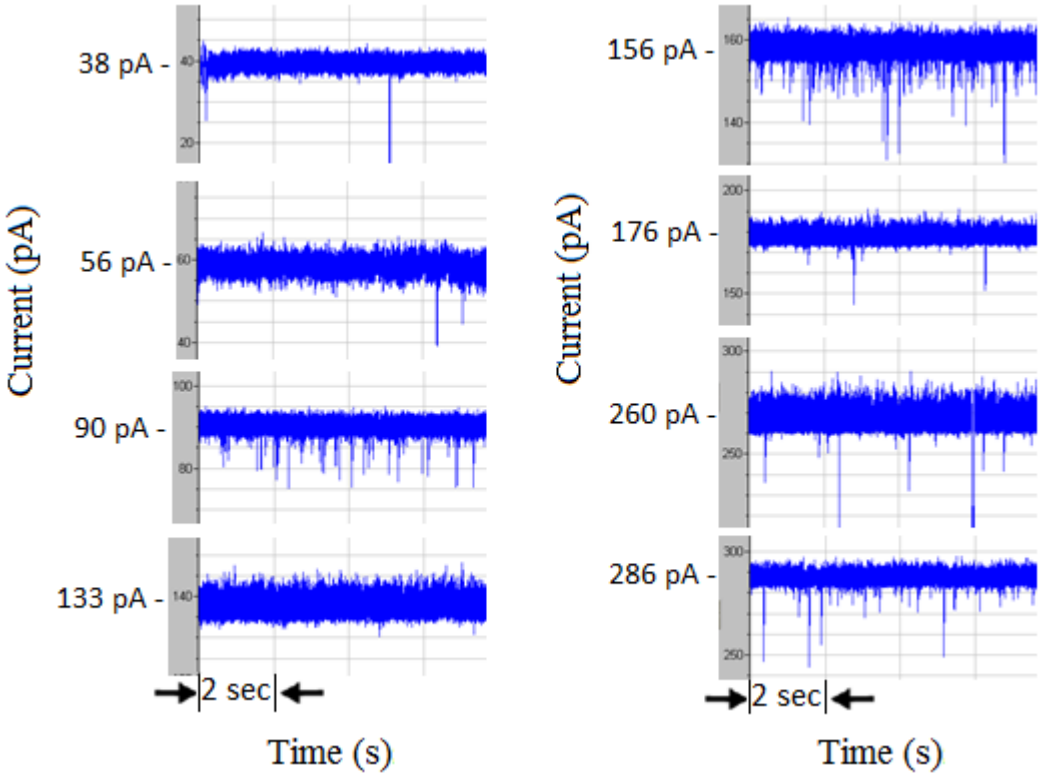

Figure 4.23. Open pore currents recorded with unidentified nanopores obtained from mock purification using OM202 strain without a plasmid. Currents were recorded during independent experiments. Open pore current values are shown on the left of each current trace.

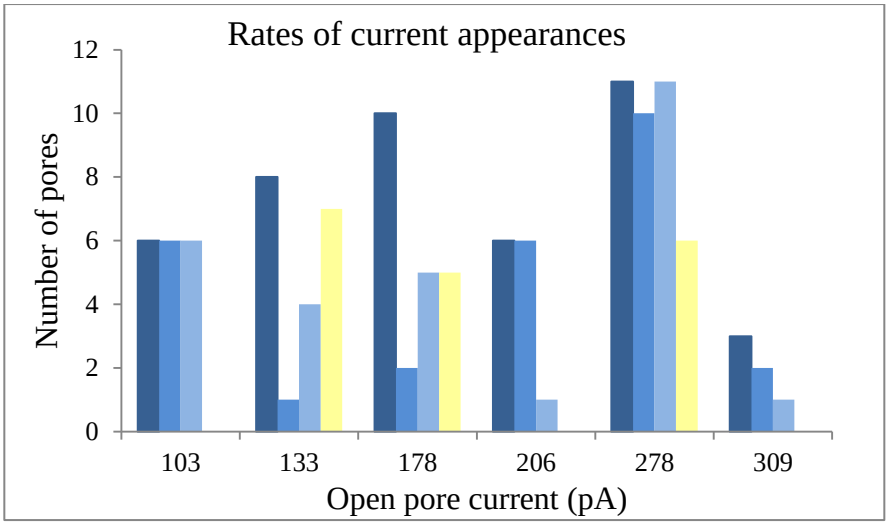

Figure 4.24. Rates of current appearances recorded for the nanopore variants and proteins from mock purification during independent experiments. Dark blue - wild type subunit *c* from *E. coli*; blue – His_6-atpES, light blue – His_6-atpES-IT, yellow - proteins from mock purification.

4.7. Electrical properties of the nanopore variants.

Open pore currents of the *c*-ring nanopore variants were recorded at different voltages. The graphs were plotted showing the current/voltage dependencies for each recorded pore. Linear current/voltage dependency indicates that all analysed pores are characterized by Ohmic behavior, which means that they obey the relationship I=V/R, where I – electric current through the open pore in A; V – voltage across the membrane in V; and R is resistance in Ω.

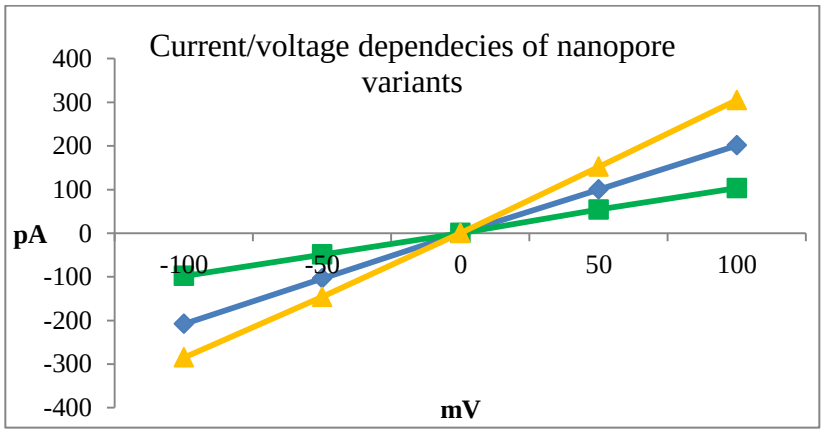

Figure 4.25. Current/voltage dependencies of nanopores produced by different nanopore variants during independent experiments. Number of inserted pores is proportional to the open pore current. Green line corresponds to 1 open pore, blue line – to 2 open pores, orange line – to 3 open pores.

All recorded pores can be classified into groups with similar electric currents. Membranes with one, two or three open pores give current-voltage relations with slopes proportional to the number of pores (Figure 4.25).

The nanopores formed by the wild type subunit *c* from *E. coli*, His_6-atpES-V15S, and His_6-atpES-IT presented good Ohmic behavior, as evidenced from linear current-voltage (I–V) curves (Figure 4.25). This behaviour indicates that the pores have cylindrical geometries (symmetric shapes) and the inner pore walls have either no charge or homogeneously distributed fixed charges resulting in absence of selectivity (Ali *et al.*, 2015).

4.8. Probing nucleic acid translocation through the nanopore.

In order to check if the solutes can pass through the pore, oligonucleotide solution (5 µM dT20) was added to the experimental system. The diameter of the ssDNA is ~1 nm. The pore, which was tested for oligonucleotide translocation had an open pore current of -289 pA at -100 mV during the recording of background noise. The current of -289 pA is too high for a single pore and most likely was created by 2 or 3 pores, which were inserted simultaneously into the membrane. It was confirmed later when one of the pores collapsed by itself and the current changed to -198 pA. Still, the open pore current of -198 pA was too high to belong to a single pore, and it was impossible to effectively discriminate which proteins formed it. This current could belong to the wild type subunit *c* (-103 pA) and some contaminating protein, which was able to form a conductive nanopore with an open pore current of -93 pA at -100 mV. The recording of translocation events after addition of oligonucleotides to the *trans*-chamber was done with the open pore current of -198 pA at -100 mV. The appearance of frequent peaks with high amplitude indicates interaction between the pore and the oligonucleotides (Figure 4.26). The number of events per minute was significantly higher after addition of oligonucleotides (Figure 4.27). Blockade current histograms were plotted showing the event distribution before and after addition of the oligonucleotides (Figure 4.28). Two peaks of 20 pA and 45 pA are clearly visible before and after addition of oligonucleotides. Events with amplitude of around 20 pA usually correspond to gating and bumping interactions. Higher amplitude events of 45 pA could also be caused by bumping or gating, or translocation of small molecules, which are present in a solution. If there are two concurrently inserted pores, the gating could be different

for each pore, resulting in two distinct peaks. A new peak of ~80 pA appears after addition of oligonucleotides, indicating their translocation through the pore.

We concluded from these data that the pores, which produced open pore current of -198 pA, responded well to the addition of a new solute and were capable of interacting with oligonucleotides. This data could be used for future examination of nanopore properties, as the blockade current histograms could represent the behaviour of novel nanopore variants.

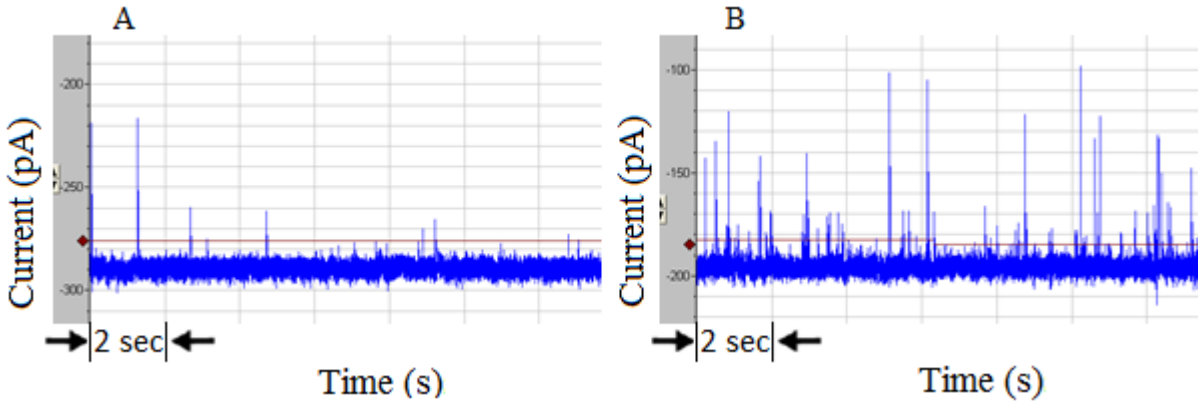

Figure 4.26. Electric current traces of the wild type subunit *c* pore before (A) and after (B) addition of oligonucleotides recorded at -100 mV.

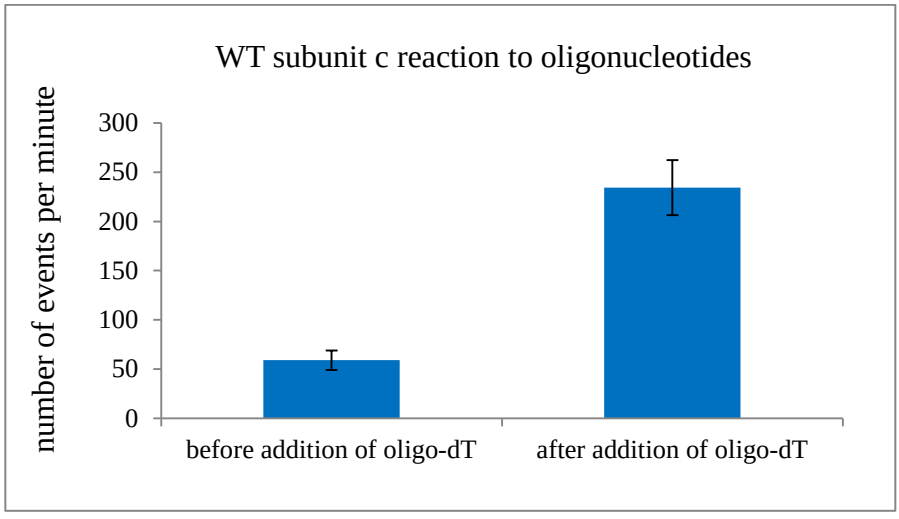

Figure 4.27. Event frequency before and after addition of oligonucleotides.

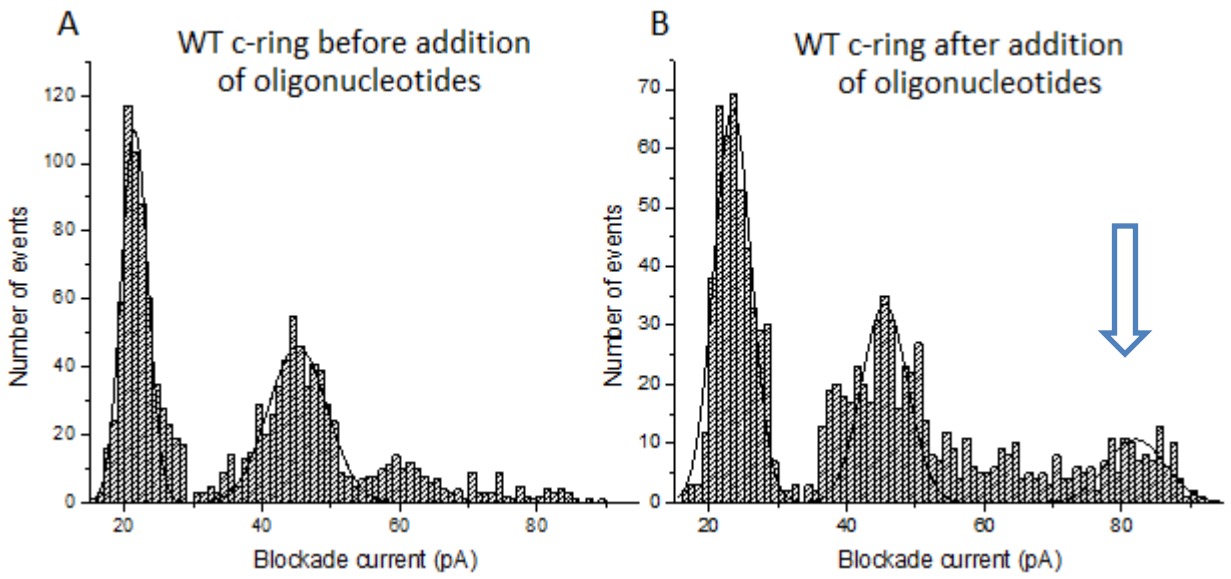

Figure 4.28. Blockade current histograms of the wild type subunit *c* before (A) and after (B) addition of oligonucleotides, recorded at -100 mV.

4.9. Testing disruption of the *c*-ring assembly by the G23D mutation.

It was shown earlier that mutation G23D in subunit *c* from *E. coli* inhibits proton transport and oxidative phosphorylation (Downie *et al.*, 1979). Further studies showed an absence of the mutated subunit *c* in membranes (Downie *et al.*, 1981; Jans *et al.*, 1983). Kol *et al.* (2006) showed that in a cell free system in the presence of the YidC chaperone, mutant subunit *c* fail to form oligomeric structures. These data indicate that the G23D mutation in the *c* subunit disrupts *c*-ring assembly, and therefore should prevent formation of a nanopore in proteoliposomes. If the observed open pore current was due to oligomerized *c* subunits, G23D variant should show no nanopore activity.

Both His_6-atpES-V15S and wild type subunit *c* with the G23D mutation (called atpES-G23D and atpE-G23D respectively) were purified and reconstituted into proteoliposomes with DPhPC lipid. Both mutant proteins were tested for the ability to form a conductive nanopore under the same conditions as the other subunit *c* variants. The open pore currents corresponding to the multiple pore insertions were observed with both proteins (Figure 4.29). The current of 309 pA is very similar to the currents observed previously with nanopore variants, such as His_6-

atpES-V15S, His_6-atpES-IT and the wild type subunit c from *E. coli* (Figure 4.22). The wild type subunit *c* with the G23D mutation, on the other hand, didn't produce currents of 103 pA, 206 pA or 309 pA. The open pore currents of 530 pA, 560 pA and 639 pA, which were detected with atpE-G23D and atpES-G23D, were too high to be effectively discriminated, as they are produced by 5 or 6 concurrently incorporated nanopores, and could belong to contaminating proteins, which are co-purified with subunit *c* variants. The open pore current of 151 pA, which was detected with atpE-G23D, may belong to the contaminant proteins forming nanopores, which were observed previously (Figure 4.23).

We conclude that the G23D mutation introduced into the polar version of the *c*-ring from *E. coli* doesn't prevent its oligomerization as evidenced from the Western blot, and potentially could result in nanopore activity. However, the wild type subunit *c* with G23D mutation didn't produce open pore currents of previously described values corresponding to the nanopore variants (Figure 4.22), which indicates its disruptive effect on the *c*-ring.

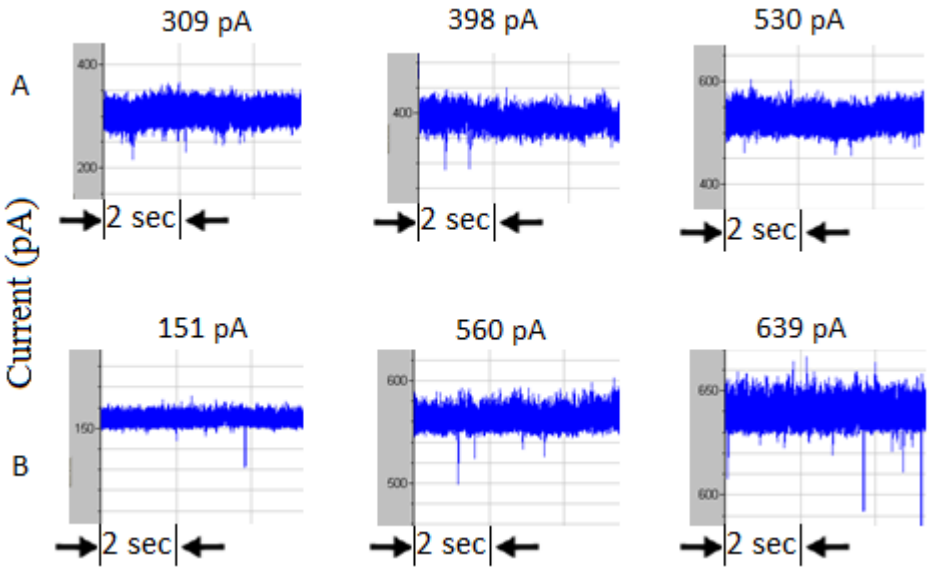

Figure 4.29. Electric current traces of the pore variants with G23D mutation. (A) atpES-G23D. (B) atpE-G23D. Open pore current values are shown above each current trace.

4.10. Effect of DCCD on nanopore assembly and conductivity.

DCCD (N,N'-Dicyclohexylcarbodiimide) specifically binds to the H^+-binding carboxyl residue of D61 of the subunit *c*. In F_1F_O ATP synthase DCCD blocks the rotation of the *c*-ring and thus inhibits proton transport (Toei and Noji, 2013). The large cyclohexyl moieties of DCCD bound to *c* subunits may interfere with their oligomerization by creating steric hindrances, thus preventing conductive pore formation. In our experiments we tested the ability of DCCD to inhibit *c*-ring formation by incubating *c* subunits with DCCD for 2 hours prior to incorporation into DPhPC liposomes.

Subunit *c* treated with DCCD produced a characteristic current of 103 pA (Figure 4.30), which was observed with the nanopore variants (Figure 4.22). Incubation of monomeric subunit *c* with DCCD didn't affect its propensity to oligomerize and form stable nanopores. This means that DCCD doesn't prevent oligomerization of the *c* subunits.

In order to prove that the proton channel segment of the subunit *c* is not involved in current creation, we added DCCD to reconstituted proteoliposomes and incubated at room temperature for 2 hours. The samples treated with DCCD were tested for the conductive pore formation under our standard conditions. The current of 103 pA was recorded with the sample of proteoliposomes treated with DCCD for 2 hours prior to the experiment (Figure 4.31). DCCD didn't change the characteristic of the *c*-ring open pore current, indicating that the D61 of the subunit *c* is not involved in creation of the observed current.

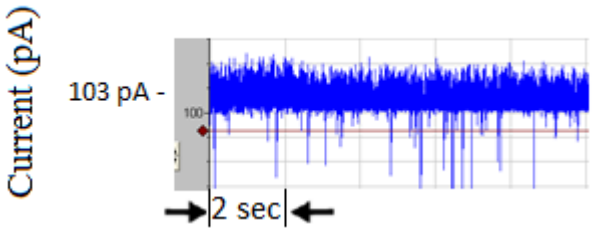

Figure 4.30. Open pore current recorded with His_6-atpES-IT treated with DCCD prior to reconstitution into lipid.

According to our experiments, all samples containing *E. coli* proteins seem to be capable of forming pores in the membrane. The currents of 103 pA and multiples of it can be considered as produced by the *c*-ring nanopore variants, as they were detected exclusively with samples containing His_6-atpES-V15S, His_6-atpES-G23D, His_6-atpES-IT and wild type subunit *c* from *E. coli*, and not detected with samples containing proteins from the mock *E. coli* purification and wild type subunit *c* from *E. coli* with G23D mutation.

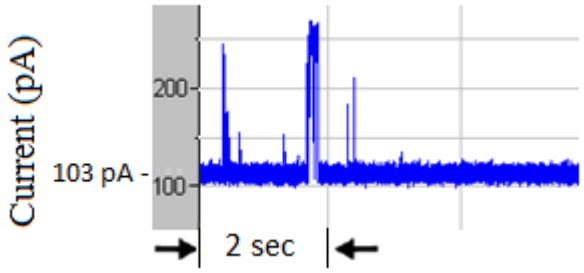

Figure 4.31. Open pore current recorded with His_6-atpES-IT treated with DCCD prior to experiment.

5. Discussion

5.1. Nanopore design

The goal of this research was to create a novel nanopore using a *c*-ring of F_1F_O ATP synthase as a scaffold. We used *c*-rings from *E. coli* and *I. tartaricus*, which have 10 and 11 subunits respectively. We aimed to replace the central plug of phospholipids in the channel with water. For that we changed amino acids inside the channel, by substituting hydrophilic non-charged serine and asparagine for hydrophobic valine, leucine, isoleucine and methionine. The polar variants of the *c*-ring are expected to form stable structures in aqueous solutions with a water-filled channel. The non-charged substituting amino acids were used to exclude ion selectivity.

As there is no high-resolution structure of the c_{10} *E. coli c*-ring, we used a model calculated from biochemical data and monomer structure to identify the residues lining the channel. We introduced six mutations into the TMH1 of the *E. coli c*-ring. We created 2 polar versions of the subunit *c* from *E. coli* – atpES-A14S (was created by mistake) and atpES-V15S.

The c_{11} ring of *I. tartaricus* was chosen as a second template because of its extreme stability, as the ring doesn't dissociate in SDS and can be purified as an intact complex (Meier *et al.*, 2005). We used the structure of the whole ring, which was obtained at resolution of 2.35 Å, to pinpoint the hydrophobic residues inside the channel. We created a polar variant of the *c*-ring from *I. tartaricus* with 5 mutations in the TMH1 – atpES-IT.

5.2. Mutations in the *c*-ring interior have different effects on ATP synthase assembly and function.

We aimed to express subunit *c* variants in the context of the *atp* operon, as the ring assembly may be facilitated by other subunits of the ATP synthase complex. We replaced wild type subunit *c* with atpES-A14S in the *atp* operon, and tested expression of the atpES-A14S and assembly of the enzyme in the F_1F_O-deficient strain. The major F_1 subunits and atpES-A14S were missing, indicating that the enzyme was not assembled. Hence, expression of the polar version of subunit *c* in the context of the *atp* operon resulted in absence of the *c*-ring in cell. This could happen because one or several introduced mutations induced disassembly of the

c-ring and prevented its incorporation into the enzyme. In order to find out which mutation disrupted *c*-ring assembly, we tested each of them separately. We introduced M11N, V15S, L19N, I22N, I26N and I30S into the subunit *c* in the *atp* operon and tested each mutant for the enzyme assembly and activity. Five of the mutations were well tolerated, and one was found to cause loss of enzyme activity and disrupt its assembly on the cell membrane. The *c*I30S substitution was characterized by the absence of the major F_1 subunits in the membrane fraction and defective ATP-driven H^+-pumping. Despite the fact that *c*I30 is not a part of the glycine-rich motif, which includes residues G23, A25, G27 and G29, its side chain can be directly involved in interactions with neighboring G29 and play important role in packing of the *c* subunits. Earlier it was shown that the glycine-rich motif is involved in tight residue packing at the c/c-subunit interface, increasing the stability of the whole complex (Press *et al.*, 2013). It is possible that the side chain of the substituting serine in position 30 caused sterical conflict with the neighboring subunits, which disrupted subunit *c* oligomerization, and prevented formation of assembled *c*-rings and their incorporation into ATP synthase complex. This explanation is plausible given that substitution of the isoleucine with threonine didn't cause any notable changes in the enzyme assembly and activity. Unlike serine, and similar to isoleucine, threonine contains β-branched side-chain and therefore is better tolerated as isoleucine substitution. Although some of the other tested mutations caused notable decrease of the enzyme activity, none of them prevented assembly of the ATP synthase complex. This indicates that they did not induce any critical structural changes in the *c*-ring and thus can be used in nanopore design.

5.3. Expression and purification of subunit *c* variants is possible only in monomeric state.

Previously we tested each introduced mutation separately, and found that *c*I30S disrupted *c*-ring assembly. We intended to eliminate disruptive effect of the *c*I30S by reintroducing isoleucine at position 30 in atpES-V15S mutant variant. We also changed the *c*I30S to the *c*I30N in atpES-V15S to test another polar variant of subunit *c*. Effect of mutations on enzyme assembly was tested by expressing polar versions of subunit *c* in the context of the *atp* operon in *E. coli* F_1F_O-deficient strain. We created three polar variants of the subunit *c* from *E. coli*, containing either 5 or 6 mutations. First polar version had intended set of six mutations including *c*I30S which proved to disrupt *c*-ring assembly; second polar version had six mutations including *c*I30N; third polar version had five mutations and the wild type isoleucine in position 30. As

none of the created polar versions of subunit *c* was present in cells, which was confirmed by the Western blot analysis, we concluded that the cumulative effect of the 5 mutations is sufficient for the *c*-ring disruption. Unlike the single *c*I30S mutation, the other five mutations together only caused the loss of subunits *a* and *c*, but did not prevent F_1-assembly and its attachment to the membrane through the subunit *b* dimer. Absence of the subunit *a* is consistent with the previous studies demonstrating importance of both subunits *b* and *c* for incorporation of subunit *a* into the membrane (Hermolin and Fillingame, 1995). So, like in the case with the *c*I30S mutation, 5 and 6 mutations in subunit *c* resulted in absence of the *c*-ring in cell. It remains unclear why individual *c*I30S mutation and 5-6 mutations together in subunit *c* lead to two different effects on the complex assembly. In case with the *c*I30S mutation the ATP synthase wasn't present in cell, while 5-6 mutations in subunit *c* result in incompletely assembled enzyme. The previously tested polar version of subunit *c*, atpES-A14S, also resulted in absence of all ATP synthase subunits in cell. As the incorrectly introduced mutation A14S is facing towards the neighboring subunit and not inside the hole, it is likely to disrupt packing of *c* subunits. The outcome of this experiment brought us to the conclusion that polar versions of subunit *c* from *E. coli*, expressed in the context of the *atp* operon result in absence of the *c*-ring in cell because of the cumulative effect of introduced mutations which disrupts assembly of the enzyme. It is possible, that the polar versions of subunit *c* assemble in different stoichiometry than the wild type, which results in its non-incorporation into the ATP synthase complex and subsequent degradation. This led us to the assumption that polar variants of subunit *c* expressed without the rest of the enzyme will not be degraded. It would be reasonable to assume that higher production of the polar variants under the control of a strong promoter would result in sufficient protein quantities for purification.

We aimed to express the polar variant of subunit *c* from *I. tartaricus*, atpES-IT, in the context of the *atp* operon. Expression of the subunit *c* in the context of the *atp* operon is beneficial, because other ATP synthase subunits can facilitate assembly of the *c*-ring. It was demonstrated that the 14 kDa protein encoded by *atpI* gene is required for assembly of the *c*-ring from *P. modestum* (Suzuki *et al.*, 2007). Also, the assembly of the enzyme can be evaluated by analysing other subunits of the ATP synthase complex, for example, subunits α and β. Previously, an attempt to express the entire *atp* operon from *P. modestum* in *E. coli atp* deletion mutant cells was unsuccessful (Gerike *et al.*, 1995), however functional chimeric ATPases were creat-

ed, containing genes from *P. modestum* and *E. coli* (Kaim and Dimroth, 1993), or *P. modestum* and *Bacillus* PS3 (Suzuki *et al.*, 2007). In this study we aimed to reproduce the described chimeras using genes from *P. modestum* and *E. coli* (Pogorelov *et al*., 2012, Meier *et al*., 2005). We used wild type subunit *c* from *P. modestum* as the control for expression, because the genes encoding subunit *c* from *P. modestum* and *I. tartaricus* are remarkably similar. We created two chimeric ATP synthases, each containing genes of F_1 complex from *E. coli*, and genes of F_O complex from *P. modestum,* with splice in either *atpA* (subunit α), or *atpF* (subunit *b*). The chimeric *atp* operon with splice in *atpA* was also modified with replacement of the *atpE-PM* with the target *atpES-IT* gene.

Although we reproduced the gene composition and splicing points in the chimeric *atp* operon constructs exactly as described in the literature, none of the chimeras was assembled in cells. It is not entirely clear why we were not able to reproduce the previously described functional chimeric enzymes.

In order to create the chimeric enzyme with splice in *atpA*, the authors (Kaim and Dimroth, 1993) used *E. coli* strain CM1470, which has chromosomal deletion of *atpI, atpB, atpE, atpF, atpH* and part of the *atpA* genes (Friedl *et al.*, 1983). They transformed this strain with a plasmid containing corresponding genes from *P. modestum*, and selected colonies, which were able to grow on succinate as a sole source of carbon, indicating presence of a functional ATP synthase in cells. We used F_1F_O-delection *E. coli* strain OM202 for transformation with the plasmid containing chimeric *atp* operon with F_1 genes from *E. coli* and F_O genes from *P. modestu*m with splice in the *atpA.* So, use of different procedures, as well as different strains and plasmids could affect the result.

Another chimeric construct was described to contain F_1 genes from *Bacillus* PS3 and F_O genes from *P. modestum* with splice in *atpF*. The authors used an F_1F_O-deficient *E. coli* strain JM103Δunc and a plasmid pTR-h$F_1F_O^{(+i)}$. Despite the use of a similar procedure, we used F_1 genes from a different organism (*E. coli* instead of *Bacillus* PS3), which could interfere with the outcome. The complete *atp* operon from *P. modestum* in pBWU13 plasmid was transformed in F_1F_O deletion strain OM202, but the ATP synthase complex wasn't present in cells. So, we were not able to express the wild type subunit *c* from *P. modestum*, or atpES-IT in the context of the *atp* operon.

We tested another possibility to obtain subunit *c* from *P. modestum* or atpES-IT by expressing it together with *atpI* under the control of a strong promoter. We intended to purify the intact *c*-ring expressed under the control of the T7 promoter in *E. coli* BL21(DE3) strain using described previously purification procedure (Meier *et al.*, 2005). We cloned the *atpI* gene upstream of the *atpES-IT* to achieve better yield of the *c*-ring versus monomer (Suzuki *et al.*, 2007). The absence of the Histidine tag made monitoring of protein expression and purification difficult. Although the molecular weights of the bands after purification were similar to the *c*-ring and monomeric subunit *c*, the qualitative examination by Mass-spec analysis showed absence of the target protein in these bands. It was confirmed later that the subunit *c* is being lost during ammonium sulphate precipitation, indicating that the procedure didn't work as described. The result demonstrates that the procedure designed for purification of the atpES-IT in the form of the c_{11}-ring didn't succeed.

Expression of the polar subunit *c* variants, including atpES-IT, was much more effective under the control of the *araBAD* promoter with subsequent purification of monomers by affinity chromatography on Ni-NTA and size exclusion chromatography. It is noteworthy that purification procedure worked much better for the polar version of subunit *c*, than for the wild type. It can be explained by the significant reduction of the hydrophobic surface of the polar version compared to the wild type, which increased the overall effectiveness of the purification procedure. The proteins, purified this way, were tested for nanopore formation.

5.4. The *c*-ring of F_1F_O ATP synthase forms a conductive nanopore.

The purpose of this study was to test the ability of the polar *c*-ring variants to form a conductive nanopore. Purified subunit *c* variants were incorporated into the DPhPC lipid and tested for nanopore formation. Previous reports (Arechaga *et al.*, 2002) demonstrated that the *c* subunits from *E. coli* can self-assemble *in vitro* in mild detergent in the absence of other ATP synthase subunits and form annular structures with internal diameter of around 23 Å, which is almost two times bigger than the calculated diameter of 12 Å from the model structure of the c_{10} oligomer. These results suggest that the ability of the subunit *c* to assemble into complete rings is predetermined by its amino acid sequence, and thus it is an inherent property of the subunit *c*. This means that the ring assembly may not require chaperone proteins and the other subunits of ATP synthase, and can be achieved by reconstitution of the monomeric subunit *c* into the lipo-

some membrane. However, it is not known whether subunit *c* can self-assemble in proteoliposomes as well as in the detergent micelles, and how the heterologous lipid would influence size and stability of the assembled *c*-ring. In our experiments we used DPhPC lipid for proteoliposome reconstitution of subunit *c* variants for its low background noise during the nanopore incorporation into the membrane. Archaebacterial lipid DPhPC, however, is not a natural environment for the subunit *c* from *E. coli* or *I. tartaricus*, and its effect on the *c*-ring assembly is unknown.

Test for nanopore formation was done with atpES-V15S, atpES-IT, wild type subunit *c* from *E. coli*, atpES-G23D, atpE-G23D, and the proteins from mock purification using OM202 strain without a plasmid. Many open pore currents were recorded with each tested protein, including proteins from mock purification. One of the regularly observed currents had a value of 103 pA for a single pore, and 206 pA and 309 pA for 2 and 3 concurrently incorporated pores. We ascribed this current to the *c*-ring, as it was consistent for the atpES-V15S, atpES-IT and wild type subunit *c* from *E. coli*, and was never observed with proteins from mock purification. The internal diameter of the nanopore can be estimated from such parameters as length of the channel and the open pore current at given voltage. So, in the case with the open pore current of 103 pA the internal diameter corresponds to ~17-18 Å, which matches the diameter of the undecameric *c*-ring of *I. tartaricus*. However, it remains unclear why *E. coli* subunit *c* variants form nanopores of the similar size as atpES-IT, as the decameric ring has smaller internal diameter according to the model calculated from biochemical data and monomer structure. We hypothesised that the heterogenous lipid used for proteoliposome reconstitution *in vitro* changed the native stoichiometry of the *c*-ring, and thus its internal diameter, which is consistent with previous observations (Arechaga *et al.*, 2002).

The proteins from mock purification produced various currents, ranging from 38 pA to 286 pA. The bacterial channels and porins, which may co-purify with subunit *c*, can account for these currents. For example, potassium channel with its internal diameter of 0.35 - 1 nm can account for the 38 - 56 pA currents (MacKinnon, 2004). The OmpF, PhoE and other bacterial porins can be responsible for higher currents (Dargert *et al.*, 1986). Considering the result, it appears to be problematic to discriminate between the tested pore variants and contaminants. This clearly demonstrates that the purity of the studied nanopore obtained from bacteria must

be much higher in order to discriminate between the protein of interest and endogenous bacterial pore-forming proteins.

5.5. Polar amino acid substitutions do not affect electrical properties and conductivity of the nanopore.

The purpose of the polar substitutions inside the channel of the *c*-ring was to remove phospholipid molecules from the cavity, so it would become water-filled. All tested subunit *c* variants, including wild type subunit *c* from *E. coli*, formed nanopores of the same characteristics, such as open pore current and current/voltage relationship. This result suggests that the polarity of the pore lining doesn't affect current flow perceptibly. Apparently, the lipid can be effectively removed by sufficiently high applied voltage. Previous findings demonstrate that the lipid, filling the internal cavity of the *c*-ring, can be removed without affecting the stability of the complex (Meier *et al.*, 2001). The more recent study indicates that the purified reconstituted *c*-ring of the bovine F_1F_O ATP synthase forms a voltage-sensitive channel and apparently works as a mitochondrial permeability transition pore (Alavian *et al.*, 2014). In agreement with this data wild type *c*-ring has the same potential to form a conductive nanopore as its polar variant.

5.6. Sensing of DNA is possible with the novel nanopore.

We tested oligonucleotide transport through the *c*-ring nanopore. We recorded current traces before and after addition of oligonucleotides to estimate the alterations of the blockade current. The current traces were recorded at -100 mV. The gating was recorded with the open pore current of -289 pA, which correspond to 2 or 3 concurrently open pores, and the translocation was recorded with the open pore current of -198 pA, which corresponds to 1 or 2 concurrently open pores. The current of -198 pA could be caused by the wild type *c*-ring with the open current of -103 pA, and the contaminating pore-forming protein, producing the current of -95 pA. The number of resistive pulses corresponding to the blockade current increased three times after addition of the oligonucleotides, indicating that the pore is interacting with the solute. Translocation of the oligonucleotides through the pore was identified by analysing blockade current histograms. The current through the nanopore without any solutes was characterized by the presence of small amplitude events, which appear as two distinct peaks of 20 and 45 pA on a blockade current histogram. This could indicate interaction of the pore with the proteolipo-

somes or other contaminants in the solution, or gating of the pore. If there are two concurrently inserted pores, the gating could be different for each pore, resulting in two distinct peaks. The result showed appearance of a new peak of 80 pA after addition of the oligonucleotides, indicating translocation of the oligonucleotides through the pore. The increase in blockade current with the oligonucleotides evidenced that the nanopore translocates solutes and therefore can be used in nanopore analysis.

5.7. Nanopore assembly is affected by the G23D mutation.

We aimed to prove that the observed open pore currents of 103 pA, 206 pA and 309 pA were produced by the *c*-ring channel. Earlier it was shown that the G23D mutation disrupts assembly of the *c*-ring (Kol *et al.*, 2006). We tested subunit *c* from *E. coli* with G23D mutation for nanopore activity. If the current is created by the *c*-ring, the mutation should disrupt nanopore formation. Most of the observed currents with atpE-G23D (wild type subunit *c* with G23D) were in the range of 400 - 600 pA. None of the observed currents corresponded to the characteristic for the nanopore variants 103 pA, 206 pA or 309 pA. This result confirmed the hypothesis that these open pore currents belong to the *c*-ring nanopores. The atpES-G23D also produced different currents; most of them were in the range of 300 - 500 pA. The current of 309 pA was observed once, and it could be produced by the *c*-ring, as it was similar to the 309 pA currents of the nanopore variants discussed above. The atpES with G23D mutation displayed increased tendency to form stable oligomers before reconstitution into proteoliposomes as evidenced from Western blot. So, addition of a single mutation to the existing ensemble of mutations in subunit *c* increased its propensity to oligomerize. It is noteworthy that a single G23D mutation in subunit *c* didn't result in increased oligomerization or subsequent nanopore formation. This observation is in agreement with the previous reports of the disruptive effect of the G23D mutation on the *c*-ring. Taken together, this data supports our previous statement that the current of 103 pA and its multiples were produced by the *c*-ring variants.

5.8. Proton channel component of the *c*-ring is not required for nanopore conductivity.

We attempted to prove that the observed currents of 103 pA are not affected by the D61 of subunit *c*, located on the outside of the ring. The D61 is involved in proton transport in ATP synthase and can potentially transport ions across the membrane bypassing the main channel of

the pore. We tested if this residue is required for the observed nanopore activity. We used DCCD as an effective proton transport inhibitor of the *c*-ring. Decrease of the open pore current after incubation with DCCD would indicate that the proton translocation is blocked through the D61 of the *c*-ring and the only remaining current flow occurs via the pore opening. As the detected current had the same value of 103 pA, we concluded that DCCD does not alter the open pore current and thus the D61 of the *c*-ring is not required for nanopore conductivity. The observed currents are not likely to relate to the proton movement through the ATP synthase proton translocator because of the lack of ion selectivity, very high pore conductance and the absence of the subunit *a* in proteoliposome preparations.

5.9. Summary

We created and tested for nanopore activity two polar variants of subunit *c*. Formation of a nanopore was evidenced from the open pore currents, which were consistent and reproducible. We found that the wild type subunit *c* from *E. coli* is also capable of nanopore formation, producing currents similar to the polar variants of subunit *c*. The nanopores were characterized by a good Ohmic behavior, indicating symmetrical shape of the channel and absence of ion selectivity. Wild type subunit *c* with G23D mutation didn't result in the characteristic for nanopore variants open pore currents, confirming that they were produced by the *c*-ring. Wild type subunit *c* nanopore reacted well to oligonucleotides and resulted in increased blockade current, indicating that the nanopore translocates solutes across the membrane. As the DCCD didn't alter the observed previously currents, the D61 is not involved in nanopore activity.

Bacterial pore-forming proteins, which were co-purified with the subunit *c* variants, produced various currents while testing subunit *c* variants for nanopore activity. This hampered examination of nanopore properties, as discrimination between the tested subunit *c* variants and contaminants was problematic.

Finally, we conclude that the novel nanopore was generated from a *c*-ring. It is characterised by a high ionic conductance and is suitable for use in nanopore analysis.

6. Conclusions

We explored the possible ways for the *c*-ring modification. Our results demonstrate that its internal cavity can be modified with creation of a polar channel. We screened various conditions for the expression of the polar variants of subunit *c* and found that they can't be expressed in the presence of other ATPase subunits. For this reason we used *E. coli* F_1F_O-deletion strain for overexpression of all proteins of interest. We also devised an effective purification procedure for the variants of subunit *c*.

We developed a highly successful method for delivering hydrophobic *c*-ring protein into the lipid bilayer membrane. For low background noise during nanopore incorporation into the membrane, we used DPhPC liposomes for reconstitution of a purified and concentrated protein with subsequent buffer exchange. Substantially, this method can be used for any hydrophobic protein nanopore.

Our results indicate that all *c*-ring variants including the wild type and atpES-IT can form relatively stable nanopores with open pore currents of ~103 pA. No such current was detected with the control subunit *c* carrying G23D mutation, or proteoliposomes lacking any subunits of ATP synthase. Addition of oligonucleotides caused changes in the recorded current implying that the pore interacts with the solute. As incubation with DCCD didn't alter the open pore current, it was concluded that D61 of the *c*-ring is not involved in current creation.

7. Future work

Purification procedure for all subunit *c* variants should be optimized further. Exceedingly high protein purity is needed to increase rates of nanopore incorporation and thus facilitate its examination. A proof of the correct nanopore assembly in proteoliposomes would be rational, and a separate confirmation of the identity of the incorporated into the membrane nanopore would be important.

The further nanopore optimisation can be done using the findings of the current study. Substituting serine for threonine in position 30 proved to be beneficial for nanopore assembly and, potentially, its stability. Removal of the histidine tag may lower gating and increase effectiveness of nanopore incorporation, as the overall charge of the protein will be significantly reduced. As a result this will make the pore more suitable for use in nanopore analysis.

8. References

Abrahams, J.P., Leslie, A.G., Lutter, R., and Walker, J.E. (1994). Structure at 2.8 Å resolution of F_1-ATPase from bovine heart mitochondria. Nature 370, 621-628.

Alavian, K. N., Beutner, G., Lazrove, E., Sacchetti, S., Park, H. A., Licznerski, P., ... and Porter, G. A. (2014). An uncoupling channel within the c-subunit ring of the F_1F_O ATP synthase is the mitochondrial permeability transition pore. Proc. Acad. Nat. Sci. U.S.A. 111, 10580-10585.

Ali, M., Nasir, S., and Ensinger, W. (2015). Bioconjugation-induced ionic current rectification in aptamer-modified single cylindrical nanopores. Chem. Commun. 51, 3454-3457.

Apel, P.Y., Korchev, Y.E., Siwy, Z., Spohr, R., and Yoshida, M. (2001). Diode-like single-ion track membrane prepared by electro-stopping. Nucl. Instrum. Methods B, 184, 337-346

Arechaga, I., Butler, P.J., and Walker, J.E. (2002). Self-assembly of ATP synthase subunit *c* rings. FEBS Lett. 515, 189-193.

Bayley, H. (1995). Pore-forming proteins with built-in triggers and switches. Bioorg. Chem. 23, 340-354.

Bayley, H., and Martin, C. R. (2000). Resistive-pulse sensing from microbes to molecules. Chem. Rev. 100, 2575-2594.

Branton, D., Deamer, D. W., Marziali, A., Bayley, H., Benner, S. A., Butler, T., *et al.* (2008). The potential and challenges of nanopore sequencing. Nature Biotechnol. 26, 1146-1153.

Butler, T. Z., Pavlenok, M., Derrington, I. M., Niederweis, M., and Gundlach, J. H. (2008). Single-molecule DNA detection with an engineered MspA protein nanopore. Proc. Acad. Nat. Sci. U.S.A. 105, 20647-20652.

Capaldi, R. A., and Aggeler, R. (2002). Mechanism of the F_1F_O-type ATP synthase, a biological rotary motor. Trends Biochem. Sci. 27, 154-160.

Chen, M., Khalid, S., Sansom, M. S., and Bayley, H. (2008). Outer membrane protein G: Engineering a quiet pore for biosensing. Proc. Acad. Nat. Sci. U.S.A. 105, 6272-6277.

Claggett, S. B., Grabar, T. B., Dunn, S. D., and Cain, B. D. (2007). Functional incorporation of chimeric *b* subunits into F_1F_O ATP synthase. J. Bacteriol. 189, 5463-5471.

Coulter, W.H. "Means for counting particles suspended in a fluid." U.S. Patent 2,656,508, issued October 20, 1953.

Dagert, M., and Ehlrich, S. (1979). Prolonged incubation in calcium chloride improves the competence of *Escherichia coli* cells. Gene 6, 23-28.

Dargent, B., Hofmann, W., Pattus, F., and Rosenbusch, J. P. (1986). The selectivity filter of voltage-dependent channels formed by phosphoporin (PhoE protein) from *E. coli*. EMBO J. 5, 773.

de Gier, J. W. L., and Luirink, J. (2003). The ribosome and YidC. EMBO rep. 4, 939-943.

Deamer, D. W., Olsen, H., Akeson, M. A., and Kasianowicz, J. J. (2002). Mechanism of ionic current blockades during polymer transport through pores of nanometer dimensions. Struct. Dynam. Conf. Pol. 165-175.

Dekker, C. (2007). Solid-state nanopores. Nat. Nanotechnol. 2, 209-215.

Dimroth, P., von Ballmoos, C., Meier, T., and Kaim, G. (2003). Electrical power fuels rotary ATP synthase. Structure 11, 1469-1473.

Dmitriev, O. Y., and Fillingame, R. H. (2007). The rigid connecting loop stabilizes hairpin folding of the two helices of the ATP synthase subunit *c*. Protein Sci. 16, 2118-2122.

Dmitriev, O.Y., Jones, P.C., and Fillingame, R.H. (1999). Structure of the subunit *c* oligomer in the F_1F_O ATP synthase: model derived from solution structure of the monomer and crosslinking in the native enzyme. Proc. Acad. Nat. Sci.U.S.A. 96, 7785-7790.

Downie, J. A., Cox, G. B., Langman, L., Ash, G., Becker, M., and Gibson, F. (1981). Three genes coding for subunits of the membrane sector (F_O) of the *Escherichia coli* adenosine triphosphatase complex. J. Bacteriol. 145, 200-210.

Downie, J. A., Senior, A. E., Gibson, F., and Cox, G. B. (1979). A fifth gene (*uncE*) in the operon concerned with oxidative phosphorylation in *Escherichia coli*. J. Bacteriol. 137, 711-718.

Dunn, S.D., and Chandler, J. (1998). Characterization of a $b_2\delta$ complex from *Escherichia coli* ATP synthase. J. Biol. Chem. 273, 8646-8651.

Eisenstein, M. (2012). Oxford Nanopore announcement sets sequencing sector abuzz. Nature Biotechnol. 30, 295.

Faller, M., Niederweis, M., and Schulz, G.E. (2004). The structure of a mycobacterial outermembrane channel. Science 303, 1189-1192.

Fleischer, R. L., and Price, P. B. (1963). Tracks of charged particles in high polymers. Science 140, 1221-1222.

Friedl, P., Hoppe, J., Gunsalus, R. P., Michelsen, O., Von Meyenburg, K., and Schairer, H. U. (1983). Membrane integration and function of the three F_O subunits of the ATP synthase of *Escherichia coli* K12. EMBO J. 2, 99.

Garaj, S., Hubbard, W., Reina, A., Kong, J., Branton, D., and Golovchenko, J.A. (2010). Graphene as a subnanometre trans-electrode membrane. Nature 467, 190-193.

Gerike, U., Kaim, G., and Dimroth, P. (1995). In vivo synthesis of ATPase complexes of Propionigenium modestum and Escherichia coli and analysis of their function. Eur. J. Biochem. 232, 596-602.

Gibbons, C., Montgomery, M., Leslie, A., and Walker, J. (2000). The structure of the central stalk in bovine F_1-ATPase at 2.4 Å resolution. Nature Struct. Biol. 7, 1055-1061.

Girvin, M.E., Rastogi, V.K., Abildgaard, F., Markley, J.L., and Fillingame, R.H. (1998). Solution structure of the transmembrane H^+-transporting subunit *c* of the F_1F_O ATP synthase. Biochemistry (Mosc) 37, 8817-8824.

Gouaux, J.E., Braha, O., Hobaugh, M.R., Song, L., Cheley, S., Shustak, C., and Bayley, H. (1994). Subunit stoichiometry of staphylococcal alpha-hemolysin in crystals and on membranes: a heptameric transmembrane pore. Proc. Acad. Nat. Sci. U.S.A. 91, 12828-12831.

Gu, L. Q. Gu, L. Q., Braha, O., Conlan, S., Cheley, S., and Bayley, H. (1999) Stochastic sensing of organic analytes by a pore-forming protein containing a molecular adapter. Nature 398, 686–690.

Hakulinen, J.K., Klyszejko, A.L., Hoffmann, J., Eckhardt-Strelau, L., Brutschy, B., Vonck, J., and Meier, T. (2012). Structural study on the architecture of the bacterial ATP synthase F_O motor. Proc. Acad. Nat. Sci. U.S.A. 109, E2050-2056.

Hermolin, J., and Fillingame, R.H. (1995). Assembly of F_O sector of *Escherichia coli* H^+ ATP synthase. Interdependence of subunit insertion into the membrane. J. Biol. Chem. 270, 2815-2817.

Howorka, S., Cheley, S. and Bayley, H. (2001) Sequence-specific detection of individual DNA strands using engineered nanopores. Nature Biotechnol. 19, 636–639.

Jans, D.A., Fimmel, A.L., Langman, L., James, L.B., Downie, J.A., Senior, A.E., Ash, G.R., Gibson, F., and Cox, G.B. (1983). Mutations in the *uncE* gene affecting assembly of the *c* subunit of the adenosine triphosphatase of *Escherichia coli*. Biochem. J. 211, 717-726.

Jiang, W., Hermolin, J., and Fillingame, R.H. (2001). The preferred stoichiometry of c subunits in the rotary motor sector of *Escherichia coli* ATP synthase is 10. Proc. Acad. Nat. Sci. U.S.A. 98, 4966-4971.

Jones, P.C., and Fillingame, R.H. (1998). Genetic fusions of subunit *c* in the F_O sector of H^+-transporting ATP synthase. Functional dimers and trimers and determination of stoichiometry by cross-linking analysis. J. Biol. Chem. 273, 29701-29705.

Kaim, G., Dimroth P. (1993). Formation of a functionally active sodium-translocating hybrid F_1F_O-ATPase in *Escherichia coli* by homologous recombination, Eur. J. Biochem. 218, 615-623

Keyser, U. F. (2011). Controlling molecular transport through nanopores. J. R. Soc. Interface rsif20110222.

Kol, S., Turrell, B.R., de Keyzer, J., van der Laan, M., Nouwen, N., and Driessen, A.J. (2006). YidC-mediated membrane insertion of assembly mutants of subunit *c* of the F_1F_O ATPase. J. Biol. Chem. 281, 29762-29768.

Kol, S., Nouwen, N., and Driessen, A.J. (2008). The charge distribution in the cytoplasmic loop of subunit *c* of the F_1F_O ATPase is a determinant for YidC targeting. J. Biol. Chem. 283, 9871-9877.

Korotkov, K. V., Gonen, T., and Hol, W. G. (2011). Secretins: dynamic channels for protein transport across membranes. Trends Biochem. Sci. 36, 433-443.

Krasniqi, B., and Lee, J. S. (2014). RNase A does not translocate the alpha-hemolysin pore. PloS one 9, e88004.

Kwok, H., Briggs, K., and Tabard-Cossa, V. (2014). Nanopore fabrication by controlled dielectric breakdown. PloS one 9, e92880.

Laubinger, W., and Dimroth, P. (1987). Characterization of the Na^+-stimulated ATPase of *Propionigenium modestum* as an enzyme of the F_1F_O type. Eur. J. Biochem, 168, 475-480.

Laubinger, W., and Dimroth, P. (1988). Characterization of the ATP synthase of *Propionigenium modestum* as a primary sodium pump. Biochemistry (Mosc) 27, 7531-7537.

Li, J., Stein, D., McMullan, C., Branton, D., Aziz, M. J., and Golovchenko, J. A. (2001). Ion-beam sculpting at nanometre length scales. Nature 412, 166-169.

Long, J., Wang, S., Vik, B. (1998). Membrane topology of subunit *a* of the F_1F_O ATP synthase as determined by labeling of unique cysteine residues. J. Biol. Chem. 273, 16235-16240

Lowry, O.H., Rosebrough, N.J., Farr, A.L., and Randall, R.J. (1951). Protein measurement with the Folin phenol reagent. J. Biol. Chem. 193, 265-275.

Madampage, C. A., Tavassoly, O., Christensen, C., Kumari, M., and Lee, J. S. (2012). Nanopore analysis: An emerging technique for studying the folding and misfolding of proteins. Prion 6, 116-123.

MacKinnon, R. (2004). Potassium channels and the atomic basis of selective ion conduction (Nobel Lecture). Angew. Chem. Int. Ed. 43, 4265-4277.

Manrao, E. A., Derrington, I. M., Pavlenok, M., Niederweis, M., and Gundlach, J. H. (2011). Nucleotide discrimination with DNA immobilized in the MspA nanopore. PloS one 6, e25723.

Matthies, D., Zhou, W., Klyszejko, A. L., Anselmi, C., Yildiz, Ö., Brandt, K., ... and Meier, T. (2014). High-resolution structure and mechanism of an F/V-hybrid rotor ring in a Na^+-coupled ATP synthase. Nat. Commun. 5.

McLachlin, D.T., and Dunn, S.D. (2000). Disulfide linkage of the *b* and δ subunits does not affect the function of the *Escherichia coli* ATP synthase. Biochemistry (Mosc) 39, 3486-3490.

Meier, T., Matthey, U., Henzen, F., Dimroth, P., and Müller, D. J. (2001). The central plug in the reconstituted undecameric *c* cylinder of a bacterial ATP synthase consists of phospholipids. FEBS Lett. 505, 353-356.

Meier, T., Matthey, U., von Ballmoos, C., Vonck, J., von Nidda, T. K., Kühlbrandt, W., and Dimroth, P. (2003). Evidence for structural integrity in the undecameric *c*-rings isolated from sodium ATP synthases. J. Mol. Biol. 325, 389-397.

Meier, T., Polzer, P., Diederichs, K., Welte, W., and Dimroth, P. (2005). Structure of the rotor ring of F-Type Na^+-ATPase from *Ilyobacter tartaricus*. Science 308, 659-662.

Meier, T., Ferguson, S. A., Cook, G. M., Dimroth, P., and Vonck, J. (2006). Structural investigations of the membrane-embedded rotor ring of the F-ATPase from *Clostridium paradoxum*. J. Bacteriol. 188, 7759-7764.

Meier, T., Krah, A., Bond, P. J., Pogoryelov, D., Diederichs, K., and Faraldo-Gómez, J. D. (2009). Complete ion-coordination structure in the rotor ring of Na^+-dependent F-ATP synthases. J. Mol. Biol. 391, 498-507.

Mosher, M. E., White, L. K., Hermolin, J., and Fillingame, R. H. (1985). H^+-ATPase of *Escherichia coli*. An *uncE* mutation impairing coupling between F_1 and F_O but not F_O-mediated H^+ translocation. J. Biol. Chem. 260, 4807-4814.

Movileanu, L., Howorka, S., Braha, O., and Bayley, H. (2000). Detecting protein analytes that modulate transmembrane movement of a polymer chain within a single protein pore. Nature Biotechnol. 18, 1091-1095.

Neumann, S., Matthey, U., Kaim, G., and Dimroth, P. (1998). Purification and properties of the F_1F_O ATPase of *Ilyobacter tartaricus*, a sodium ion pump. J. Bacteriol. 180, 3312-3316.

Niederweis, M., Ehrt, S., Heinz, C., Klocker, U., Karosi, S., Swiderek, K.M., Riley, L.W., and Benz, R. (1999). Cloning of the *mspA* gene encoding a porin from *Mycobacterium smegmatis*. Mol. Microbiol. 33, 933-945.

Ozaki, Y., Suzuki, T., Kuruma, Y., Ueda, T., and Yoshida, M. (2008). UncI protein can mediate ring-assembly of *c*-subunits of F_OF_1-ATP synthase *in vitro*. Biochem. Biophys. Res. Commun. 367, 663-666.

Parker, M. W., Buckley, J. T., Postma, J. P., Tucker, A. D., Leonard, K., Pattus, F., and Tsernoglou, D. (1994). Structure of the Aeromonas toxin proaerolysin in its water-soluble and membrane-channel states. Nature 367, 292-295.

Pastoriza-Gallego, M., Rabah, L., Gibrat, G., Thiebot, B., van der Goot, F. G., Auvray, L., ... and Pelta, J. (2011). Dynamics of unfolded protein transport through an aerolysin pore. J. Am. Chem. Soc. 133, 2923-2931.

Pogoryelov, D., Yildiz, Ö., Faraldo-Gómez, J. D., and Meier, T. (2009). High-resolution structure of the rotor ring of a proton-dependent ATP synthase. Nature Struct. Mol. Biol. 16, 1068-1073.

Pogoryelov, D., Klyszejko, A. L., Krasnoselska, G. O., Heller, E. M., Leone, V., Langer, J. D., ... and Meier, T. (2012). Engineering rotor ring stoichiometries in the ATP synthase. Proc. Acad. Nat. Sci. U.S.A. 109, E1599-E1608.

Preiss, L., Yildiz, Ö., Hicks, D. B., Krulwich, T. A., and Meier, T. (2010). A new type of proton coordination in an F_1F_O-ATP synthase rotor ring. PLoS Biol. 8, e1000443.

Preiss, L., Klyszejko, A. L., Hicks, D. B., Liu, J., Fackelmayer, O. J., Yildiz, Ö., ... and Meier, T. (2013). The *c*-ring stoichiometry of ATP synthase is adapted to cell physiological requirements of alkaliphilic *Bacillus pseudofirmus* OF4. Proc. Acad. Nat. Sci. U.S.A. 110, 7874-7879.

Reichow, S. L., Korotkov, K. V., Hol, W. G., and Gonen, T. (2010). Structure of the cholera toxin secretion channel in its closed state. Nature Struct. Mol. Biol. 17, 1226-1232.

Rodgers, A.J., and Capaldi, R.A. (1998). The second stalk composed of the *b*- and δ-subunits connects F_O to F_1 via an α-subunit in the *Escherichia coli* ATP synthase. J. Biol. Chem. 273, 29406-29410.

Sakmann, B., Neher, E. (1984). Patch clamp techniques for studying ionic channels in excitable membranes. Annu. Rev. Physiol. 46, 455–472.

Senior, A. E. (1988). ATP synthesis by oxidative phosphorylation. Physiol. Rev. 68, 177-231.

Schagger, H., and von Jagow, G. (1987). Tricine-sodium dodecyl sulfate-polyacrylamide gel electrophoresis for the separation of proteins in the range from 1 to 100 kDa. Anal. Biochem. 166, 368-379.

Schneider, E., and Altendorf, K. (1984). Subunit *b* of the membrane moiety (F_O) of ATP synthase (F_1F_O) from *Escherichia coli* is indispensable for H^+ translocation and binding of the water-soluble F_1 moiety. Proc. Acad. Nat. Sci. U.S.A. 81, 7279-7283.

Song, L., Hobaugh, M.R., Shustak, C., Cheley, S., Bayley, H., and Gouaux, J.E. (1996). Structure of staphylococcal alpha-hemolysin, a heptameric transmembrane pore. Science 274, 1859-1866.

Stahlberg, H., Müller, D. J., Suda, K., Fotiadis, D., Engel, A., Meier, T., ... and Dimroth, P. (2001). Bacterial Na^+-ATP synthase has an undecameric rotor. EMBO rep. 2, 229-233.

Steed, P. R. and Fillingame, R. H. (2013). Residues in the polar loop of subunit *c* in *Escherichia coli* ATP synthase function in gating proton transport to the cytoplasm. J. Biol. Chem. 289, 2127-2138.

Stefureac, R., Long, Y. T., Kraatz, H. B., Howard, P., and Lee, J. S. (2006). Transport of α-helical peptides through α-hemolysin and aerolysin pores. Biochemistry 45, 9172-9179.

Stein, D., Kruithof, M., and Dekker, C. (2004). Surface-charge-governed ion transport in nanofluidic channels. Phys. Rev. Lett. 93, 035901.

Stock, D., Leslie, A. G., and Walker, J. E. (1999). Molecular architecture of the rotary motor in ATP synthase. Science 286, 1700-1705.

Storm, A. J., Chen, J. H., Ling, X. S., Zandbergen, H. W., and Dekker, C. (2003). Fabrication of solid-state nanopores with single-nanometre precision. Nat. Mater. 2, 537-540.

Suzuki, T., Ozaki, Y., Sone, N., Feniouk, B.A., and Yoshida, M. (2007). The product of *uncI* gene in F_1F_O-ATP synthase operon plays a chaperone-like role to assist *c*-ring assembly. Proc. Acad. Nat. Sci. U.S.A. 104, 20776-20781.

Tabard-Cossa, V., and *et al*. (2007). Noise analysis and reduction in solid-state nanopores. Nanotechnology 18, 305505.

Toei, M., and Noji, H. (2013). Single-molecule analysis of F_OF_1-ATP synthase inhibited by N, N-dicyclohexylcarbodiimide. J. Biol. Chem. 288, 25717-25726.

Towbin, H., Staehelin, T., and Gordon, J. (1979). Electrophoretic transfer of proteins from polyacrylamide gels to nitrocellulose sheets: procedure and some applications. Proc. Acad. Nat. Sci. U.S.A. 76, 4350-4354.

Uhlin, U., Cox, G., and Guss, J. (1997). Crystal structure of the ε subunit of the protontranslocating ATP synthase from *Escherichia coli*. Structure 5, 1219-1230.

Valiyaveetil, F.I., and Fillingame, R.H. (1998). Transmembrane topography of subunit *a* in the *Escherichia coli* F_1F_O ATP synthase. J. Biol. Chem. 273, 16241-16247.

van Bloois, E., Jan Haan, G., de Gier, J. W., Oudega, B., and Luirink, J. (2004). F_1F_O ATP synthase subunit c is targeted by the SRP to YidC in the *E. coli* inner membrane. FEBS lett. 576, 97-100.

van der Laan, M., Bechtluft, P., Kol, S., Nouwen, N., and Driessen, A. J. (2004). F_1F_O ATP synthase subunit c is a substrate of the novel YidC pathway for membrane protein biogenesis. J. Cell Biol. 165, 213-222.

Vik, S. B., and Ishmukhametov, R. R. (2005). Structure and function of subunit *a* of the ATP synthase of *Escherichia coli*. J. Bioenerg. Biomembr. 37, 445-449.

Vollmar, M., Schlieper, D., Winn, M., Büchner, C., and Groth, G. (2009). Structure of the c_{14} rotor ring of the proton translocating chloroplast ATP synthase. J. Biol. Chem. 284, 18228-18235.

von Ballmoos, C., Wiedenmann, A., and Dimroth, P. (2009). Essentials for ATP synthesis by F_1F_O ATP synthases. Annu. Rev. Biochem. 78, 649-672.

Vonck, J., von Nidda, T.K., Meier, T., Matthey, U., Mills, D.J., Kuhlbrandt, W., and Dimroth, P. (2002). Molecular architecture of the undecameric rotor of a bacterial Na^+-ATP synthase. J. Mol. Biol. 321, 307-316.

Wada, T., Long, JC., Zhang, D., Vik, SB. (1999). A novel labeling approach supports the five transmembrane model of subunit *a* of the *Escherichia coli* ATP synthase. J. Biol. Chem. 24, 17353-17357.

Walker, J. E. (2013). The ATP synthase: the understood, the uncertain and the unknown. Biochem. Soc. Trans. 41, 1-16.

Watt, I. N., Montgomery, M. G., Runswick, M. J., Leslie, A. G., and Walker, J. E. (2010). Bioenergetic cost of making an adenosine triphosphate molecule in animal mitochondria. Proc. Acad. Nat. Sci. U.S.A. 107, 16823-16827.

Wilkens, S., and Capaldi, R. A. (1998). Solution structure of the ε subunit of the F_1-ATPase from *Escherichia coli* and interactions of this subunit with β subunits in the complex. J. Biol. Chem. 273, 26645-26651.

Wilkens, S., Rodgers, A., Ogilvie, I., and Capaldi, R. (1997). Structure and arrangement of the δ subunit in the *E. coli* ATP synthase. Biophys. Chem., 68, 95-102.

Yi, L., Jiang, F., Chen, M., Cain, B., Bolhuis, A., and Dalbey, R.E. (2003). YidC is strictly required for membrane insertion of subunits *a* and *c* of the F_1F_O ATP synthase and SecE of the SecYEG translocase. Biochemistry (Mosc) 42, 10537-10544.

Yi, L., Celebi, N., Chen, M., and Dalbey, R.E. (2004). Sec/SRP requirements and energetics of membrane insertion of subunits *a*, *b*, and *c* of the *Escherichia coli* F_1F_O ATP synthase. J. Biol. Chem. 279, 39260-39267.

Yoshida, M., Muneyuki, E., and Hisabori, T. (2001). ATP synthase - a marvellous rotary engine of the cell. Nature Rev. Mol. Cell Biol. 2, 669-677.

Yoshida, M., Sone, N., Hirata, H., Kagawa, Y., and Ui, N. (1979). Subunit structure of adenosine triphosphatase. Comparison of the structure in thermophilic bacterium PS3 with those in mitochondria, chloroplasts, and *Escherichia coli*. J. Biol. Chem. 254, 9525-9533.

Zhao, Q., Jayawardhana, D. A., Wang, D., and Guan, X. (2009). Study of peptide transport through engineered protein channels. J. Physiol. Chem. B, 113, 3572-3578.